MOLECULAR MECHANISMS OF A RETINAL

CYCLIC NUCLEOTIDE-GATED CHANNEL

Juan Ramon Martinez-Francois

A DISSERTATION

in

Neuroscience

Presented to the Faculties of the University of Pennsylvania

in

Partial Fulfillment of the Requirements for the

Degree of Doctor of Philosophy

2009

Supervisor of Dissertation Zhe Lu

Zhe Lu, M.D., Ph.D.

Graduate Group Chair Michael Nusbaum

Michael P. Nusbaum, Ph.D.

Dissertation Committee

Toshinori Hoshi, Ph.D.

Stephen M. Baylor, M.D.

Paul De Weer, M.D., Ph.D.

Brian M. Salzberg, Ph.D.

Acknowledgments

A great number of people have been invaluable in the completion of this thesis. I wish to thank everyone that has been a part of my life during the past seven years.

Zhe. I'm incredibly lucky to be your student. Working with you has not only made me a better scientist, but most importantly, a better person.

Yanping. For your outstanding contributions in the projects we did together and for all your excellent advice. Above all, for being such a wonderful friend.

The Lu lab. All of you have been incredible friends and have always been there to help me and encourage me through the hard times. You guys are really the best lab I could have ever hoped to work in.

My thesis committee. For really caring about my work and hugely assisting in my improvement.

My dad. For supporting me all along and for always cheering me on. I am sure I would not have made it this far without you. I love you.

My friends. You have kept me sane all these years. Thanks for being there for me every single time I have needed you.

ABSTRACT

MOLECULAR MECHANISMS OF A RETINAL
CYCLIC NUCLEOTIDE-GATED CHANNEL

Juan Ramon Martinez-Francois

Zhe Lu

Cyclic nucleotide-gated (CNG) channels mediate the transduction of light signals to electrical signals in vertebrate photoreceptors. These channels are non-selective for cations and open upon cGMP binding. The intracellular cGMP concentration is elevated in darkness, and the current through CNG channels maintains the membrane of the rod photoreceptor at around -40 mV. When light enters the retina, it triggers a signal transduction cascade that decreases intracellular cGMP, and therefore CNG channels close. A reduction in CNG current hyperpolarizes the rod. Two molecular mechanisms are crucial for the proper physiological function of retinal CNG channels. First, block of these channels by physiological agents reduces membrane noise in rods. This feature enables rods to detect photons with high sensitivity. Second, CNG channels must be able to conduct current in response to the light-triggered changes in intracellular cGMP. In other words, they should open and close gradually in response to cGMP binding, not other stimuli such as voltage. This thesis addresses these two fundamental mechanisms of CNG channel function. We present the biophysical investigation of the mechanism

underlying voltage sensitivity of ion channel block. That is, affinity of blocking agents for the pore of ion channels varies with membrane voltage. Two models have been postulated to explain this phenomenon. Here we use the retinal CNG channel (CNGA1) as a model to illustrate the analytical solutions and electrophysiological hallmarks of these two models. In addition, we show through a systematic mutagenesis study, that certain point mutations around the outer, narrow part of the channel close the channel at the relevant physiological voltages. However, these mutant channels can open in response to voltage at positive potentials only when bound by cGMP. This mutation-caused voltage gating reflects the inherent voltage gating capabilities of the wild-type channel, which must be suppressed to avoid their closure in a physiological setting. These results support the notion that the selectivity filter of the channel must be properly anchored to the surrounding protein structure in order for CNGA1 channels to achieve their physiological role.

Table of contents

List of tables

List of figures

Abbreviations

bis-QA_{C10}	decane-*bis*-trimethylammonium
cAMP	3',5'-cyclic adenosine monophosphate
cGMP	3',5'-cyclic guanosine monophosphate
CNG	cyclic nucleotide-gated
DTT	dithiothreitol
EDTA	ethylenediaminetetraacetic acid
ΔG	change in free energy
G-V	conductance-voltage
HCN	hyperpolarization-activated cyclic nucleotide-modulated
HEPES	4-(2-hydroxyethyl)-1-piperazineethanesulfonic acid
I/I_o	fraction of current not blocked
I-V	current-voltage
Kir	inward-rectifier potassium channel
Kv	voltage-gated potassium channel
MTS	methanethiosulfonate
PCR	polymerase chain reaction
PDE	phosphodiesterase E
PhTx	philanthotoxin
QAs	quaternary ammoniums
SPM	spermine
$V_{1/2}$	half-activation voltage
WT	wild type
Z	effective valence

Chapter 1

General introduction

1.1 Ion channels

Cells have membranes that allow them to separate their intracellular space from the environment. This hydrophobic lipid membrane represents an enormous energy barrier for the movement of small ions. During evolution, a class of proteins, known as ion channels, were developed to facilitate ion movements through the intracellular and extracellular aqueous compartments. These proteins are integrally embedded in the membrane, spanning the lipid bilayer to provide an efficient and selective pathway for ions to move down their electrochemical gradient. Ion channels are not simple open holes of different diameter; they can discriminate between different ions with great efficiency and specificity and can conduct ions at extremely high rates (>10^6 ions per second). For example, potassium-selective channels, or K^+ channels, let over one hundred K^+ ions go through for every Na^+ ion, in spite of both types of ions having similar sizes.

Ion channels are widely distributed throughout the biological world, appearing in membranes of animal cells, prokaryotes, protozoa, and plant cells. Although ion channels share a common function, namely, allowing the passage of ions through the plasma membrane, they also specifically respond to stimuli that induce the opening (or closing) of the permeation pathway in a process called gating. Gating stimuli include the membrane voltage, the concentration of extracellular or intracellular ligands, temperature

and membrane tension, i.e., electrical, chemical and mechanical forces.

The biophysical description of ion channels and their role in producing electric currents in cell membranes was carried out more than fifty years ago by Hodgkin and Huxley as well as Curtis and Cole in their studies of Na^+ and K^+ currents in the squid giant axon (Hille, 2001). Since then, fundamental knowledge about ion channel function and structure has been obtained in great part due to outstanding technological advances in electrophysiology, molecular biology and protein chemistry (reviewed by Bezanilla, 2008).

One of the most popular electrophysiological methods is the patch-clamp technique (Hamill et al., 1981; Sakmann and Neher, 1995). It is widely used to record currents formed by a large number of channels (called macroscopic currents) as well as single-channel currents, in a plethora of preparations *in vitro* and *in vivo*. By means of the patch-clamp technique and other electrophysiological methods great insight can be obtained about the function of ion channels; however, the tool that allows correlation of specific functional channel properties with protein elements is molecular cloning.

Since the cloning of the first ion channel (Noda et. al., 1983), hundreds of different other channel types have been cloned and thus the classification of channels into families, based on their amino acid sequence and molecular topology, has become possible (e.g., Jan and Jan, 1990). Furthermore, using molecular biology techniques in conjunction with efficient heterologous expression systems, such as *Xenopus laevis* oocytes, it is possible to study the functional properties of cloned channels that have been altered in their primary structure. Through such structure-function studies an enormous amount of mechanistic information has been obtained at the molecular level.

The next breakthrough that led to the detailed molecular understanding of ion channels was the determination of the crystal structure of a potassium channel (Doyle et. al., 1998). Molecular models obtained from crystal structures of different channels now guide the efforts of the structure-function studies and the understanding of ion channel function at the atomic level.

1.2 Cyclic nucleotide-gated channels

Cyclic nucleotide-gated (CNG) channels open in response to the direct binding of the cyclic nucleotides 3',5'-cyclic guanosine monophosphate (cGMP) and 3',5'-cyclic adenosine monophosphate (cAMP). The fact that these channels are activated by cGMP binding was discovered in membranes of the outer segment of vertebrate rod photoreceptors (Fesenko et al., 1985). Subsequently, similar channels were identified in cone photoreceptors (Haynes and Yau, 1985) and chemosensitive cilia of olfactory sensory neurons (Nakamura and Gold, 1987). Molecular cloning of CNG channels became possible when the channel protein was purified and identified by functional reconstitution into artificial liposomes and lipid bilayers (Cook et al., 1986; Hanke et al., 1988). Presently, by means of sequence similarity and functional studies, CNG channels have been identified in many vertebrate tissues such as heart, aorta (Biel et al., 1993, 1994), pineal gland (Dryer and Henderson, 1991; Distler et al., 1994), kidney, sperm (Biel et al., 1994; Weyand et al., 1994) and brain (Bradley et al., 1997). CNG channels are also expressed in the membranes of plants (Leng et al. 1999), prokaryotes (Nimigean et al., 2004) and invertebrates (Bacigalupo et al. 1991; Delgado et al. 1991; Zufall and Hatt; 1991; Baumann et al.1994; Komatsu et al. 1996). Whereas the function of CNG

channels has been clearly demonstrated in primary sensory transduction (see below; Yau and Baylor, 1989; Kaupp and Seifert, 2002), their role in other physiological processes is currently not well understood. For example, in the retina, CNG channels have been implicated in nitric oxide signaling (Ahmad et al., 1992). In the nematode *Caenorhabditis elegans*, the tax-2 and tax-4 genes which encode proteins that are closely related to CNG channels, were shown to be essential for formation of the appropriate synaptic connections between chemosensory neurons and the nerve ring (Coburn and Bargmann, 1996; Komatsu et al., 1996). In addition, Ca^{2+} imaging studies found that an influx of Ca^{2+} in hippocampal neurons, probably through a CNG channel, results from an increase in intracellular cyclic nucleotide concentrations, suggesting that CNG channels play a role in the synaptic plasticity underlying learning and memory (Bradley et al., 1997).

1.3 Role of retinal CNG channels in phototransduction

As mentioned before, the role of CNG channels is best understood in sensory transduction. In both olfactory and visual transduction, CNG channels transform external sensory stimuli into electric signals that can be propagated to the brain. In retinal rods specifically, CNG channels mediate the generation of an electric response to light. Rod photoreceptors contain the visual pigment rhodopsin and are mainly responsible for vision under dark or dim conditions. In the dark, cGMP levels are high and binding of cGMP to CNG channels causes the channels to open, allowing a steady flow of Na^{+} and Ca^{2+} into the cell. This inward current, called the dark current, maintains the rod's membrane potential at a relatively depolarized voltage in darkness. When light hits the

retina, it activates the phototransduction cascade on the disc membranes of rod photoreceptor outer segments (Fig. 1.1; Burns and Baylor, 2001). Light activates rhodopsin in the membrane. This process causes the activation of a phosphodiesterase (PDE) via the heteromeric G-protein transducin. PDE hydrolyzes cGMP to 5`-GMP. The resulting decrease in the intracellular cGMP concentration causes the closure of CNG channels, and decreases the dark current, which hyperpolarizes the rod photoreceptors. Membrane hyperpolarization causes a decrease in the tonic release of glutamate from the presynaptic terminals. In this way, the inhibition of a neurotransmitter signal indicates the detection of photons to the downstream retinal cells and neurons.

1.4 Diversity and structure of CNG channels

In vertebrates, six genes coding for CNG channel subunits have been identified. These genes are grouped according to sequence similarity into two subtypes, CNGA and CNGB (Bradley et al., 2001). Physiologically, specific combinations of subunits form the different tetrameric channels present in specific tissues. Functional features of these channels, such as ligand sensitivity and selectivity, ion permeation, and gating vary with the subunit composition of the respective channel complex. The first cDNA clone for a subunit of the CNG channel family (CNGA1) was isolated from bovine retina (Kaupp et al., 1989). CNGA1 is expressed in rod photoreceptors and produces functional homotetramers that are gated by binding of cGMP when expressed heterologously in *Xenopus laevis* oocytes. Later, a second subunit of the rod CNG channel (CNGB1) was isolated and cloned (Chen et al., 1993). CNGB1 expressed alone does not produce

functional channels, but coexpression of CNGA1 and CNGB1 yields heterotetrameric channels with characteristics similar to those of native channels (Chen et al., 1993; Körschen et al., 1995). Studies using a combination of different approaches show that native CNG channels from rod photoreceptors are composed of three CNGA1 subunits and one CNGB1 subunit (Weitz et al., 2002; Zheng et al., 2002; Zhong et al., 2002).

CNG channels have the same basic architecture, four subunits arranged around a centrally located pore (Fig. 1.2 A; Liu et al., 1996; Clayton et al., 2008). Each subunit contains six transmembrane segments (S1-S6). The permeation pathway of the channel, or pore region, is formed by the S6 and the loop that connects it to S5, this loop is called the pore loop. This loop has an alpha-helical portion called the pore helix followed by a region that forms the selectivity filter of the channel which is a narrow constriction at the extracellular part of the pore (Fig. 1.2 B; Doyle et al., 1998). These structural motifs are also present in other channels, for example, voltage-gated K^+ (Kv) channels and hyperpolarization-activated cyclic nucleotide-modulated (HCN) channels (Craven and Zagotta, 2006; Anselmi et al., 2007). Intriguingly, the S4 segment in CNG channels resembles that of Kv channels, which is a major part of the voltage sensor. However, the role of S4 in CNG channels is still unknown as the channels show little voltage dependence (Karpen et al., 1988; Benndorf et al., 1999; Nache et al., 2006). CNG channels also possess a large intracellular C-terminus that forms the cyclic nucleotide-binding domain site (Kaupp et al., 1989; Molday et al., 1991; Wohlfart et al., 1992; Henn et al., 1995; Liu et al., 1996).

The CNG channel pore is thought to be structurally similar to those of other pore-loop containing ion channels (Heginbotham et al., 1992; Clayton et al., 2008). The

general architecture of the pore of this family of channels was initially revealed by the crystal structure of a KcsA, a bacterial potassium channel from *Streptomyces lividans* (Doyle et al., 1998). Later, an open channel conformation was determined in the crystal structure of another channel, MthK (Jiang et al., 2002). This channel is structurally similar to KcsA in the pore-loop but has a different conformation of the inner helix (corresponding to S6 in CNG or Kv channels) that lines the pore. The inner helices contain a "gating hinge" that bends upon opening of the channel. In a straight conformation, the four inner helices form a bundle, closing the pore near its intracellular end. In a bent configuration, the inner helices stay open creating a wide (12 Å) intracellular mouth. Amino acid conservation among a wide range of pore-loop containing channels suggests that the KcsA and MthK structures may serve as general structural models for the closed and open state conformations of this family of ion channels. In addition, functional approaches have established that Kv channels open and close their permeation pathway at the intracellular end of the pore (Yellen, 1998; Swartz, 2004). In contrast, CNG channels appear to lack a gating mechanism at the intracellular end of the pore. For example, when the permeation pathway of CNG channels is occluded by charged molecules or ions added from the cytoplasmic side, the channels are blocked equally in conditions where they are mostly open or mostly closed. In other words, these agents do not block CNG channels in a state-dependent manner (Karpen et al., 1993; Fodor et al., 1997a,b; Contreras and Holmgren, 2006) as in the case of Kv channels (e.g. Armstrong, 1971; Choi et al., 1993; Holmgren et al., 1997). Additionally, methanethiosulfonate (MTS) reagents applied intracellularly modify cysteine residues located in the most intracellular region of the CNG channel pore in a non-state-dependent

manner (Sun et al., 1996; Flynn and Zagotta, 2001; Contreras and Holmgren, 2006). Again, these latter studies are in direct opposition with the location of the gate in the S6 segment, as shown in Kv channels using a similar approach (Liu et al., 1997; del Camino and Yellen, 2001). Therefore, it seems that instead of gating at the intracellular end of the pore, the gate of the CNG channel appears to be located at the selectivity filter. Several lines of evidence seem to indicate that conformational changes in the selectivity filter of CNG channels are associated with gating: (1) mutations in the selectivity filter have significant effects on gating (Bucossi et al., 1996; Gavazzo et al., 2000); (2) in the presence of low concentrations of cGMP, CNG channels produce different single-channel currents compared to channels in high cGMP concentrations (Ruiz and Karpen, 1997; Hackos and Korenbrot, 1999; Kusch et al., 2004); (3) accessibility of cysteine modifying reagents applied from either side of the membrane perturbs normal gating by cGMP when wild-type residues are replaced with cysteines along the entire pore-loop. (Becchetti et al., 1999; Beccheti and Roncaglia, 2000; Liu and Siegelbaum, 2000; Contreras et al., 2008). The location of the CNG channel gate is yet to be conclusively determined, however, these observations suggest that the basic gating mechanism differs in CNG and Kv channels.

1.5 Retinal CNG channel selectivity

The permeation properties of retinal CNG channels have been extensively studied in native and heterologous systems. These channels are very selective for cations over anions, and do not discriminate well among monovalent cations. The selectivity for monovalent cations is determined by calculating the relative permeabilities of different

cations under conditions where one type of ion is present in one side of the membrane and a different type is in the other side, i.e. biionic conditions. In these conditions it is possible to examine the reversal potential of the currents through the channels upon changing either the type of ion or its concentration at one side of the membrane. Using this approach, homomeric recombinant channels formed by the CNGA1 subunit were found to have the following sequence of permeability ratios: $NH_4^+ > Na^+ \sim K^+ > Li^+ > Rb^+ > Cs^+ = 2.93:1.01:1:0.63:0.56:0.37$ (Kaupp et al., 1989; Goulding et al., 1993; Nizzari et al., 1993). Native amphibian (Fesenko et al., 1985; Menini, 1990; Furman and Tanaka, 1990; Zimmerman and Baylor, 1992) and mammalian (Kaupp et al., 1988) retinal CNG channels have similar relative ion permeabilities.

1.6 Retinal CNG channel block

Permeation of monovalent cations through retinal CNG channels is blocked by physiological agents, such as divalent cations (Haynes et al., 1986; Stern et al., 1987; Colamartino et al., 1991; Zimmerman and Baylor, 1992; Root and MacKinnon, 1993; Eismann et al., 1994; Park and MacKinnon 1995; Nasi and del Pilar Gomez, 1999; Seifert et al., 1999) and polyamines (Lu and Ding, 1999; Guo and Lu, 2000). These channels can also be blocked by diverse pharmacological agents, for example, quaternary ammonium ions (Goulding et al., 1993; Stotz and Haynes, 1996; Contreras and Holmgren, 2006), amiloride 3',4'-dichlorobenzamil (Nicol et al., 1987), tetracaine and its derivatives (Fodor et al., 1997a,b; Ghatpande et al., 2002; Strassmaier et al., 2005), and dequalinium (Rosenbaum et al., 2002; 2004). Under physiological conditions, channel block lowers the effective single-channel conductance of retinal CNG channels from ~25

pS to ~0.1 pS. Thus, a single channel at the rod's resting membrane potential in darkness (-40 mV) conducts a current of about 4 fA instead of 1 pA. The dark current of 40 pA in a single rod then flows through ten thousand open channels whereas, in the absence of block, a macroscopic current of the same size would require only forty open channels (Yau and Baylor, 1989). Block of CNG channels thus decreases the membrane electrical noise for a similar current size. This feature allows rods to detect single photons because photon detection is encoded by small currents, ~1 pA or less (Penn and Hagins, 1972; Baylor et al., 1979; Rieke and Baylor, 1998). Additionally, having channels with a very small effective conductance contributes in great part to making single-photon detection a reproducible event. In rods, a single photon inhibits 3% of the dark current, or about 300 channels. Given that ion channels open and close with a known average rate and independently of the time since the last event, their gating can be described with a Poisson distribution, where the standard deviation is the square root of the mean. Therefore, when a large pool of open channels contributes to the dark current, the expected variation in the number of channels closing is 17 when a photon is absorbed. If channels were not blocked and had a large conductance, the mean number of channels that would need to close to give a 1 pA single-photon response would be close to one, thereby making the single-photon response much less reproducible (Baylor et al., 1979, 1984; Yau and Baylor, 1989).

1.7 Studies in this thesis

As discussed above, CNG channel block in the retina has critical importance in phototransduction. Moreover, block of ion channels underlies many physiological

processes, for example, neurotransmission (Dingledine et al., 1999), shaping of the cardiac action potential (Nichols and Lopatin, 1997), or potassium regulation in the retina (Newman, 1993). In addition, ion channel blockers serve as therapeutic agents to treat clinical disorders such as epilepsia (Macdonald and Kelly, 1995), heart arrhythmia (Carmeliet and Mubagwa, 1998) and neuropathic pain (Bräu et al., 2001). In some cases, channel block may produce severe adverse pharmacological effects, such as the lethal acquired long-QT syndrome (Keating and Sanguinetti, 2001). CNG channels provide a good model to study the mechanism of ion channel block as their block by physiological and pharmacological agents has been well characterized. In addition, their molecular architecture is similar to voltage-gated channels that are responsible for the generation of electric signals in living organisms.

The first study in this thesis, presented in Chapter 2, consists on the biophysical investigation of the mechanism underlying voltage sensitivity of channel block. It is a well-known phenomenon that the apparent affinity of blockers for the pore of the channel varies with membrane voltage. Two models have been proposed to explain this phenomenon. We used the CNGA1 channel to illustrate the analytical solutions and electrophysiological hallmarks of both models that explain the voltage-dependent block.

During this study, we found that certain point mutations around the extracellular part of the CNGA1 channel pore produced mutant channels that displayed voltage sensitivity. This observation interested us because, as already mentioned, the region where modest voltage sensitivity originates in CNG channel is unknown. The second study, presented in Chapter 3, describes the characterization and analysis of more than one hundred CNGA1 mutants. We found that mutation-caused voltage gating originates

from the region around the selectivity filter, not from either the positively charged S4 or the intracellular part of S6, which in Kv channels function as voltage sensor and activation gate, respectively. We conclude that proper attachment of the selectivity filter to the surrounding pore structure is essential to avoid voltage gating in CNG channels. Mutations that render the channels voltage gated would cause their closure at physiological voltages. Thus, the suppression of the inherent voltage sensitivity in CNGA1 channels is critical for keeping the channels active in the range of membrane potentials where they convert cGMP concentrations to electric signals.

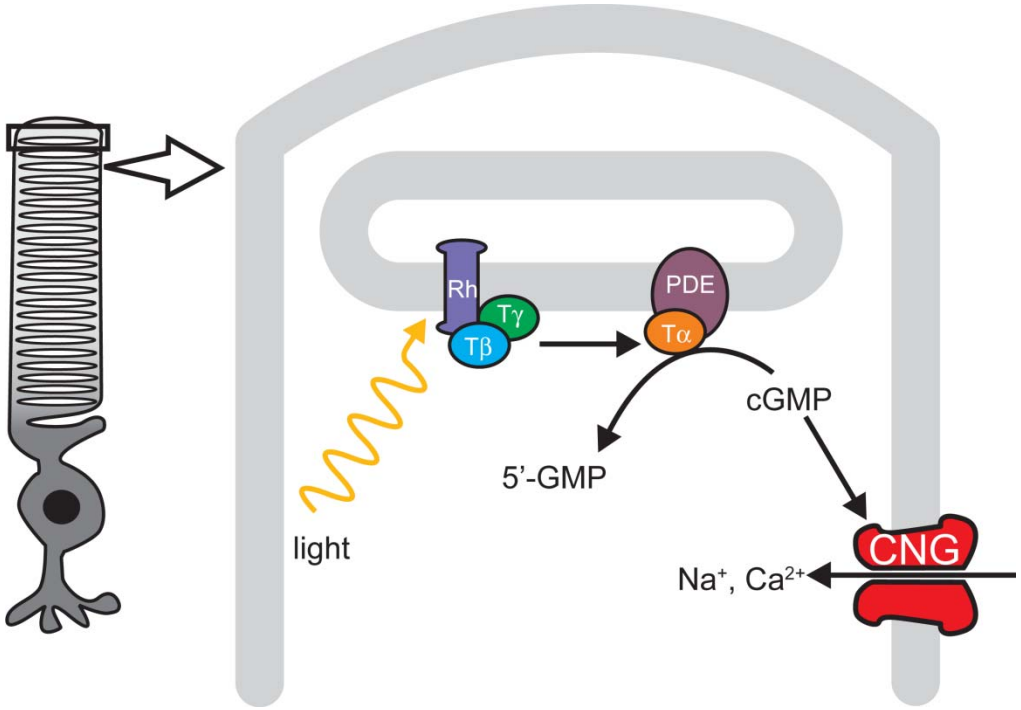

Figure 1.1. Phototransduction cascade in the rod photoreceptor. Signal transduction cascade activated by light in rod photoreceptors (left) takes place in their outer segment (right). Light activates rhodopsin (Rh), which activates the heteromeric G protein transducin (Tα, Tβ, Tγ), whose α subunit activates phosphodiesterase E (PDE). PDE catalyzes the hydrolysis of cGMP. The subsequent decrease in the cytoplasmic concentration of cGMP leads to the closure of CNG channels.

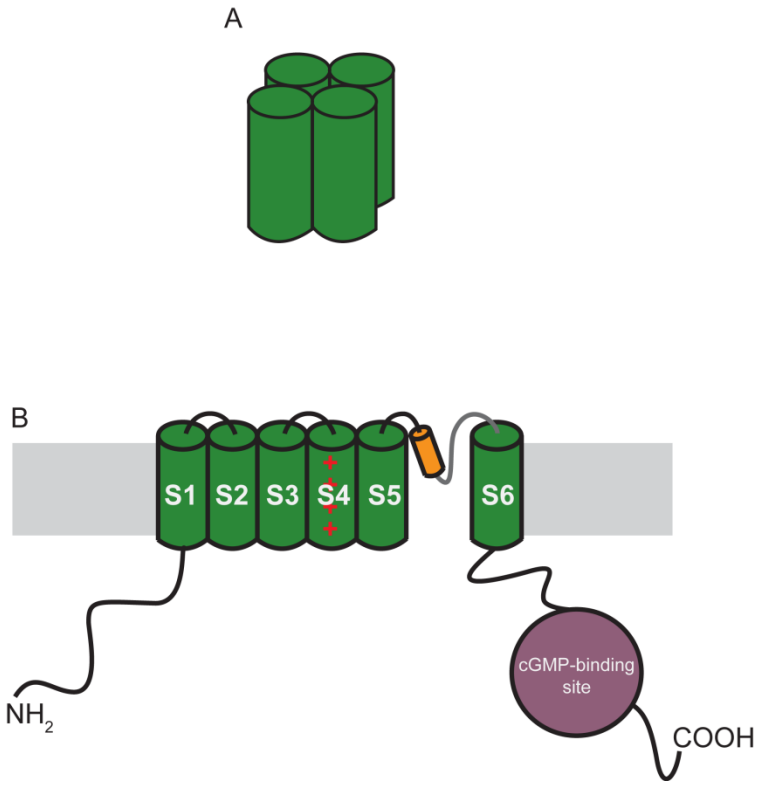

Figure 1.2. Molecular architecture of CNG channels. (A) Cartoon representation of the tetrameric structure of CNG channels. (B) Membrane topology of each subunit of the CNG channel. The transmembrane segments (S1-S6) are shown in green. The pore loop is formed by the S5-S6 linker that contains the pore helix in orange and the selectivity filter in grey. The voltage sensor region is indicated by red positive charges. The C-terminal region contains the cyclic nucleotide-binding domain in maroon.

Chapter 2

Intrinsic versus extrinsic voltage sensitivity of blocker interaction with an ion channel pore

2.1 Abstract

Many agents produce physiological or pharmacological effects by occluding the conduction pore of ion channels. A hallmark of channel block by charged blocking agents is that their apparent affinity for the pore often varies with membrane voltage. Two models have been proposed to explain voltage dependence of channel block. One model – prevalent during the past three decades – assumes that the charged blocker itself directly senses the transmembrane electric field, in other words, blocker binding is intrinsically voltage dependent, e.g., by binding to a site within the field. In the alternative model, the blocker does not directly interact with the electric field; instead, blocker binding acquires apparent voltage dependence through the concurrent movement of permeant ions across the field. Although less frequently invoked, this latter model may better explain voltage dependence of channel block by large organic compounds that are too bulky to fit into the narrow part of the pore where the electric field is steep. To date no systematic protocol has been described for distinguishing between the two types of mechanism. In the present study we use an analytic approach to identify the defining features of the two models, and find that a retinal cyclic nucleotide-gated (CNG) channel can be blocked via either mechanism, depending on the blocker's characteristics. With

this channel as a model, we have systematically and quantitatively examined both intrinsic and extrinsic types of voltage dependence of channel block.

2.2 Introduction

The conduction pore of ion channels can be physically blocked by natural or synthetic agents. Ion channel pores are generally much longer than blocker molecules. Blockers may therefore interact with parts of the pore before reaching their deepest and energetically most stable site. These interactions would result in a multiple, sequential binding scheme (Shin and Lu, 2005; Shin et al., 2005). In the limit that the blocker affinity for any part of the pore, beside the final binding site, is negligible, a single-step binding scheme suffices to describe the binding reaction.

Most pore blockers are charged, and the apparent affinity of channels for these blockers often varies dramatically with membrane voltage. Two general types of model have been proposed to explain this voltage dependence. According to one model, the voltage dependence is intrinsic to the binding of the blocking ion within the transmembrane electric field (Woodhull, 1973), and the extent of block is expected to vary exponentially with membrane voltage according to a Boltzmann function. During the past three decades, this model has been invoked over a thousand times to account for voltage dependence of channel block (e.g., Neher and Steinbach, 1978; Hagiwara et al., 1978; Coronado and Miller, 1979; Blatz and Magleby, 1984; Mayer and Westbrook, 1987; Blaustein and Finkelstein, 1990). The alternative model posits that the blocker does not bind within the electric field, but that the apparent voltage dependence of block reflects the concurrent movement of permeant ions displaced across the electric field by

the blocker (Armstrong, 1971). This model has been used to explain how raising the permeant ion concentration on the opposite side of the membrane lowers the apparent blocker affinity, a phenomenon sometimes dubbed the trans knock-off effect (Armstrong and Binstock, 1965; Hille and Schwarz, 1978; Yellen, 1984b; Neyton and Miller, 1988). However, it has only occasionally been used to interpret the voltage dependence of channel block itself (e.g., MacKinnon and Miller, 1988; Ruppersberg et al., 1994; Spassova and Lu, 1998; Thompson and Begenisich, 2001; 2003; Nimigean and Miller, 2002; Guo et al., 2003), even though it is more plausible in the case of large organic compounds that are too bulky to fit into the narrow part of the pore where the electric field is steep (Jiang et al., 2002; Bernèche and Roux, 2003). In the present study, we use a cyclic nucleotide-gated (CNG) channel as a model to illustrate the analytical characteristics and electrophysiological hallmarks of both types of model for voltage-dependent channel block.

CNG channels mediate visual signal transduction in vertebrate retinal rods and are activated by cGMP (Yau and Baylor, 1989). They open in darkness when the intracellular cGMP concentration is elevated, and close when it is reduced in light. These channels can be blocked by divalent cations and polyamines from either side of the membrane in a voltage-dependent manner (Stern et al., 1987; Colamartino et al., 1991; Zimmerman and Baylor, 1992; Root and MacKinnon, 1993; Eismann et al., 1994; Guo and Lu, 2000). Physiological block of the channels reduces the relative contribution of individual channel currents to the overall macroscopic current, a property that allows accurate phototransduction of light intensity (Yau and Baylor, 1989; Rieke and Baylor, 1998).

2.3 Materials and methods

2.3.1 Molecular biology and oocyte preparation

Complementary DNA for CNGA1 (Kaupp et al., 1989) was cloned into the pGEM-HESS plasmid (Liman et al., 1992). The cRNA was synthesized with T7 polymerase (Promega) using linearized cDNA as a template. Oocytes harvested from *Xenopus laevis* were incubated in a solution containing (in mM): 82.5 NaCl, 2.5 KCl, 1.0 $MgCl_2$, 5.0 HEPES (pH 7.6), and 2-4 mg/ml collagenase (Worthington). The oocyte preparation was agitated at 100 rpm and 30°C for 40-60 min. It was then rinsed thoroughly and stored in a solution containing (in mM): 96 NaCl, 2.5 KCl, 1.8 $CaCl_2$, 1.0 $MgCl_2$, 5 HEPES (pH 7.6), and 50 mg/ml gentamicin. Defolliculated oocytes were selected and injected with RNA at least 2 and 16 h, respectively, after collagenase treatment. All oocytes were stored at 18°C.

2.3.2 Recordings and solutions

Macroscopic currents were recorded from inside-out membrane patches of *Xenopus* oocytes heterologously expressing CNGA1 channels with an Axopatch 200B voltage-clamp amplifier (MDS Analytical Technologies), filtered at 5 kHz, and sampled at 25 kHz using an analog-to-digital converter (Digidata 1322A; MDS Analytical Technologies) interfaced with a personal computer. pClamp8 software was used for amplifier control and data acquisition. To elicit macroscopic currents the voltage across the membrane patch was first hyperpolarized from the 0 mV holding potential to the most hyperpolarizing or depolarizing potential indicated, and then stepped to various test

voltages in 10-mV increments and back to 0 mV. The currents in the absence of cGMP were used as templates for subsequent off-line background-current corrections. Both the internal and external solutions contained (in mM): 0.1 EDTA, 5 HEPES, pH 7.6, and, unless otherwise specified, 130 mM NaCl. To activate the channel a saturating (2 mM) concentration of cGMP was included in the internal solution. All chemicals were purchased from Sigma-Aldrich.

2.3.3 Data analysis

Data analysis and curve fitting were performed with Origin 8.0 (OriginLab Corp.). The figures were made using OriginPro 8.0 and CorelDRAW X14 (Corel Corp.).

2.4 Results

2.4.1 CNGA1 channel block by extracellular PhTx

We first constructed a dose-response curve for cGMP activation of retinal CNGA1 channels in our recording system. Fig. 2.1 A shows currents recorded from an inside-out membrane patch in the presence of four concentrations of intracellular cGMP. Consistent with previous reports (Kaupp et al., 1989; Goulding et al., 1994; Zagotta and Siegelbaum, 1996; Benndorf et al., 1999), cGMP stimulates current with an EC_{50} of ~70 μM, approaching saturation at 2 mM cGMP. The dose-response curve differs little for steps to -100 and 100 mV (Fig. 2.1 B).

The polyamine spermine (SPM) not only blocks but also robustly permeates CNGA1 channels (Lu and Ding, 1999; Guo and Lu, 2000). As the latter property complicates the study of the mechanism of block, we used philanthotoxin (PhTx) instead, which can be thought of as a spermine molecule with a bulky chemical group attached to one end (Fig. 2.2 A). The spermine portion of the PhTx molecule, like spermine itself, can bind in the narrow selectivity filter, but the bulky group will prevent PhTx from sliding through to the opposite side (Bähring et al., 1997; Guo and Lu, 2000). Fig. 2.2 B shows CNGA1 currents in the absence or presence of three concentrations of extracellular PhTx. The channels were activated with 2 mM intracellular cGMP, and currents were elicited with the voltage protocol shown. The corresponding steady-state I-V curves are shown in Fig. 2.2 C. In the absence of PhTx, the I-V curve is approximately linear. PhTx blocks the channels in a voltage dependent manner, rendering the I-V curve outwardly rectifying. To better illustrate the voltage dependence of channel block, we made a plot of the fraction of current not blocked (I/I_o) against voltage, which we will call the (voltage-dependent) blocking curve (Fig. 2.2 D). As one might expect for a blocking mechanism where a positively charged blocker enters the transmembrane electric field, the fraction of current not blocked obeys a Boltzmann function that approaches zero at extreme negative potentials. A fit of the data yields an $^{app}K_d$ at 0 mV of $2.71 \pm 0.20 \times 10^{-5}$ M and an effective valence of 1.76 ± 0.02.

At low blocker concentrations the "on" rates of current block are sufficiently slow to allow kinetic analysis. Fig. 2.3 A shows an example of current block by 0.1 μM PhTx initiated by a voltage step from 100 mV to -150 mV; the time course follows a single exponential. Similar records were made for three PhTx concentrations (0.03, 0.1 and 1

μM) at eight voltages between -110 and -180 mV. In Fig. 2.3 B we plot the reciprocals of the corresponding averaged time constants against PhTx concentration. At each PhTx concentration the data points for all eight voltages are superimposed; there is thus no discernible trend in the value of the individual slopes (a measure of the second-order rate constant for blocker binding) as a function of voltage (Fig. 2.3 C). Linear extrapolation of Fig. 2.3 C to 0 mV yields a second-order rate constant k_{on} (0 mV) of $1.04 \pm 0.06 \times 10^9$ $M^{-1}s^{-1}$ for blocker binding to the pore, with valence (z_{on}, estimated from the extrapolating slope) not significantly different from zero (0.01 ± 0.01).

Unblocking kinetics were examined from the time course of depolarization-induced current recovery. Fig. 2.4 A shows an example of current recovery from block by 0.1 μM PhTx, initiated by a voltage step from -200 mV to -50 mV; the time course of current recovery again follows a single exponential. The reciprocal of the time constant ($1/\tau_{off}$ or k_{off}) is independent of PhTx concentration but varies with voltage (Fig. 2.4 B). The averages (over the three concentrations tested) of the natural logarithm of k_{off} are plotted against voltage in Fig. 2.4 C. A Boltzmann fit of the plot yields k_{off} (0 mV) = $9.65 \pm 0.35 \times 10^3$ s^{-1} and valence (z_{off}) = 1.31 ± 0.02. The calculated ratio $k_{off}/k_{on} = 9.28 \times 10^{-6}$ M (at 0 mV) is within a factor of three of the $^{app}K_d$ (0 mV) = 2.71×10^{-5} M determined from equilibrium measurements, and $z_{on} + z_{off} = 1.32$ is comparable to Z = 1.76 determined from equilibrium measurements (Fig. 2.2).

2.4.2 CNGA1 channel block by intracellular PhTx

In similar fashion we examined CNGA1 block by intracellular PhTx. Fig. 2.5 A shows currents recorded in the absence or presence of 0.3 μM PhTx. Intracellular PhTx,

like extracellular PhTx, also blocks the channels in a voltage-dependent manner. To examine the voltage dependence of channel block by intracellular PhTx we plotted the blocking curves for four concentrations of intracellular PhTx in Fig. 2.5 B. As expected if PhTx were binding in the electric field, the fraction of current not blocked decreases with membrane depolarization and approaches zero at extreme positive potentials. A Boltzmann function fits the data well and yields $^{app}K_d$ (0 mV) = $8.58 \pm 0.38 \times 10^{-7}$ M and valence = 2.67 ± 0.04.

We also performed kinetic analyses of the development of, and recovery from, channel block by intracellular PhTx, initiated with voltage jumps. Fig. 2.5, C and D plots the natural logarithm of the second-order blocking rate constant (k_{on}) and of the unblocking rate (k_{off}), respectively, against membrane voltage. The constant k_{on} is weakly, and k_{off} strongly, voltage dependent. Analyzing the data with a Boltzmann function, we obtained k_{on} (0 mV) = $4.23 \pm 0.34 \times 10^7$ $M^{-1}s^{-1}$ with valence $z_{on} = 0.23 \pm 0.01$, and k_{off} (0 mV) = 33 ± 1 s^{-1} with valence $z_{off} = 1.60 \pm 0.01$. The calculated ratio $k_{off}/k_{on} = 7.80 \times 10^{-7}$ M is comparable to $^{app}K_d = 8.58 \times 10^{-7}$ M determined from equilibrium measurements. Valence $z_{on} + z_{off} = 1.83$ is significantly smaller than Z = 2.67 obtained at equilibrium. As discussed later, this discrepancy signifies that a two-step (at least) model is required to account for block by intracellular PhTx.

The simplest way to reveal a possible low-affinity blocking state would be to apply much higher PhTx concentrations, which was however cost prohibitive. We therefore increased the apparent affinity of the intracellular toxin by lowering the Na^+ concentration on both sides of the membrane from 130 mM (used in all experiments described above) to 30 mM. As shown in Fig. 2.6, A and B, under low-Na^+ conditions

PhTx indeed produces voltage-dependent block with significantly higher affinity. Lowering Na^+ also reveals the existence of dose-dependent but voltage-independent channel block at highly hyperpolarized voltages (-100 to -150 mV). Thus, intracellular PhTx apparently produces both voltage-dependent and -independent blocked states.

We also analyzed the kinetics of block and unblock in low-Na^+ conditions. The logarithms of k_{on} and k_{off} are plotted against voltage in Fig. 2.6, D and E, respectively. As in the case of high-Na^+ conditions, k_{on} ($8.42 \pm 0.68 \times 10^8$ M^{-1} s^{-1} at 0 mV) exhibits little voltage dependence ($z_{on} = 0.14 \pm 0.01$), whereas k_{off} (27 ± 2 s^{-1} at 0 mV) exhibits considerable dependence ($z_{off} = 1.10 \pm 0.02$).

We noticed (Fig. 2.6 C) that the steady-state voltage-dependent blocking curve was right shifted (with an unaltered plateau at hyperpolarized voltages) when the cGMP concentration was lowered from 2 mM (saturating) to 20 μM where only 14.1 ± 1.9% (n = 8) of maximal current was activated . To further investigate the gating state dependence of channel block, we compared the kinetics of intracellular PhTx interaction with channels activated by either 2 mM or 20 μM cGMP. As already shown, block of current activated by 2 mM cGMP follows a single-exponential time course. In the presence of 20 μM cGMP, the time course of current block initially tracks that in 2 mM cGMP and then becomes slower (Fig. 2.7 A; lower red trace). A slow component is expected because, at low cGMP concentrations, outward current elicited by a depolarizing voltage pulse also develops in two phases: a nearly instantaneous step followed by a slow phase that reflects the modest further enhancement (by voltage) of channel activation that is seen only at non-saturating cGMP concentrations (Fig. 2.7 A; upper traces). It follows then that only the fast phase of voltage step-induced current

block in 20 μM cGMP reflects the actual kinetics of channel block, whereas the slow phase is rate-limited by the voltage-dependent additional channel activation that occurs at subsaturating cGMP concentrations. Since the fast phase in 20 μM cGMP tracks faithfully the time course of current block in 2 mM cGMP, we conclude that the kinetics of current block by intracellular PhTx are not significantly influenced by cGMP concentration. Additionally, the time courses of current recovery at low and high cGMP concentrations are superimposable (Fig. 2.7 B). As for the kinetics of channel gating interaction with extracellular PhTx we found that they are also virtually independent of cGMP concentration (Fig. 2.7 C, D).

2.4.3 CNGA1 channel block by intracellular quaternary ammonium ions

CNGA1 channels are blocked by millimolar concentrations of quaternary ammoniums (QAs) from the intracellular but not extracellular side (Goulding et al., 1993; Stotz and Haynes, 1996; Contreras and Holmgren, 2006). Since QAs are generally too bulky to enter the narrow selectivity filter, the voltage sensitivity of their block of CNGA1 channels must arise indirectly, as in the case of their block of K^+ channels. We thus examined the voltage-dependent behavior of CNGA1 block by a series of QAs to learn how it differs from that by PhTx. Using decane-*bis*-trimethylammonium (bis-QA_{C10}; Fig. 2.8 A) as an example, we will first illustrate the basic properties of QA block.

Fig. 2.8 B shows CNGA1 current records in the absence or presence of three concentrations of bis-QA_{C10}, a molecule of the same length as spermine but with wider head groups. Like PhTx, bis-QA_{C10} blocks the channels in a voltage dependent manner, rendering the I-V curve inwardly rectifying (Fig. 2.8 C). The fraction of current not

blocked by 5 mM bis-QA_{C10} is plotted against voltage in Fig. 2.8 D. This blocking curve is roughly similar to that of PhTx in that it exhibits a voltage-independent blocking component at very negative voltages, followed by a voltage-dependent component. However, unlike that of PhTx, the blocking curve of bis-QA_{C10} does not proceed to completion but reaches a non-zero plateau value at extreme positive voltages, i.e., it deviates markedly from a Boltzmann function.

We tested six additional QA derivatives that block in a voltage-dependent manner (Fig. 2.9), rendering the I-V curve inwardly rectifying (Fig. 2.10). To further illustrate the voltage dependence of channel block, we plotted the fraction of current not blocked against voltage for all seven QAs (Figs. 2.11 and 2.12 A). These QAs differ in size, shape, and chemistry, exhibiting various affinities and somewhat different voltage dependence. Despite their differences, the blocking curves for all eight QAs share these characteristics: they exhibit two voltage-independent blocking phases, one at extreme positive and one at extreme negative voltages, with an intervening voltage-dependent phase. Thus, QA blockers appear to create more than one blocked state.

Again using bis-QA_{C10} as an example, we show that altering the permeant Na^+ concentration affects the voltage-dependent phase of the curve but not the two voltage-independent ones, whereas altering blocker concentration affects all three phases (Fig. 2.12 A).

2.5 Discussion

Two general types of model have been proposed to account for the voltage dependence of ion channel block by charged blockers. One model assumes that the

blocker itself traverses (a portion of) the transmembrane electric field to reach its binding site in the pore (Woodhull, 1973), and the voltage dependence is thus a property intrinsic to blocker binding. Characteristically, this intrinsic voltage dependence model predicts that the fraction of current not blocked (I/I_o) decreases exponentially with membrane voltage over the entire voltage range, as described by a Boltzmann function (Fig. 2.13),

$$\frac{I}{I_0} = \frac{1}{1 + \frac{[B]}{{}^{app}K_d \, e^{-\frac{ZVF}{RT}}}}, \tag{2.1}$$

where ${}^{app}K_d$ is the apparent equilibrium dissociation constant for the blocker-binding reaction in the absence of a membrane potential, [B] is the concentration of blocker, Z is the effective valence (sometimes denoted as zδ), V is the membrane voltage, and F, R, and T have their usual meaning. As shown here, PhTx block of CNGA1 channels can be well accounted for by this type of mechanism, as equilibrium channel block varies with voltage according to a Boltzmann function (Figs. 2.2 D and 2.5 B).

The other model assumes that the blocker itself does not bind within the electric field, and that the voltage dependence reflects phenomena extrinsic to the blocker binding itself, namely, the blocker displacing permeant ions across the field (Armstrong, 1971). This extrinsic voltage dependence model predicts that voltage dependence of blocker binding will vanish upon removal of all permeant ions, a prediction not testable electrophysiologically because removing permeant ions would abolish current. However, the following argument suggests an alternative approach. In this permeant ion-displacement model, where voltage dependence arises from the displaced permeant ions

traversing the transmembrane electric field, the blocker binds at a site outside the field, occupied by a permeant ion before it enters the electric field (Armstrong and Binstock, 1965; Yellen, 1984b; MacKinnon and Miller, 1988; Park and Miller, 1992; Spassova and Lu, 1998; Spassova and Lu, 1999; Guo et al., 2003). As a sufficiently strong depolarization will lower the permeant ion occupancy of that site, the blocker may occupy it without encountering a permeant ion. When blocker binding is no longer linked to the movement of permeant ions, channel block loses its extrinsic voltage dependence. As we show below, the ion-displacement model predicts that, for blocker added intracellularly, the extent of channel block increases as voltage becomes more positive but deviates from a Boltzmann function at extreme depolarization, and tends toward a current plateau (Fig. 2.13) whose amplitude diminishes with increasing blocker concentration. This behavior was seen with seven intracellular QA blockers too bulky to enter the ion selectivity filter (Figs. 2.11 and 2.12 A) (Goulding et al., 1993). We will now quantitatively examine these two types of voltage-dependent block, using PhTx and QAs as examples.

2.5.1 Analysis of PhTx block with the intrinsic voltage-dependence model

PhTx blocks the channel from either side of the membrane in a strongly voltage-dependent manner (Figs. 2.2 and 2.5). As already discussed, the voltage-dependent blocking curve for either intracellular or extracellular PhTx is well described by a Boltzmann function, exhibiting no non-zero plateau phase at extreme voltages in the respective direction that favors their binding. This behavior is expected for a blocker that binds within the electric field from either side of the membrane.

Channel block by extracellular PhTx appears to be a simple one-step bimolecular reaction since voltage jump-induced blocking and unblocking transients follow single-exponential time courses and k_{off}/k_{on} at 0 mV is comparable to $^{app}K_d$ at 0 mV. The only non-intuitive observation is that the entire voltage dependence associated with $^{app}K_d$ is attributable to k_{off}, whereas k_{on} is practically voltage independent. As discussed below, this phenomenon may reflect more complex blocking kinetics.

Many aspects of CNGA1 block by intracellular PhTx are similar to those by extracellular PhTx, with one notable exception. The sum of z_{off} (1.60) and z_{on} (0.23) from kinetic measurements is only about half the Z value (2.67) measured at equilibrium. This discrepancy indicates that the blocking process is not a one-step bimolecular reaction. At least one other transition must exist, which we have not been able to measure directly. For example, there may be a blocked state with such low affinity that it is insignificantly populated at the blocker concentrations we used. Higher PhTx concentrations could reveal a potential low-affinity state, but this is impractical given the high cost of PhTx. An alternative approach is to raise the apparent blocker affinity by lowering the permeant ion concentration to reduce competition and/or knock-off by permeant ions (Armstrong and Binstock, 1965). Having lowered the Na^+ concentration on both sides of the membrane from 130 mM to 30 mM, we found that at negative potentials PhTx indeed blocks current in a dose-dependent but voltage-independent manner (Fig. 2.6 A). Therefore, as seen with QAs, binding of PhTx to the channel evidently produces at least two blocked states: a voltage-dependent state plus a voltage-independent state.

The two blocked states (ChB_1 and ChB_2) could be formed via either sequential or parallel transitions (Fig. 2.14 A or B). For either model the fraction of current not blocked is given by:

$$\frac{I}{I_0} = \frac{[Ch]}{[Ch] + [ChB_1] + [ChB_2]}. \tag{2.2}$$

For the sequential model, the equilibrium constants in the absence of an electric field are defined as $K_1 = [Ch][B]/[ChB_1]$ and $K_2 = [ChB_1]/[ChB_2]$. In the presence of an electric field the fraction of current not blocked is then given by:

$$\frac{I}{I_0} = \frac{1}{1 + [B]\left(\frac{1}{K_1 e^{-\frac{Z_1 VF}{RT}}} + \frac{1}{K_1 K_2 e^{-\frac{(Z_1+Z_2)VF}{RT}}}\right)}, \tag{2.3}$$

where Z_1 and Z_2 are the effective valences associated with K_1 and K_2 respectively. For parallel transitions the fraction of current not blocked is given by:

$$\frac{I}{I_0} = \frac{1}{1 + [B]\left(\frac{1}{K_1 e^{-\frac{Z_1 VF}{RT}}} + \frac{1}{K_2' e^{-\frac{Z_2 VF}{RT}}}\right)}, \tag{2.4}$$

where $K_1 = [Ch][B]/[ChB_1]$, $K_2' = [Ch][B]/[ChB_2]$. Eqs. 2.3 and 2.4 are equivalent, except that K_2 in the sequential model (Eq. 2.3) and K_2' in the parallel model (Eq. 2.4) have different physical meanings. The free energy change for the blocked states, with respect to the unblocked state is $\Delta G_{ChB2} = -RT \times \ln [K_1K_2/(1+K_2)]$ in the sequential

model but $\Delta G_{ChB2} = -RT \times \ln K'_2$ in the parallel model; in both models $\Delta G_{ChB1} = -RT \times \ln K_1$.

We now discuss the sequential model in detail using intracellular PhTx as an example. As previously demonstrated with inward-rectifier K^+ channels (Shin and Lu, 2005; Shin et al., 2005) the sequential model is physically plausible, given that the length of an ion channel pore greatly exceeds that of a blocker. The blocker is likely to transiently contact parts of the pore with some affinity on its way to the energetically most stable site. That is, a realistic blocking scheme likely consists of sequential interactions.

We fitted the blocking curves in Fig. 2.6 B with Eq. 2.3 to obtain equilibrium constants $K_1 = 1.04 \pm 0.03 \times 10^{-5}$ M and $K_2 = 2.03 \pm 0.14 \times 10^{-3}$, and valence $Z_2 = 2.08 \pm 0.04$. Z_1 was set to zero because formation of the first (shallow) blocked state is voltage insensitive (witness the voltage-insensitive but dose-dependent asymptotes at extreme negative voltages). As for the individual constants at 0 mV, analysis of the blocking and unblocking kinetics yields $k_{on} = 8.42 \times 10^8$ M^{-1} s^{-1} with $z_{on} = 0.14$; and $k_{off} = 27$ s^{-1} with $z_{off} = 1.10$ (Fig. 2.6 C, D). Given that the experimental blocking rate k_{on} reflects k_1 in the model (and thus $z_1 = z_{on}$) we could then calculate k_{-1} from $K_1 k_1 = 8.76 \times 10^3$ s^{-1}. This value of k_{-1} is about 300-fold larger than the experimental unblocking rate k_{off}, which must therefore approximate the off rate-limiting k_{-2} (and z_{off} must approximate z_{-2}). Finally, we can obtain k_2 as $k_{-2}/K_2 = 1.33 \times 10^4$ s^{-1} with z_2 as $Z_2 - z_{-2} = 0.98$. The above kinetic analysis in terms of a sequential two-step blocking model shows that most of the voltage sensitivity of channel block by intracellular PhTx resides in the transition

between the two blocked states, with k_2 and k_{-2} exhibiting comparable voltage dependence.

According to Eq. 2.3 derived for the sequential two-step blocking model, the apparent equilibrium constant at 0 mV is given by:

$$^{app}K_d = \frac{1}{\frac{1}{K_1} + \frac{1}{K_1 K_2}} = \frac{k_{-1}k_{-2}}{k_1(k_2 + k_{-2})} \tag{2.5}$$

Because in the present case k_{-2} (27 s^{-1}) << k_2 (1.3 × 10^4 s^{-1}), $^{app}K_d$ reduces to

$$^{app}K_d = \frac{k_{-1}k_{-2}}{k_1 k_2} \tag{2.6}$$

and because the values of k_{-1} and k_2 differ by less than twofold, $^{app}K_d$ is approximately equal to k_{-2}/k_1. Given that we used very low PhTx concentrations, the pseudo-first order "on" rates were sufficiently low to rate-limit the blocking reaction (and be resolvable by our recording system). As for the experimental "off" rate, the rate constant k_{-2} rate-limits the recovery from PhTx block. Thus, our observation that $^{app}K_d \sim k_{off}/k_{on}$ is merely a coincidence and, by no means, indicates that the blocking reaction under investigation is a one-step process. A clear indication that the blocking reaction involves more than one step is the discrepancy between the overall equilibrium valence, Z, and the sum of the valences z_{on} and z_{off} associated with kinetic constants k_{on} and k_{off}. In the framework of the sequential two-step blocking model, the equilibrium valence $Z = z_1 + z_{-1} + z_2 + z_{-2} = 2.08$ is greater than z_{on} (z_1) + z_{off} (z_{-2}) = 1.24 from the kinetic measurements.

For not only intracellular but also extracellular PhTx block, k_{off} is voltage dependent and k_{on} independent. In the framework of the one-step blocking model, almost all voltage dependence for equilibrium block would be attributed exclusively to that associated with observed k_{off}. However, in the sequential two-step model, blocker binding to, and unbinding from, the first (shallow) site are voltage insensitive, but its transitions to and from the deeper site are sensitive in a manner that the voltage dependence is almost evenly distributed between the forward and backward reactions. It is thus possible that extracellular PhTx, like intracellular PhTx, also interacts with the channel in more than one step.

2.5.2 Implications of a sequential blocking mechanism for probing the channel gate through examining blocking kinetics

We now comment on how the existence of multiple, sequentially-connected blocked states may prevent distinguishing the channel gate behavior from the dependence of the blocking kinetics on the channel open probability. The apparent rate of channel inhibition caused by the binding of an open-channel blocker on the opposite side of the channel gate (or by chemical modification of a cysteine residue) is expected to vary with the gating state. Such a variation has been exploited to delineate the channel gate, an approach that was successfully used in voltage-gated K^+ channels (Liu et al., 1997). To our surprise, the apparent rate of PhTx block from both extracellular and intracellular sides exhibits little dependence on the channel open probability, even though the block is strongly voltage dependent in either case. As discussed below, this unexpected finding may help us better understand certain necessary conditions under which one may infer

properties about the channel gate from the dependence of blocking kinetics on channel gating.

Kinetics of channel block or unblock are essentially unaltered by lowering the cGMP concentration from the saturating 2 mM to 20 μM. This is true regardless of whether PhTx was present in the extracellular or the intracellular solution. There are two possible explanations for these unexpected results. First, the gate is located in a region that PhTx cannot access from either side of the membrane, such as the selectivity filter (Sun et al., 1996; Bucossi et al., 1997; Becchetti et al., 1999; Liu and Siegelbaum, 2000; Becchetti and Roncaglia, 2000; Flynn and Zagotta, 2001; Contreras et al., 2008). This would mean that the long spermine portion of the PhTx molecule cannot reach deep into the filter, even though spermine can readily permeate the channel from both directions. Additionally, if this were the case, the strong voltage dependence of channel block must then arise from the movement of permeant ions displaced by PhTx across the selectivity filter. This predicts that the blocking curve would not follow a Boltzmann function, and would exhibit a plateau at highly depolarized or hyperpolarized potentials, depending on which side of the membrane PhTx was applied. However, we found that the blocking curve can be well described by a Boltzmann function.

Alternatively, invariability of the apparent channel-blocking rate with cGMP concentration may reflect the fact that the rate-liming transition in the PhTx-blocking sequence is not affected by channel gating. As the first step in the blocking sequence, PhTx associates with the channel, docking at a site which may, in principle, be as shallow as the innermost part of the pore. It then travels deeper along the pore, resulting in a second blocked state. If a gate were located between the shallow and the deep sites,

formation of only the deep, not the shallow, blocked state would depend on the open probability of the gate. The second-order rate constant for PhTx associating with the channel to form the first blocked state (k_{on}) in symmetric 30 mM Na^+ is 8.42×10^8 M^{-1} s^{-1} (or 4.23×10^7 M^{-1} s^{-1} in 130 mM), a rate that is arguably near diffusion limited. However, the pseudo-first-order blocking rate (k_1[PhTx]) is what we actually measured. Experimentally, we used sufficiently low PhTx concentrations to achieve resolvable blocking rates. Because these rates are much slower than the transit rate of PhTx from the shallow to the deep site (k_2), we cannot observe any variation of the apparent blocking rate with channel gating, even though k_2 is inherently gating dependent. While k_2 might be sensitive to the gating state, the reverse rate constant k_{-2} is not, because the rate of current recovery from PhTx block, which reflects k_{-2} (see above), is insensitive to cGMP concentration. If only k_2 is gating sensitive, this sensitivity will be reflected in K_2. Indeed, lowering cGMP from 2 mM to 20 μM decreases the macroscopic current (and thus P_o) by 8.6 ± 1.2 fold (n = 8), which is accompanied by a 7.5-fold increased K_2 (Fig. 2.6 C). Therefore, the lack of cGMP dependence of the apparent PhTx-blocking rate may simply be a property of the sequential mechanism of channel block. In any case, probing the gate through examining the kinetics of channel block by a blocker (or a cysteine modifying reagent) is conceptually straightforward for a single-step blocking reaction. However, for a blocking reaction with multiple steps arranged sequentially, this kinetic approach is only possible if the apparent rate is limited by the gating-dependent transition in the actual experiments. Otherwise, it may lead to a false negative result as exemplified above. We wish to emphasize that a mere demonstration that the second-order association rate constant (k_{on}) is diffusion limited does not ensure that the actual

association step is not rate limiting under specific experimental conditions, because it depends on the actual value of the apparent (pseudo-first-order) association rate (k_{on}[B]).

2.5.3 Analysis of quaternary ammonium block with the ion-displacement model

We now discuss extrinsic voltage dependence of channel block by QAs in the framework of an ion-displacement model. The most parsimonious form of this type of model with the features described in Results (section 2.4.3) and illustrated in Figs. 2.8 - 2.12 has three states: one blocked plus two non-blocked states (Fig. 2.14 C). In this model, the narrow external part of the channel (Ch) can only be occupied by permeant ions, whereas the wide internal part can accommodate either a permeant (Na^+) ion or a blocking (B) ion. The transmembrane electric field exists exclusively across the narrow part of the pore. Na^+ binding to the internal shared site from both sides of the membrane is consolidated in the left transition of the model. Extracellular Na^+ traverses the narrow part of the pore to reach the internal site, a process that is voltage sensitive. The upper blocking transition is voltage independent as the blocker site (outside the field) is unoccupied in the Ch state. The left and upper transitions together describe the competition of Na^+ and blocker for the internal site. In the limit that Na^+ and blocker move in a concerted manner, the competition becomes displacement as described by the lower transition. This latter transition is voltage sensitive as the blocker site is already occupied by a permeant Na^+ ion which must then enter the field. For presentation, we have referred to this model as an ion-displacement model, it however contains both ion-displacement and ion-competition reactions, indistinguishable at equilibrium. The equilibrium constants associated with any two transitions can be used to express the

equilibrium solution of the model (Spassova and Lu, 1998; Spassova and Lu, 1999; Lu, 2004). We will use the constants for the two blocking transitions to illustrate a novel feature of the model, namely, channel block loses voltage dependence at extreme positive potentials.

For this three-state model the fraction of current not blocked is given by:

$$\frac{I}{I_0} = \frac{1}{1 + \frac{[B]}{{}^{app}K_d}}. \tag{2.7}$$

The apparent equilibrium blocker dissociation constant is

$${}^{app}K_d = K_B + K_{B-Na} e^{-\frac{ZVF}{RT}} [Na^+], \tag{2.7.1}$$

where the equilibrium constants for the blocker-binding transitions without and with concomitant Na^+ displacement are $K_B = [Ch][B]/[ChB]$ and $K_{B\text{-}Na} = [ChNa][B]/([ChB][Na^+])$, respectively. Eq. 2.7 parses how the two blocking transitions contribute to the overall blocking process, for the simplest case where the concentrations of Na^+ ions on both sides of the membrane are equal.

At sufficiently hyperpolarized voltages where $K_{B-Na} e^{-\frac{ZVF}{RT}} >> K_B$, Eq. 2.7 reduces to:

$$\frac{I}{I_0} = \frac{1}{1 + \frac{[B]}{K_{B-Na} e^{-\frac{ZVF}{RT}} [Na^+]}}, \tag{2.8}$$

an equation dominated by the voltage-dependent blocking transition that involves Na^+ displacement. Conversely, at highly depolarized potentials, $K_{B-Na}e^{-\frac{ZVF}{RT}}$ approaches zero and Eq. 2.7 reduces to

$$\frac{I}{I_0} = \frac{1}{1+\frac{[B]}{K_B}}, \tag{2.9}$$

which describes voltage-insensitive block unaffected by Na^+ displacement. Eq. 2.9 accounts for the voltage-independent plateau at depolarized potentials whose amplitude varies with the blocker concentration. Indeed, the voltage-dependent blocking curve for all the intracellular QAs tested becomes voltage independent at strongly depolarized potentials. Using bis-QA_{C10} as an example, we show below that this ion-displacement model accounts well for channel block by QAs that are too bulky to enter the selectivity filter.

As shown in Fig. 2.8 D for bis-QA_{C10}, the blocking curve clearly deviates from a Boltzmann function (dotted line) at depolarized potentials but is well fitted by the ion displacement model (solid line). As already discussed for PhTx, the voltage-insensitive block at extreme negative potentials must be accounted for by an additional blocked state. A detailed treatment of this additional blocked state will be presented in the next section. To concentrate on discussing the properties of the three-state ion-displacement model, we simply scaled the fraction of current not blocked at hyperpolarized potentials (Fig. 2.12 A) to unity (Fig. 2.12 B). Eq. 2.7 derived from the three-state model makes the following experimental prediction: increasing the blocker concentration would not only shift the

blocking curve to the left but also decrease the plateau at positive potentials. This is consistent with our experimental observations (Fig. 2.12 B; compare black to red symbols). Mathematically, at a higher blocker concentration 50% block will occur at a lower voltage (Eq. 2.7) and, consequently, the blocking curve shifts leftward. Thermodynamically, the total energy for producing a given extent of block remains the same, and thus the relative energy contribution from the electric and the chemical sources is inversely related. At highly depolarized potentials, Eq. 2.7 is reduced to Eq. 2.9, showing that the extent of channel block in this voltage range is independent of voltage and is solely determined by the blocker concentration. Therefore, the plateau of the blocking curve at very depolarized potentials decreases with increasing blocker concentration. These predictions make intuitive sense in that strong depolarization reduces the permeant ion occupancy at the shared site, so the blocker will be able to occupy the site without the need to displace permeant Na^+. At the limit, the binding reaction becomes a standard bi-molecular chemical reaction, and the extent of block is thus expected to increase with the blocker concentration.

Another prediction is that decreasing the permeant ion concentration would shift the blocking curve leftward without affecting the plateau level at positive potentials, as in fact we observed when we lowered the Na^+ concentration from 130 mM to 65 mM (Fig. 2.12 B; compare filled to open symbols). From Eq. 2.7, it is evident that for a given blocker concentration, lower voltage is needed to produce 50% block at a lower Na^+ concentration because lesser electric energy is needed to generate the same probability of vacancy for the blocker. Eq. 2.9, on the other hand, indicates that the extent of channel

block at extreme positive potentials is independent of Na^+ concentration, because at sufficiently strong depolarization Na^+ occupancy will vanish.

2.5.4 Ion displacement model with sequential blocked states for QA block

When we analyzed (in the above section) intracellular QA block in the framework of the ion-displacement model, we deferred the discussion of voltage-independent block at extreme negative potentials. To account for it, we now extend the ion-displacement model to include a sequential blocking scheme, as formulated above with PhTx, into the ion-displacement model (Fig. 2.14 D). Inserting an extra blocked state in each of the two blocking transitions brings the total number of states in the model to five. The additional blocked states ChB_1 and $ChNaB_1$ represent a blocker bound at a shallow site with and without a Na^+ at the deep site, respectively. For simplicity, we assume the equilibrium between either shallow blocked state and the unblocked state is characterized by the same equilibrium dissociation constant K_{B1}. $K_{B2\text{-}Na}$ and K_{B2} are the equilibrium constants for the two subsequent transitions to form the deeper blocked state (ChB_2) with and without Na^+ displacement, respectively. For this five-state model, the fraction of current not blocked is given by:

$$\frac{I}{I_0} = \frac{1}{1 + \frac{[B]}{{}^{app}K_d}}, \tag{2.10}$$

where

$$ {}^{app}K_d = K_{B1}\left(1 + \frac{1}{K_{B2} + K_{B2-Na}e^{-\frac{ZVF}{RT}}[Na^+]}\right)^{-1}. \qquad (2.10.1) $$

The equilibrium constant for blocker binding to the shallow site is

$$ K_{B1} = \frac{[Ch][B]}{[ChB_1]} = \frac{[ChNa][B]}{[ChNaB_1]}, \qquad (2.11) $$

whereas that for blocker movement between the two sites is given by

$$ K_{B2} = \frac{[ChB_1]}{[ChB_2]}, \qquad (2.12) $$

describing blocker partition to the empty deep site;

$$ K_{B2-Na} = \frac{[ChNaB_1]}{[ChB_2][Na^+]}, \qquad (2.13) $$

describes blocker binding to the deep site displacing Na^+. The latter is the only step that is assumed to be voltage dependent; this is accounted for by the exponential term in Eq. 2.10.

At sufficiently hyperpolarized voltages where the ratio

$$ \frac{1}{K_{B2} + K_{B2-Na}e^{-\frac{ZVF}{RT}}[Na^+]} $$

approaches zero, Eq. 2.10 reduces to a simple voltage independent blocking mechanism:

$$\frac{I}{I_0} = \frac{1}{1 + \frac{[B]}{K_{B1}}}. \tag{2.14}$$

This latter equation accounts for voltage independent block at hyperpolarized potentials. At these potentials, block involves primarily the two left transitions, and the fraction of current not blocked is a function of the blocker concentration.

At extreme positive voltages, the term

$$K_{B2-Na} e^{-\frac{ZVF}{RT}} [Na^+]$$

approaches zero and Eq. 2.10 reduces to

$$\frac{I}{I_0} = \frac{1}{1 + [B]\left(\frac{1}{K_{B1}} + \frac{1}{K_{B2}}\right)}, \tag{2.15}$$

where, again, block becomes voltage independent. At depolarized potentials, block involves primarily the two upper transitions, and Eq. 2.15 thus contains both K_{B1} and K_{B2}. The curves superimposed on the blocking curves of all seven QAs (Figs. 2.8 C, 2.11 and 2.12 A) are fits with Eq. 2.10 (all fitted parameters are listed in Table 2.1). Thus, the five-state model fully accounts for QA block.

In conclusion, given that blockers are generally much shorter than ion channel pores, they are likely to block the pore in sequential steps. Blocker association with the

shallow site may be the rate-limiting step of current block, regardless of equilibrium occupancy of blocker at this site. Penetration of blocker into the pore produces voltage sensitivity in two ways with experimentally distinguishable characteristics. First, the charged blocker itself enters the transmembrane electric field (with and without displacing permeant ions), and the observed voltage dependence is an intrinsic property of the blocker. Such voltage dependence arising from a direct interaction of the charged blocker with the electric field follows a Boltzmann function. Second, the blocker does not bind within the electric field, and its binding indirectly derives voltage dependence solely through displacing permeant ions across the electric field. This extrinsic voltage dependence does not follow a Boltzmann function as it gradually vanishes with raising voltage.

Figure 2.1. cGMP-dependent activation of CNGA1 channels. (A) Macroscopic current traces recorded in symmetric 130 mM Na^+ from an inside-out patch containing CNGA1 channels in the presence of the indicated concentrations of intracellular cGMP. Currents were elicited by stepping from the 0 mV holding potential to voltages between -200 and 200 mV in 50-mV increments. Currents in the absence of cGMP were used as templates for subsequent off-line background-current corrections. Dotted lines indicate zero current levels. (B) Fraction of maximal current (I/I_{max}; mean ± SEM; n = 3-7) plotted against cGMP concentration for -100 mV (squares) and 100 mV (circles). Solid curves are Hill equation fits yielding EC_{50} = 79 ± 1 μM and h = 1.37 ± 0.03 at -100 mV, and EC_{50} = 64 ± 2 μM and h = 1.39 ± 0.05 at 100 mV.

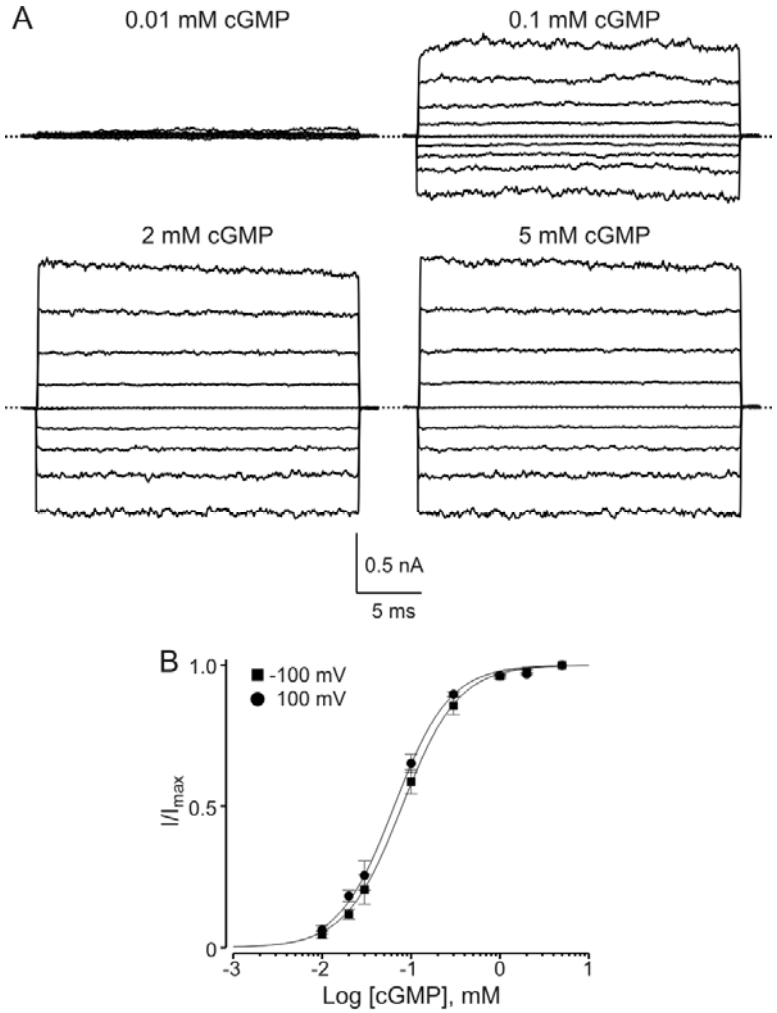
A
0.01 mM cGMP
0.1 mM cGMP
2 mM cGMP
5 mM cGMP
0.5 nA
5 ms
B
-100 mV
100 mV
I/I_max
1.0
0.5
0
-3
-2
-1
0
1
Log [cGMP], mM

Figure 2.1

Figure 2.2. Voltage-dependent CNGA1 block by extracellular PhTx. (A) Structures of philanthotoxin (PhTx) and spermine (SPM). (B) Macroscopic current traces recorded from inside-out patches containing CNGA1 channels in the presence of the indicated concentrations of extracellular PhTx (in the pipette solution). Currents were activated with 2 mM intracellular cGMP and elicited with the protocol shown. Dotted lines indicate zero current levels. (C) Mean I-V curves (mean ± SEM; n = 3-11) determined at the end of the test pulses in the absence or presence of three concentrations of extracellular PhTx. (D) Fraction of current not blocked (mean ± SEM; n = 4-6) by extracellular PhTx, plotted against membrane voltage. Curves are fits of a Boltzmann function (Eq. 2.1) to the three data sets simultaneously with parameters: $^{app}K_d$ (0 mV) = $2.71 \pm 0.20 \times 10^{-5}$ M and $Z = 1.76 \pm 0.02$.

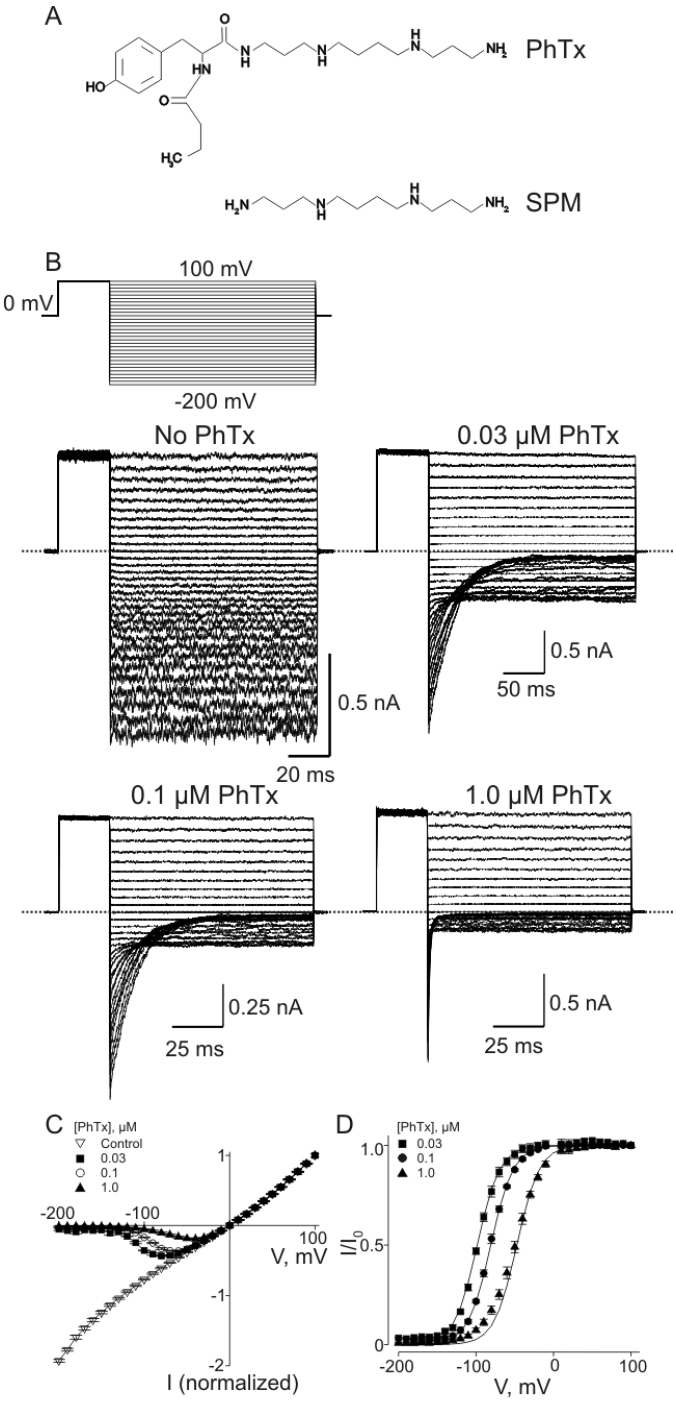
A
PhTx
SPM
B
100 mV
0 mV
-200 mV
No PhTx
0.03 µM PhTx
0.5 nA
50 ms
0.5 nA
20 ms
0.1 µM PhTx
1.0 µM PhTx
0.25 nA
25 ms
0.5 nA
25 ms
C
[PhTx], µM
Control
0.03
0.1
1.0
V, mV
I (normalized)
D
[PhTx], µM
0.03
0.1
1.0
I/I0
V, mV

Figure 2.2

Figure 2.3. Kinetics of hyperpolarization induced CNGA1 block by extracellular PhTx. (A) Current transient elicited by stepping membrane voltage from 100 to -150 mV in the presence of 0.1 μM extracellular PhTx. The superimposed curve is a single-exponential fit. (B) Circles are reciprocal of the time constant (mean ± SEM; n = 4-6) for channel block ($1/\tau_{on}$), obtained from fits as shown in panel A, plotted against the extracellular concentration of PhTx, for eight voltages. The (unresolved) lines through the data are linear fits whose slope for each voltage gives the apparent second-order rate constant (k_{on}) for blocker binding at that voltage. (C) Natural logarithm of k_{on} from panel B, plotted against membrane voltage. The fitted line is a Boltzmann function with parameters k_{on} (0 mV) = $1.04 \pm 0.06 \times 10^9$ $M^{-1}s^{-1}$ (open circle) and $z_{on} = 0.01 \pm 0.01$.

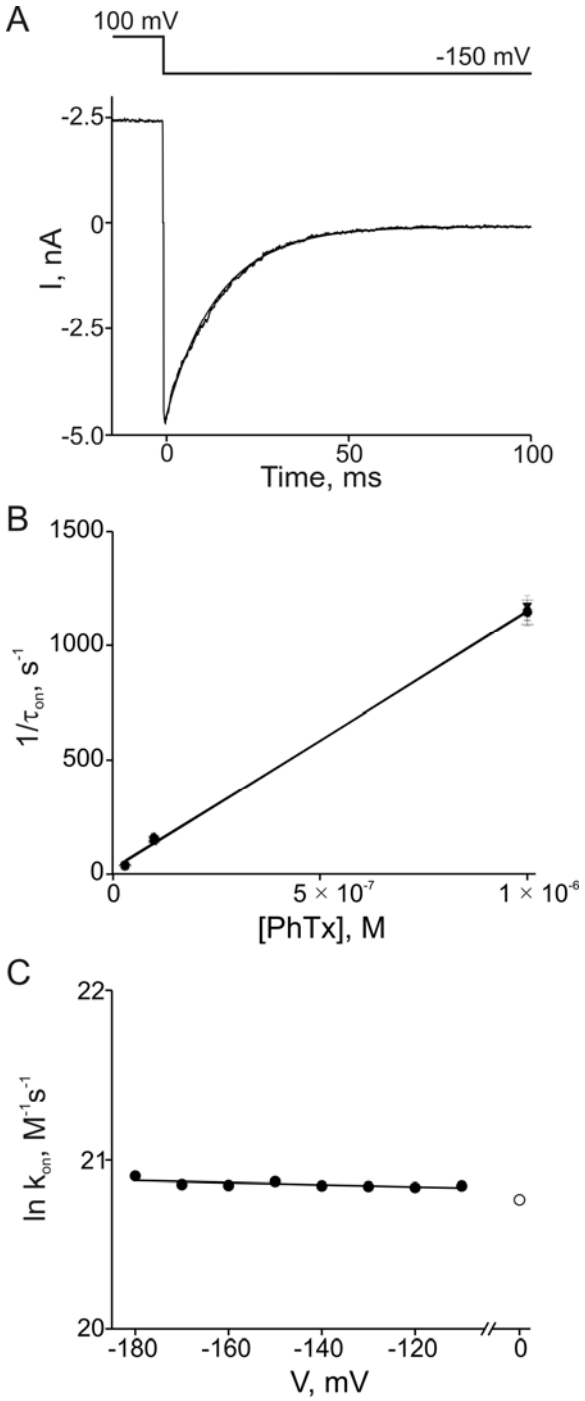
A
100 mV
-150 mV
-2.5
0
-2.5
-5.0
I, nA
0
50
100
Time, ms
B
1500
1000
500
0
1/τon, s-1
0
5 × 10-7
1 × 10-6
[PhTx], M
C
22
21
20
ln kon, M-1s-1
-180
-160
-140
-120
0
V, mV

Figure 2.3

Figure 2.4. Kinetics of depolarization induced recovery from CNGA1 block by extracellular PhTx. (A) Current transient elicited by stepping the membrane voltage from -200 to -50 mV in the presence of 0.1 μM extracellular PhTx. The superimposed curve is a single-exponential fit. (B) Logarithm of the reciprocal of the time constant (mean ± SEM; n = 4-6) for channel unblock ($1/\tau_{off}$, an estimate of the apparent off rate constant k_{off}) at four voltages, obtained from fits as shown in panel A, plotted against the concentration of extracellular PhTx. Lines through the data represent averages over the three concentrations tested at each voltage. (C) Logarithm of $\underline{k}_{off}$ from panel B, is plotted against membrane voltage. The fitted line is a Boltzmann function with parameters k_{off} (0 mV) = $9.65 \pm 0.35 \times 10^3$ s^{-1} and $z_{off} = 1.31 \pm 0.02$.

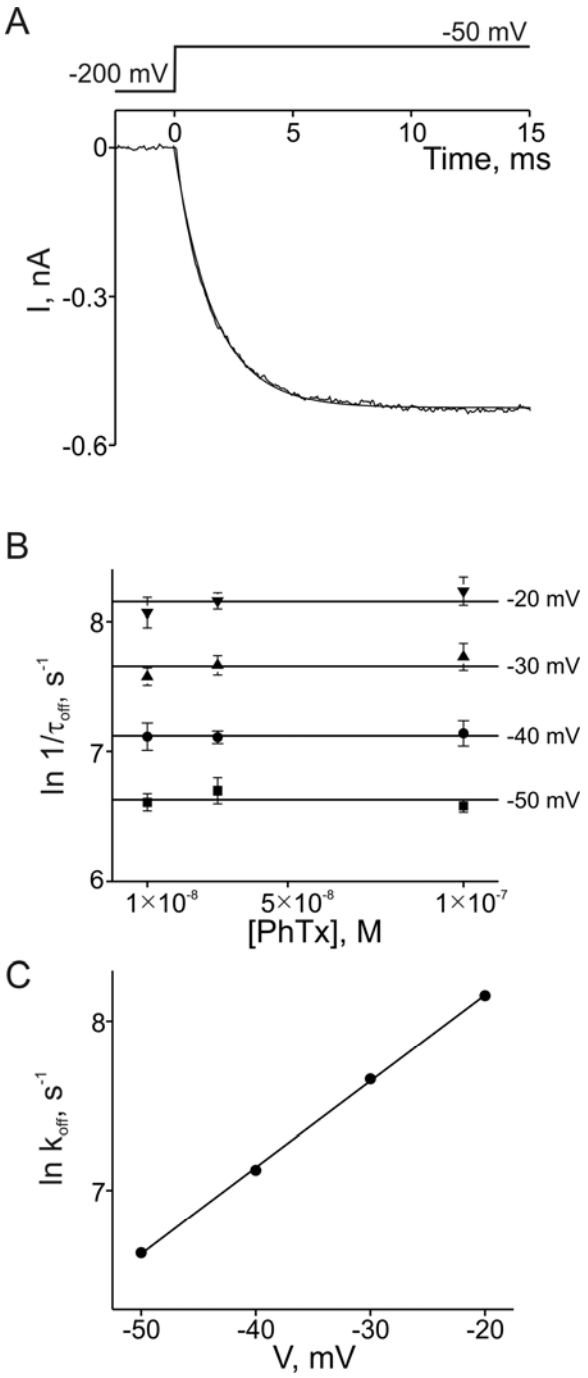
A
-50 mV
-200 mV
0
5
10
15
Time, ms
0
-0.3
-0.6
I, nA
B
-20 mV
-30 mV
-40 mV
-50 mV
8
7
6
ln 1/τoff, s-1
1×10-8
5×10-8
1×10-7
[PhTx], M
C
8
7
ln koff, s-1
-50
-40
-30
-20
V, mV

Figure 2.4

Figure 2.5. Voltage dependent block by intracellular PhTx. (A) Macroscopic current traces recorded from an inside-out patch containing CNGA1 channels in the absence or presence of 0.3 μM intracellular PhTx. Currents were activated with 2 mM intracellular cGMP and elicited with the protocol shown. Dotted line indicates zero current level. (B) Fraction of current not blocked (mean ± SEM; n = 5-10) by intracellular PhTx, plotted against membrane voltage. Curves are fits of a Boltzmann function to the four data sets simultaneously with parameters: $^{app}K_d$ (0 mV) = 8.58 ± 0.38 × 10^{-7} M and Z = 2.67 ± 0.04. (C) Kinetics of depolarization induced CNGA1 block by intracellular PhTx. Logarithm of k_{on}, determined as in Fig. 2.3 using three concentrations of intracellular PhTx (0.3, 1, and 10 μM; n = 8), plotted against membrane voltage. The fitted line is a Boltzmann function with parameters k_{on} (0 mV) = 4.23 ± 0.34 × 10^7 $M^{-1}s^{-1}$ and z_{on} = 0.23 ± 0.01. (D) Kinetics of hyperpolarization induced recovery from CNGA1 block by intracellular PhTx. Logarithm of k_{off}, determined as in Fig. 2.4 with three concentrations of intracellular PhTx (0.1, 0.3, and 1 μM; n = 5), plotted against membrane voltage. The fitted line is a Boltzmann function with parameters k_{off} (0 mV) = 33 ± 1 s^{-1} and z_{off} = 1.60 ± 0.01.

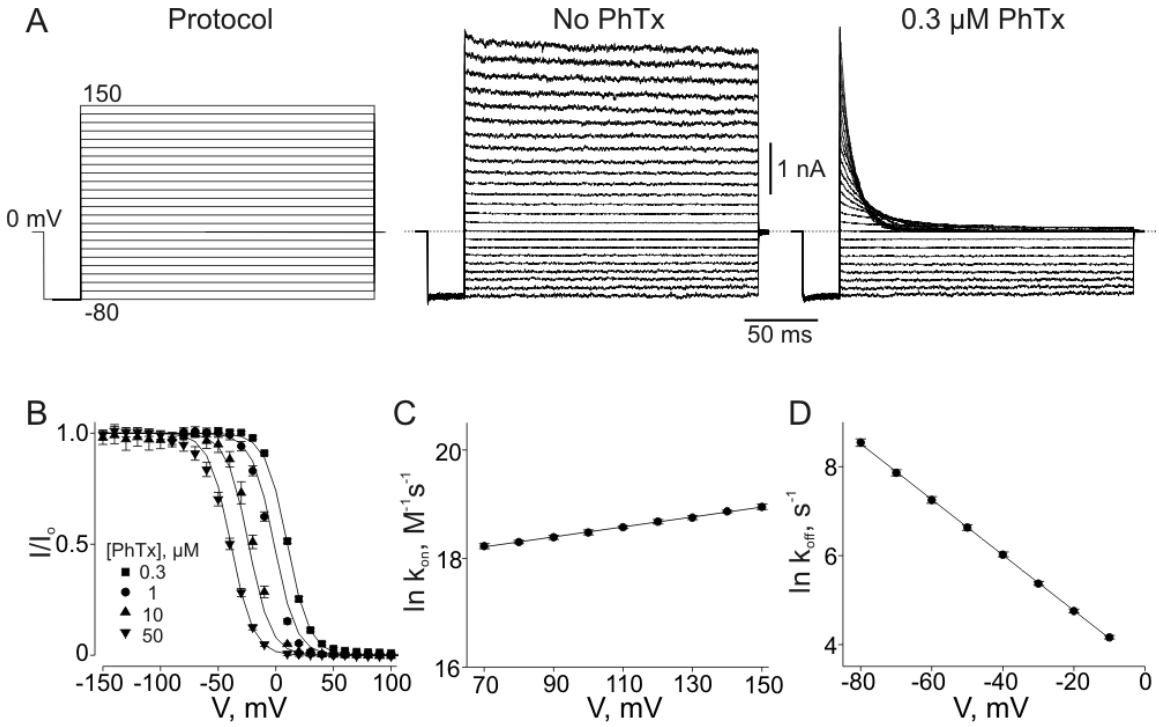
A
Protocol
No PhTx
0.3 μM PhTx
150
0 mV
-80
1 nA
50 ms
B
1.0
0.5
0
I/I$_o$
[PhTx], μM
0.3
1
10
50
-150 -100 -50 0 50 100
V, mV
C
20
18
16
ln k$_{on}$, M^{-1}s^{-1}
70 90 110 130 150
V, mV
D
8
6
4
ln k$_{off}$, s^{-1}
-80 -60 -40 -20 0
V, mV

Figure 2.5

Figure 2.6. Voltage dependence of intracellular PhTx block in symmetrical 30 mM Na^+. (A) Macroscopic current traces recorded in an inside-out patch containing CNGA1 channels in the absence or presence of 5 μM intracellular PhTx in symmetrical 30 mM Na^+. Currents were activated with 2 mM intracellular cGMP and elicited with the protocol shown. Dotted line indicates zero current level. (B) Fraction of current not blocked (mean ± SEM; n = 4-8) by the indicated concentrations of intracellular PhTx, plotted against membrane voltage. Curves are fits of Eq. 2.3 to the three data sets simultaneously with Z_1 fixed to zero. The best-fit parameters were: $K_1 = 1.04 \pm 0.03 \times 10^{-5}$ M, $K_2 = 2.03 \pm 0.14 \times 10^{-3}$ and $Z_2 = 2.08 \pm 0.04$. (B) Fraction of current not blocked (mean ± SEM; n = 8) by 1 μM intracellular PhTx in the presence of 0.02 mM (closed circles) or 2 mM (open circles; replotted from Fig. 2.6 B) cGMP, plotted against membrane voltage. Curves are fits of Eq. 2.3 to both data sets simultaneously, with Z_1 set to zero and K_1 common to both cGMP curves. The best-fit parameters were: $K_1 = 7.65 \pm 0.22 \times 10^{-6}$ M for both cGMP concentrations; $K_2 = 1.29 \pm 0.08 \times 10^{-2}$ and $Z_2 = 1.92 \pm 0.05$ for 0.02 mM cGMP; and $K_2 = 1.72 \pm 0.18 \times 10^{-3}$ and $Z_2 = 2.29 \pm 0.06$ for 2 mM cGMP. (D) Kinetics of depolarization induced CNGA1 block by intracellular PhTx in 30 mM Na^+. Logarithm of k_{on}, determined as in Fig. 2.3, at four concentrations (0.03, 0.1, 0.3 and 1 μM; n = 6) of intracellular PhTx, is plotted against membrane voltage. The fitted line is a Boltzmann function with k_{on} (0 mV) $= 8.42 \pm 0.68 \times 10^8$ $M^{-1}s^{-1}$ and $z_{on} = 0.14 \pm 0.01$. (E) Kinetics of hyperpolarization induced recovery from CNGA1 block by intracellular PhTx in 30 mM Na^+. Logarithm of k_{off}, determined as in Fig. 2.4, at four concentrations (0.1, 0.3, 0.6 and 1 μM; n = 6) of intracellular PhTx, plotted against membrane voltage. The fitted line is a Boltzmann function with k_{off} (0 mV) $= 27 \pm 2$ s^{-1} and $z_{off} = 1.10 \pm 0.02$.

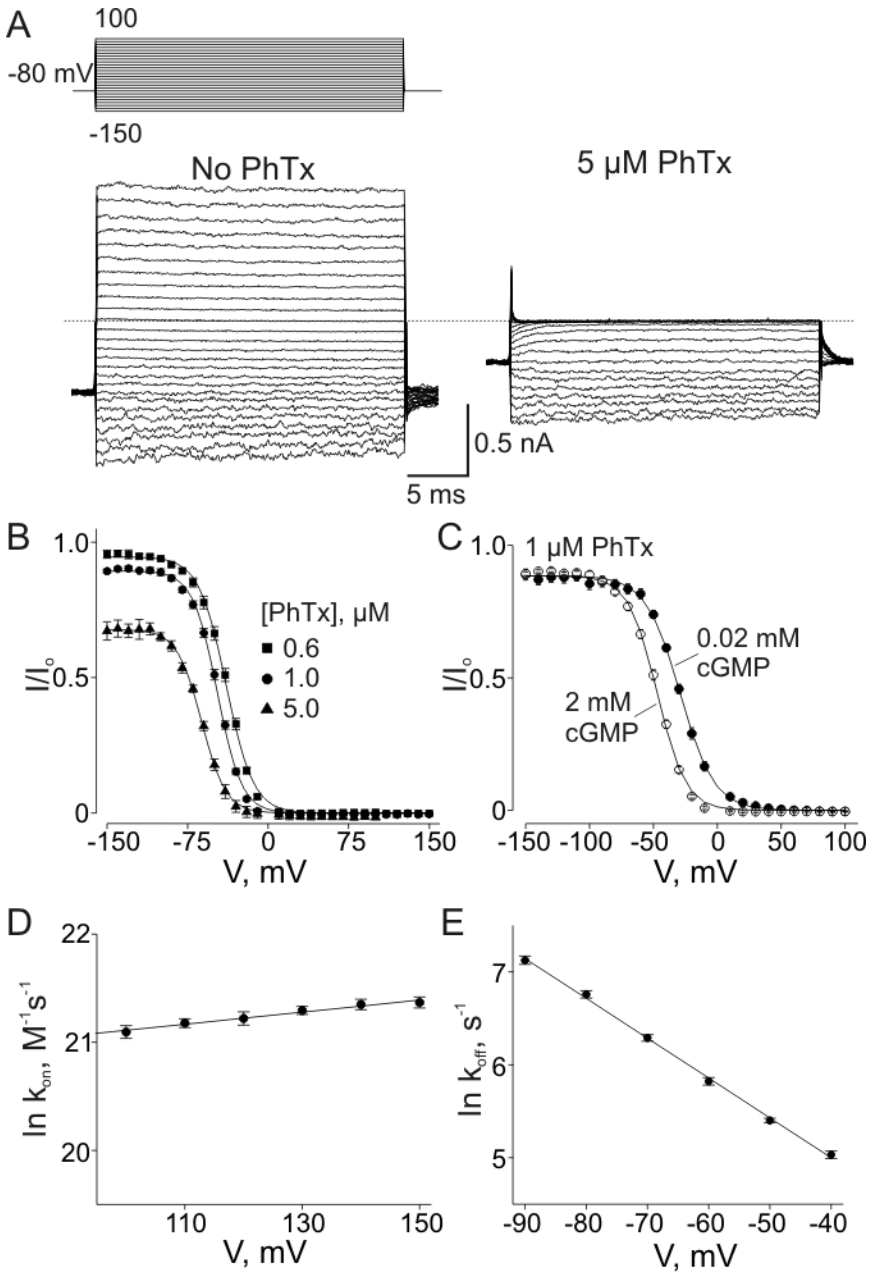
A
100
-80 mV
-150
No PhTx
5 μM PhTx
0.5 nA
5 ms
B
1.0
0.5
0
I/I$_o$
[PhTx], μM
0.6
1.0
5.0
-150 -75 0 75 150
V, mV
C
1.0
0.5
0
I/I$_o$
1 μM PhTx
0.02 mM cGMP
2 mM cGMP
-150 -100 -50 0 50 100
V, mV
D
22
21
20
ln k$_{on}$, M^{-1}s^{-1}
110 130 150
V, mV
E
7
6
5
ln k$_{off}$, s^{-1}
-90 -80 -70 -60 -50 -40
V, mV

Figure 2.6

Figure 2.7. Voltage dependence of intracellular and extracellular PhTx block at saturating and subsaturating cGMP concentrations. (A) Normalized current transients elicited by stepping membrane voltage from -80 to +120 mV in the absence (top) or presence (bottom) of 0.3 μM intracellular PhTx; and of 2 mM (black) or 20 μM cGMP (red; average of 20 consecutive traces from the same patch). The current in 20 μM cGMP is 7 fold smaller than that in 2 mM. (B) Normalized current transients elicited by stepping membrane voltage from +120 to -80 mV in the presence of 0.3 μM intracellular PhTx and of 2 mM (black; average of 5 traces) or 20 μM cGMP (red; average of 10 traces). (C) Normalized current transients elicited by stepping membrane voltage from +100 to -150 mV in the presence of 0.1 μM extracellular PhTx and of 2 mM (black) or 20 μM cGMP (red). (D) Normalized current transients elicited by stepping membrane voltage from -200 to -50 mV in the presence of 0.1 μM intracellular PhTx and of 2 mM (black) or 20 μM cGMP (red).

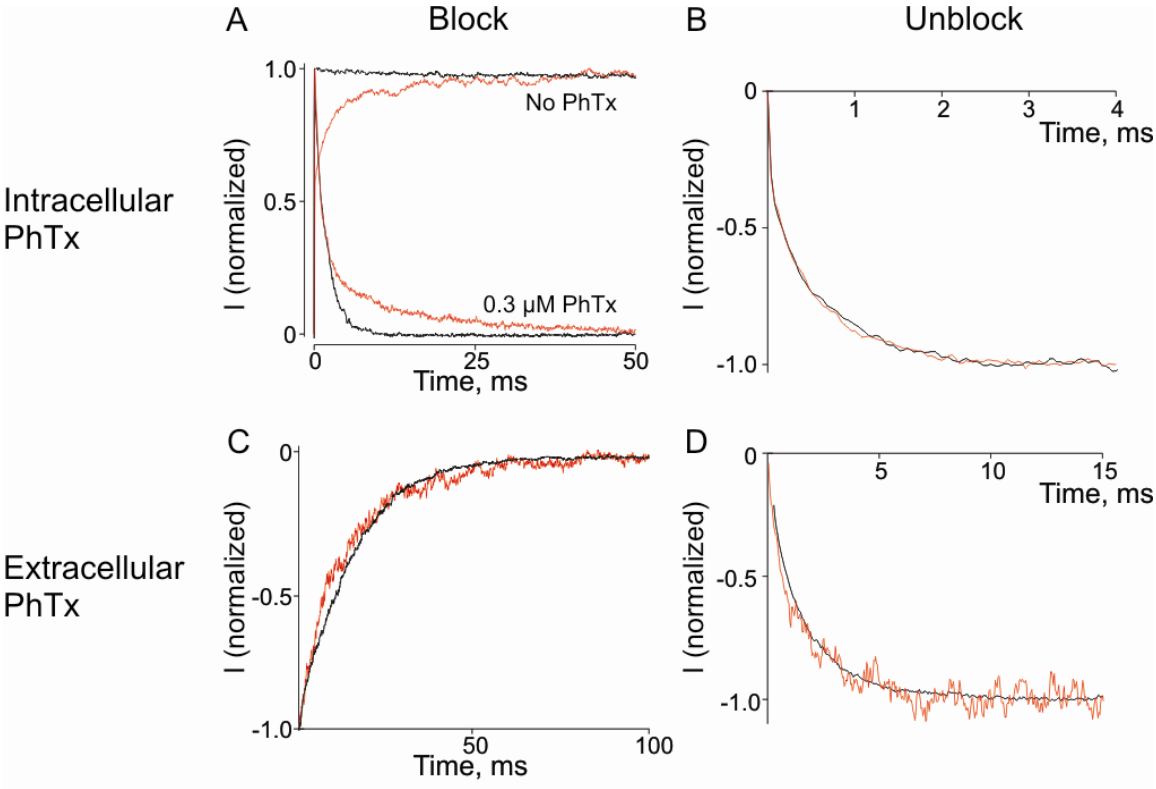
A
Block
B
Unblock
Intracellular PhTx
Extracellular PhTx
No PhTx
0.3 μM PhTx
I (normalized)
Time, ms
C
D

Figure 2.7

Figure 2.8. Voltage-dependent block by intracellular bis-QA_{C10}. (A) Chemical structure of bis-QA_{C10}. (B) Macroscopic current traces recorded from an inside-out patch containing CNGA1 channels in the absence or presence of the indicated concentrations of intracellular bis-QA_{C10}. Currents were elicited by stepping the voltage from the 0 mV holding potential to -150 mV and then to test voltages between -150 and +150 mV in 10 mV increments before returning to the holding potential. Dotted lines indicate zero current levels. (C) I-V curves (mean ± SEM; n = 5) determined at the end of the test pulses in the absence or presence of 5 mM bis-QA_{C10}. (D) Fraction of current not blocked (mean ± SEM; n = 5) by 5 mM bis-QA_{C10}, plotted against membrane voltage. The solid curve is a fit of Eq. 2.10 to the data from -150 to 90 mV (arrow) with K_{B1} = $3.17 \pm 0.05 \times 10^{-2}$ M, $K_{B2} = 2.23 \pm 0.14 \times 10^{-2}$, $K_{B2\text{-}Na} = 2.67 \pm 0.09$ M^{-1} and $Z = 1.11 \pm 0.02$. Dotted curve is a fit to the data from -150 to 90 mV (arrow) of a Boltzmann function (similar to Eq. 2.1 except for a non-unity asymptote at hyperpolarized potentials) with parameters $^{app}K_d = 1.23 \pm 0.08 \times 10^{-2}$ M and $Z = 0.83 \pm 0.03$.

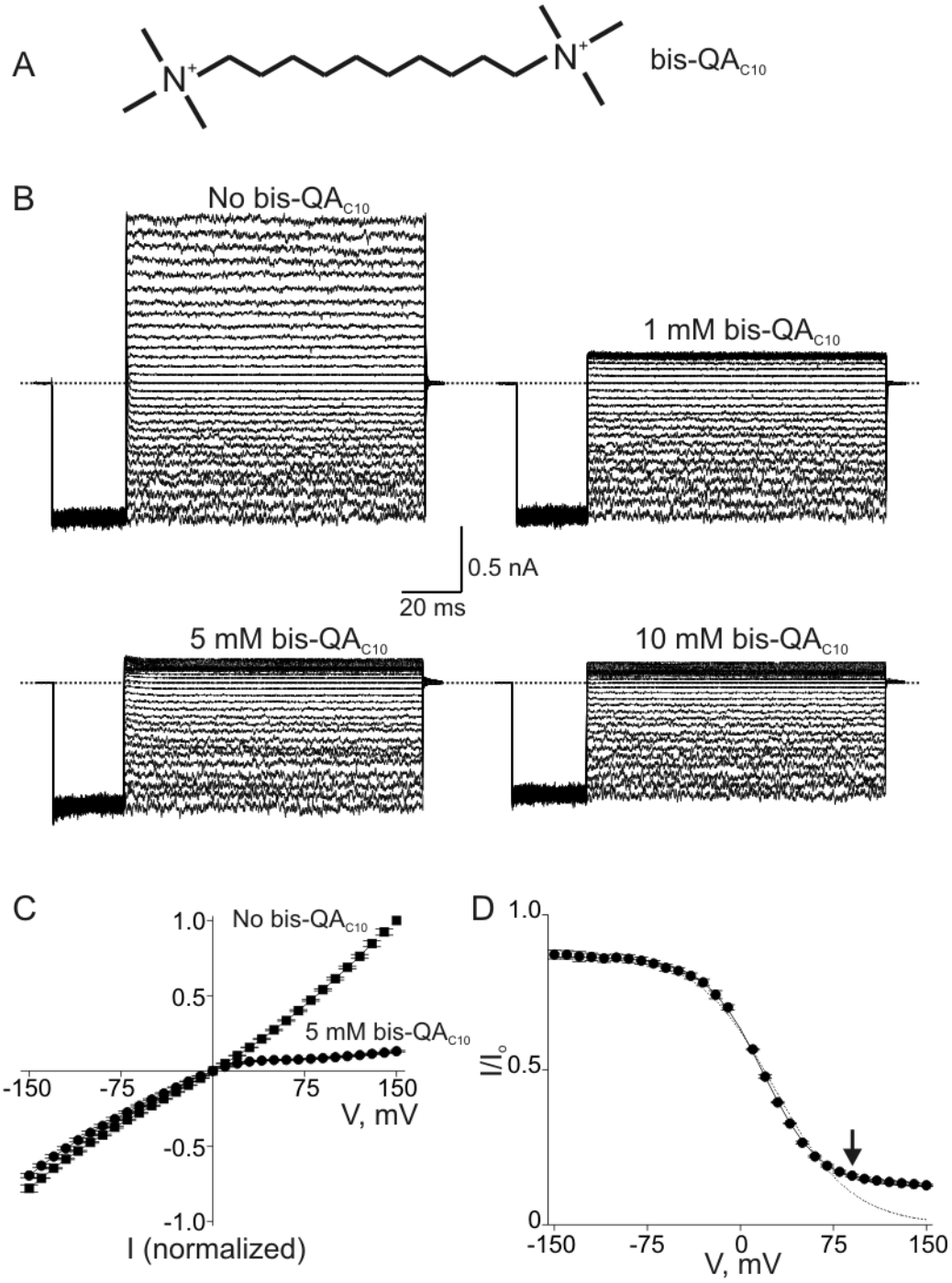
A
bis-QA$_{C10}$
B
No bis-QA$_{C10}$
1 mM bis-QA$_{C10}$
0.5 nA
20 ms
5 mM bis-QA$_{C10}$
10 mM bis-QA$_{C10}$
C
No bis-QA$_{C10}$
5 mM bis-QA$_{C10}$
1.0
0.5
-0.5
-1.0
-150
-75
75
150
V, mV
I (normalized)
D
1.0
0.5
0
I/I$_o$
-150
-75
0
75
150
V, mV

Figure 2.8

Figure 2.9. CNGA1 block by six intracellular QA compounds. Macroscopic currents recorded in the absence (left column) or presence (middle column) of the indicated blocker concentration. Scale bars are 1 nA (vertical) and 20 ms (horizontal). Chemical structures of the blockers are shown on the right.

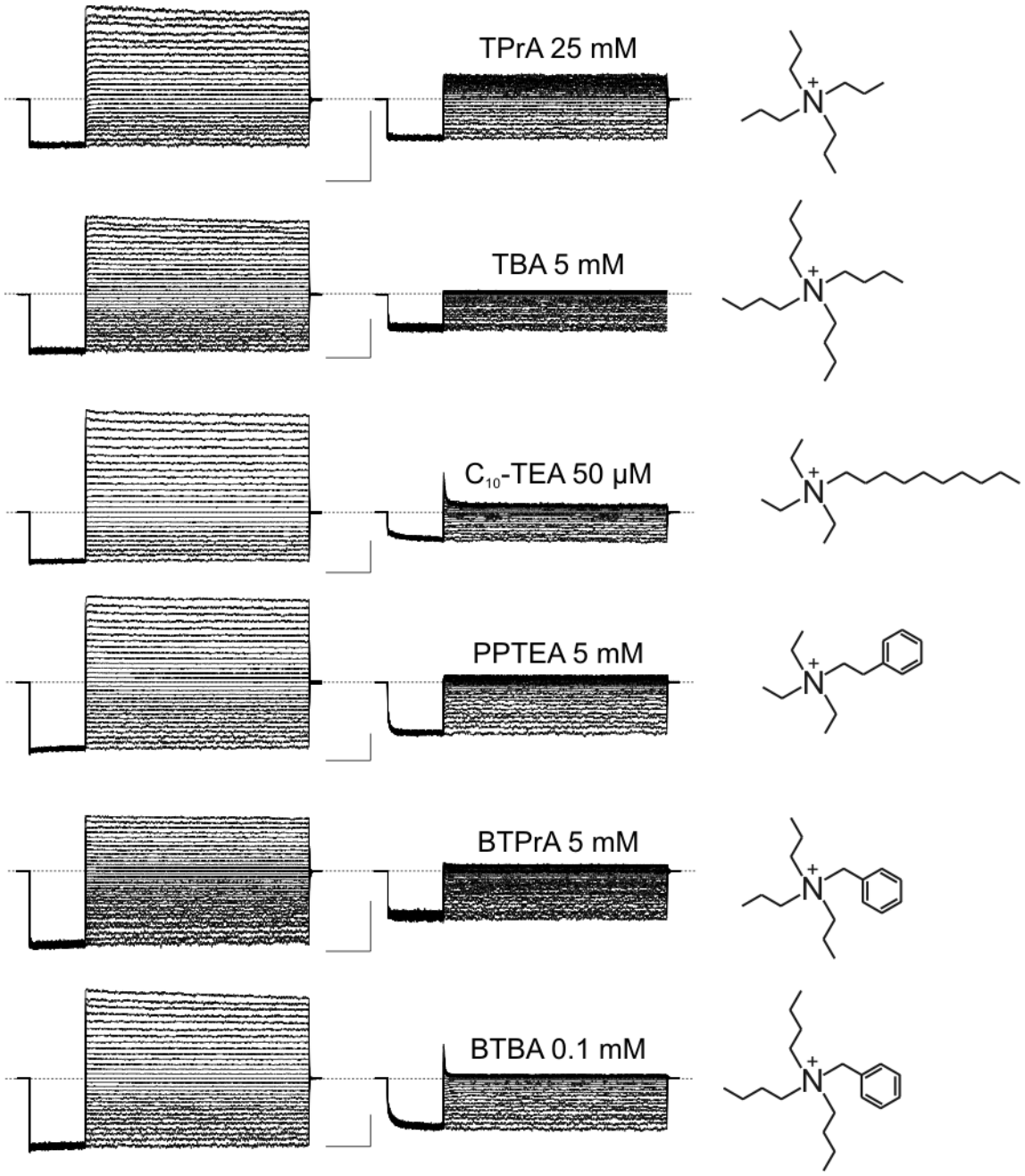

Figure 2.9

Figure 2.10. QA blockers render current-voltage relations of CNGA1 channels inwardly rectifying. Mean I-V curves (mean ± SEM; n = 3-8) in the absence (control) or presence of six QAs, each at two concentrations.

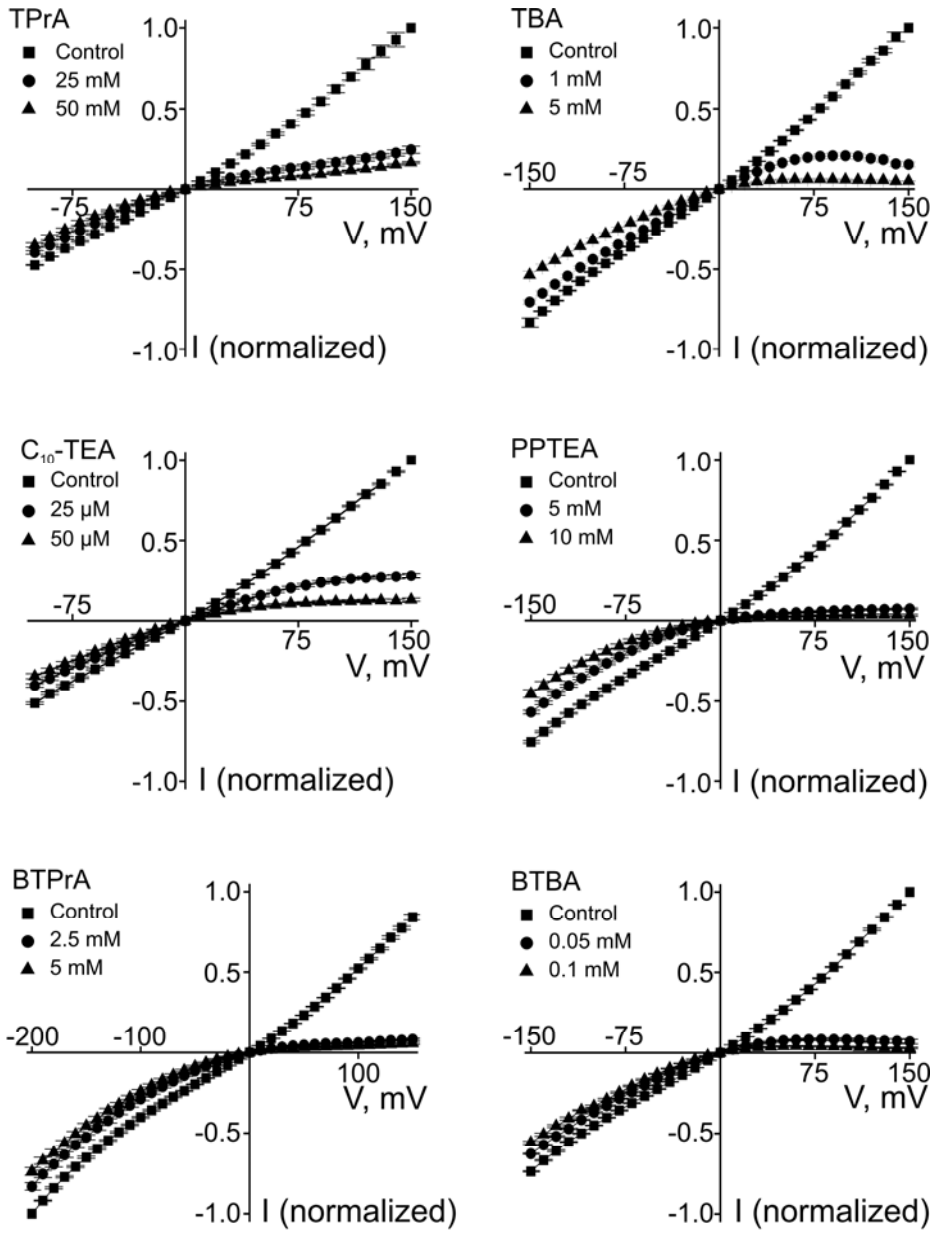
TPrA
Control
25 mM
50 mM
1.0
0.5
-0.5
-1.0
-75
75
150
V, mV
I (normalized)
TBA
Control
1 mM
5 mM
-150
-75
75
150
V, mV
I (normalized)
C10-TEA
Control
25 µM
50 µM
-75
75
150
V, mV
I (normalized)
PPTEA
Control
5 mM
10 mM
-150
-75
75
150
V, mV
I (normalized)
BTPrA
Control
2.5 mM
5 mM
-200
-100
100
V, mV
I (normalized)
BTBA
Control
0.05 mM
0.1 mM
-150
-75
75
150
V, mV
I (normalized)

Figure 2.10

Figure 2.11. Voltage dependent block by six QAs. Fraction of current not blocked (mean ± SEM; n = 3-8), plotted against voltage for six QAs, each at two concentrations. Curves were obtained by fitting Eq. 2.10 to the two data sets in each plot simultaneously. The resulting parameters are summarized in Table 2.1.

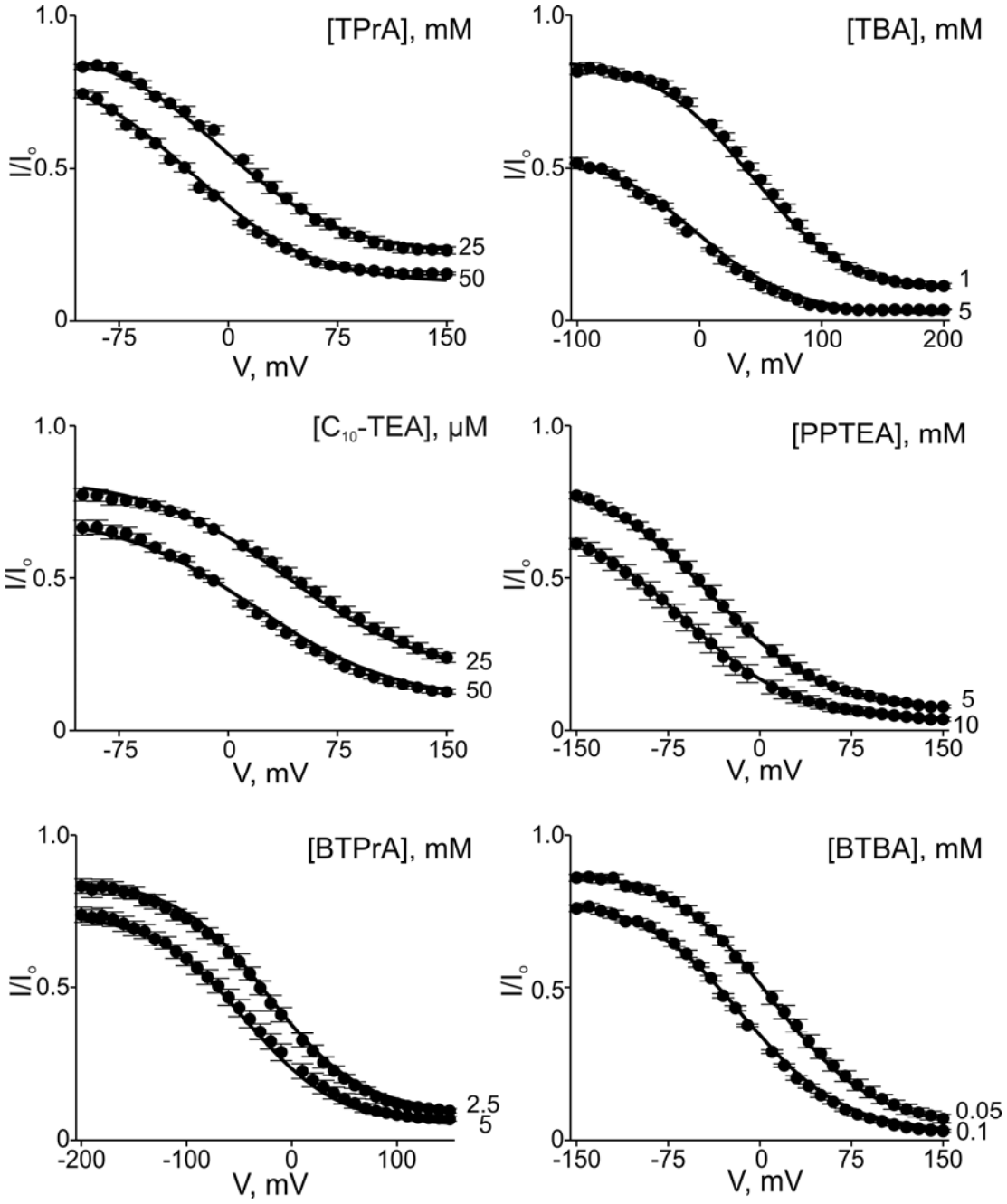
[TPrA], mM
25
50
[TBA], mM
1
5
[C10-TEA], µM
25
50
[PPTEA], mM
5
10
[BTPrA], mM
2.5
5
[BTBA], mM
0.05
0.1
I/I∘
V, mV

Figure 2.11

Figure 2.12. CNGA1 block by bis-QA_{C10} in 65 mM and 130 mM symmetrical Na^+. (A) The fraction of current not blocked (mean ± SEM; n = 4-7) in the presence of 65 mM (open symbols) and 130 mM (filled symbols) symmetrical Na^+ by 5 mM (black symbols) and 25 mM (red symbols) bis-QA_{C10}. Curves were obtained by fitting Eq. 2.10 to the four data sets simultaneously. The resulting parameters are summarized in Table 2.1. (B) Data in panel A scaled to unity at -150 mV. Curves were obtained by fitting Eq. 2.7 to the four data sets simultaneously. The best-fit parameters were: $K_B = 7.97 \pm 0.31 \times 10^{-4}$ M, $K_{B\text{-}Na} = 8.97 \pm 0.16 \times 10^{-2}$ and $Z = 1.00 \pm 0.01$.

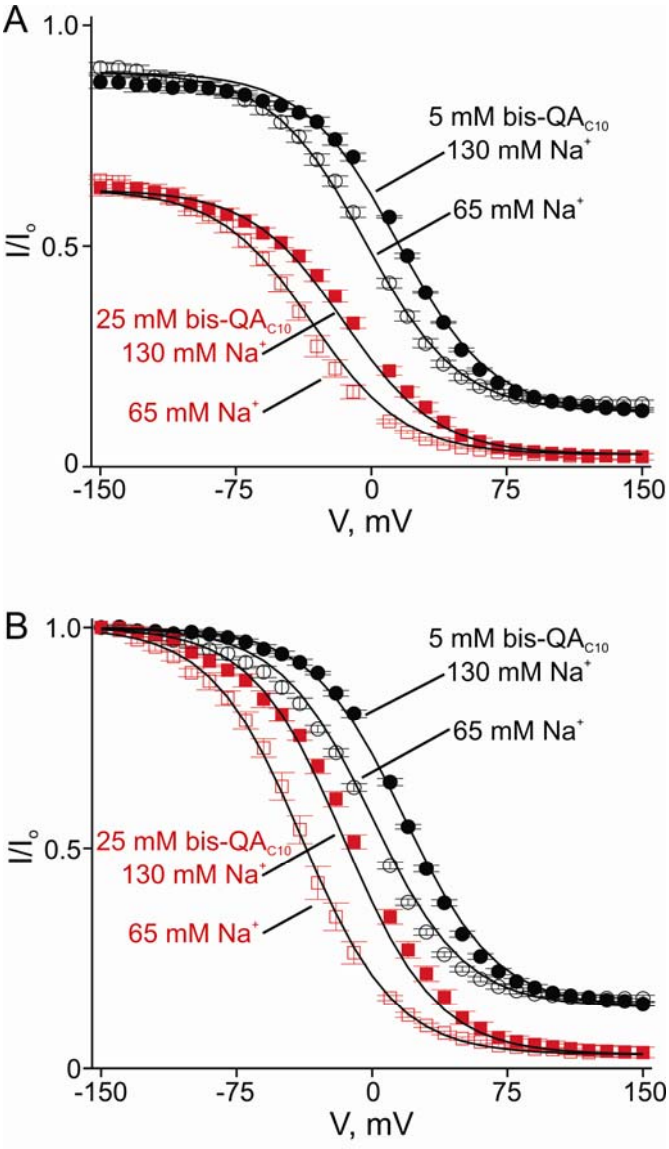
A
1.0
0.5
0
I/I$_o$
5 mM bis-QA$_{C10}$
130 mM Na$^+$
65 mM Na$^+$
25 mM bis-QA$_{C10}$
130 mM Na$^+$
65 mM Na$^+$
-150
-75
0
75
150
V, mV
B
1.0
0.5
0
I/I$_o$
5 mM bis-QA$_{C10}$
130 mM Na$^+$
65 mM Na$^+$
25 mM bis-QA$_{C10}$
130 mM Na$^+$
65 mM Na$^+$
-150
-75
0
75
150
V, mV

Figure 2.12

Figure 2.13. Simulated curves of a Boltzmann function (dotted line) and of the 3-state ion-displacement model (solid line). The Boltzmann curve was generated from Eq. 2.1 with [B] = 5 mM, $^{app}K_d$ = 6.5 mM and Z = 1. The solid curve was generated from Eq. 2.7 with [B] = 5 mM, $[Na^+]$ = 130 mM, K_B = 1 mM, $K_{B\text{-}Na}$ = 0.05 and Z = 1.

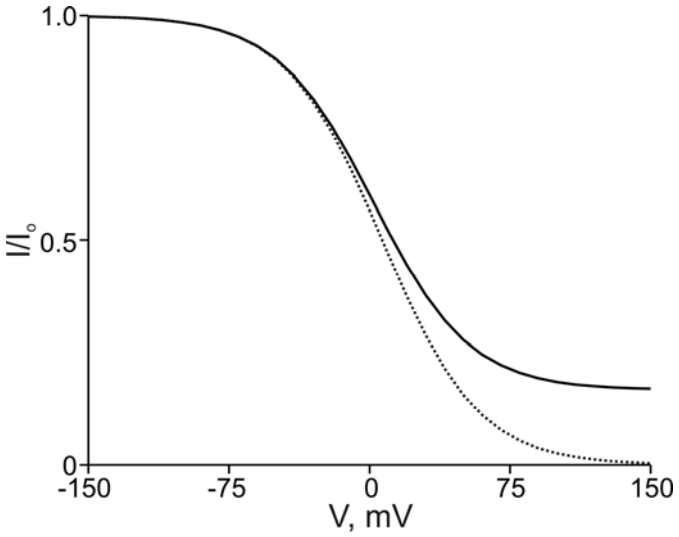

Figure 2.13

Figure 2.14. Models of channel block. (A and B) Models for multiple blocked steps. Binding of a blocker denoted as "B" to a channel (Ch) produces two blocked states (ChB_1 and ChB_2) in sequential (A) or parallel (B) steps. K_i are equilibrium constants with effective valences Z_i; k_i are rate constants and z_i their effective valences. (C) Minimal three-state ion-displacement model for voltage-dependent block. The transmembrane voltage drops exclusively across the narrow part of the pore which can only be occupied by permeant ions. The number of permeant ions in the selectivity filter is inconsequential to the model, and the number ion in the inner pore is set as the minimum of one. The channel can exist in two non-blocked states with (ChNa) or without (Ch) a permeant Na^+ ion at the inner pore (internal to the narrow selectivity filter), and one blocked state (ChB). The top blocking transition indicated by the equilibrium constant K_B is voltage independent as the blocker binds in the empty inner pore, whereas the bottom transition (with the equilibrium constant $K_{B\text{-}Na}$) is voltage dependent, as the blocker displaces the Na^+ ion. (D) Ion-displacement model with sequential blocking steps. The two leftmost non-blocked states are equivalent to those of the minimal three-state model in panel C, with (ChNa) and without (Ch) a Na^+ ion in the inner pore. The blocker may bind to the shallow site of channels in either non-blocked states characterized by a common equilibrium constant, K_{B1}. It may then bind at the deep binding site (ChB_2). The transition that involves Na^+ displacement is characterized by $K_{B2\text{-}Na}$, and is voltage dependent, whereas the one that does not involve Na^+ displacement is characterized by K_{B2}, and is voltage independent.

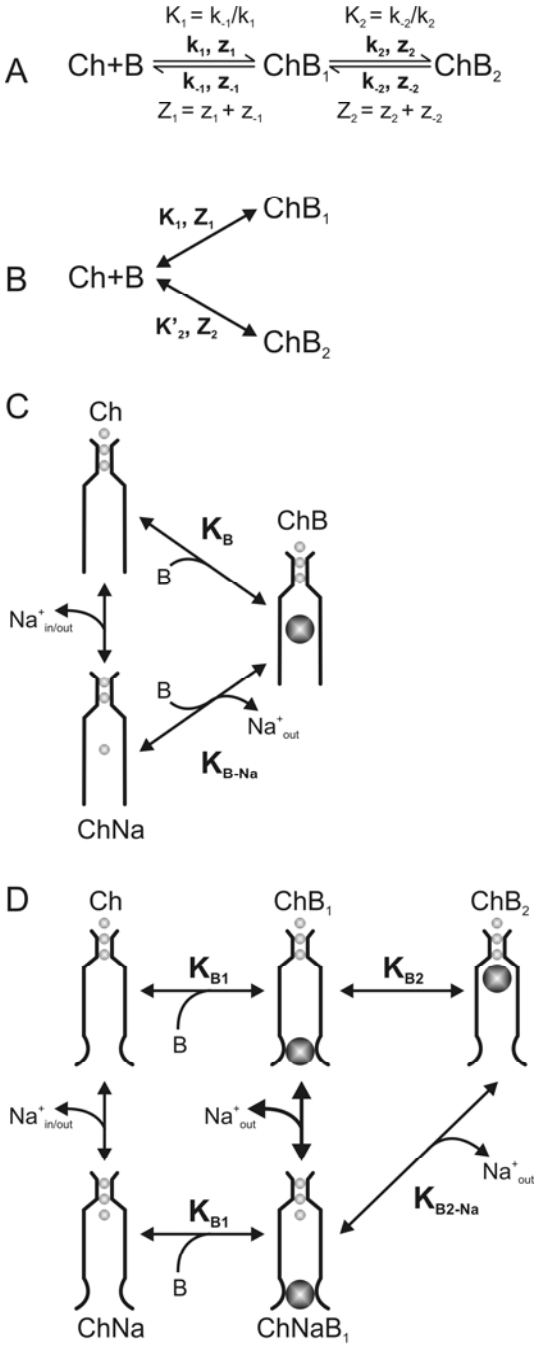
A
Ch+B
ChB1
ChB2
B
Ch+B
ChB1
ChB2
C
Ch
ChB
B
Na+ in/out
B
Na+ out
ChNa
D
Ch
ChB1
ChB2
B
Na+ in/out
Na+ out
Na+ out
B
ChNa
ChNaB1

Figure 2.14

Table 2.1
Five-state ion-displacement model parameters for QA block

	Z	K_{B1} (M)	K_{B2}	$K_{B2\text{-}Na}$ (M^{-1})
TPrA	0.63 ± 0.03	$2.49 \pm 0.36 \times 10^{-1}$	$2.93 \pm 0.53 \times 10^{-2}$	0.84 ± 0.15
TBA	0.65 ± 0.03	$6.12 \pm 0.38 \times 10^{-3}$	$1.72 \pm 0.27 \times 10^{-2}$	3.50 ± 0.40
C_{10}-TEA	0.54 ± 0.03	$1.24 \pm 0.01 \times 10^{-4}$	$4.75 \pm 0.89 \times 10^{-2}$	3.95 ± 0.51
PPTEA	0.55 ± 0.01	$2.38 \pm 0.01 \times 10^{-2}$	$1.49 \pm 0.10 \times 10^{-2}$	0.61 ± 0.02
BTPrA	0.58 ± 0.01	$1.44 \pm 0.04 \times 10^{-2}$	$1.70 \pm 0.16 \times 10^{-2}$	0.77 ± 0.03
BTBA	0.62 ± 0.01	$3.87 \pm 0.12 \times 10^{-4}$	$5.88 \pm 0.84 \times 10^{-3}$	1.16 ± 0.04
bis-QA_{C10}	0.99 ± 0.02	$4.21 \pm 0.07 \times 10^{-2}$	$1.72 \pm 0.01 \times 10^{-2}$	1.67 ± 0.05

Best-fit parameters of Eq. 2.10

Chapter 3

Mutations reveal voltage sensitivity of CNGA1 channels in saturating cGMP

3.1 Abstract

Activity of cyclic nucleotide-gated (CNG) cation channels underlies signal transduction in vertebrate visual receptors. These highly specialized receptor channels open when they bind cGMP. In the present study, we find that certain mutations restricted to the region around the ion selectivity filter render the channels essentially fully voltage gated, in such a manner that the channels remain mostly closed at physiological voltages, even in the presence of saturating concentrations of cGMP. This voltage-dependent gating resembles the selectivity filter-based mechanism seen in KcsA K^+ channels, not the S4-based mechanism of voltage-gated K^+ channels. Mutations that render CNG channels gated by voltage, loosen the attachment of the selectivity filter to its surrounding structure, thereby shifting the channel's gating equilibrium toward closed conformations. Significant pore opening in mutant channels occurs only when positive voltages drive the pore from a low-probability open conformation toward a second open conformation to increase the channels' open probability. Thus, the structure surrounding the selectivity filter has evolved to (nearly completely) suppress the expression of inherent voltage-dependent gating of CNGA1, ensuring that the binding of cGMP by itself suffices to open the channels at physiological voltages.

3.2 Introduction

Cyclic nucleotide-gated (CNG) cation channels in photoreceptors are activated by intracellular cGMP whose concentration varies with light intensity (Stryer, 1986; Yau and Baylor, 1989). The activity of these channels thereby translates light signals into electric signals. External divalent cations block the channels and, consequently, reduce the contribution of individual channels to the overall light-sensitive current, a feature critical to the high sensitivity and reliability of phototransduction (Yau and Baylor, 1989).

Given that the role of CNG channels in the retina is to convert cGMP concentration changes into electric signals, these channels should be gated primarily by ligands not voltage. Indeed, retinal CNGA1 channels exhibit essentially no voltage gating in the presence of high concentrations of cGMP. However, in the presence of low concentrations of cGMP they do display modest voltage sensitivity of unknown physical origin (Karpen et al., 1988; Benndorf et al., 1999; Nache et al., 2006). Specifically, at low cGMP concentrations, depolarization-induced currents undergo noticeable relaxation, and the steady-state macroscopic current-voltage (I-V) relation exhibits modest outward rectification. The degree of rectification decreases with increasing cGMP concentration and eventually becomes negligible. This modest voltage gating at low but not high cGMP concentrations is interpreted as follows (Karpen et al., 1988; Benndorf et al., 1999; Nache et al., 2006): a step in the ligand-gating sequence is modestly voltage sensitive with an effective valence (Z) of ~0.2, and the apparent voltage

sensitivity decreases when the gating equilibrium is already biased toward the open state in the presence of saturating cGMP concentrations.

The cGMP-binding sites are formed by the carboxy terminus, whereas the primary activation gate, in the current view, is located within the ion selectivity filter (Sun et al., 1996; Bucossi et al., 1997; Becchetti et al., 1999; Liu and Siegelbaum, 2000; Becchetti and Roncaglia, 2000; Flynn and Zagotta, 2001; Contreras et al., 2008). In the present study, we find that many mutations around the selectivity filter render the channels practically fully voltage gated even in the presence of saturating concentrations of cGMP. We present a simple model to account for these observations.

3.3 Materials and methods

3.3.1 Molecular biology and oocyte preparation

Complementary DNA for CNGA1 (Kaupp et al., 1989) was cloned into the pGEM-HESS plasmid (Liman et al., 1992). Mutant cDNAs were obtained through PCR-based mutagenesis and confirmed by DNA sequencing. The cRNAs were synthesized with T7 polymerase (Promega) using linearized cDNA as a template. Oocytes harvested from *Xenopus laevis* were incubated in a solution containing (in mM): 82.5 NaCl, 2.5 KCl, 1.0 $MgCl_2$, 5.0 HEPES (pH 7.6), and 2-4 mg/ml collagenase (Worthington). The oocyte preparation was agitated at 100 rpm and 30°C for 40-60 min. It was then rinsed thoroughly and stored in a solution containing (in mM): 96 NaCl, 2.5 KCl, 1.8 $CaCl_2$, 1.0 $MgCl_2$, 5 HEPES (pH 7.6), and 50 mg/ml gentamicin. Defolliculated oocytes were

selected and injected with RNA at least 2 and 16 h, respectively, after collagenase treatment. All oocytes were stored at 18°C.

3.3.2 Recordings and solutions

Currents were recorded from inside-out membrane patches of *Xenopus laevis* oocytes previously injected with the desired cRNA using an Axopatch 200B amplifier (MDS Analytical Technologies). Macroscopic currents were filtered at 5 kHz and sampled at 50 kHz using an analog-to-digital converter (Digidata 1322A; MDS Analytical Technologies) interfaced to a personal computer. Single-channel currents were filtered at 1 kHz and sampled at 10 kHz. pClamp 8 software was used for amplifier control and data acquisition.

Channels were activated with intracellular cGMP and the currents were elicited by stepping the voltage from the -80 mV holding potential to voltages between -200 and 200 mV in 10-mV increments. The currents in the absence of cGMP were used as template for subsequent off-line background current corrections. Internal and external solutions both contained (in mM): 130 NaCl, 0.1 EDTA, and 5 HEPES, pH 7.6. All chemicals were purchased from Sigma-Aldrich.

3.3.3 Data analysis

Conductance-voltage (G-V) curves were calculated by dividing the steady-state current value at each voltage by the electrochemical driving force and then normalizing to the value at 200 mV. In the case of the F380A mutant, the G-V curve was also obtained by isochronal measurements of the tail currents at -80 mV and normalized to the

maximum value. Data analysis and curve fitting were performed with Origin 8.0 (OriginLab Corp.). Molecular models were prepared with PyMOL 1.0 (DeLano Scientific). I-V curve simulations were performed using New Barrier (http://tedlab.urmc.rochester.edu/BarrierModel.htm). The figures were made with Origin 8.0 (OriginLab Corp.) and CorelDRAW X4 (Corel Corp.).

3.4 Results

For ease of later comparison we first illustrate some known properties of CNGA1 channels. Fig. 3.1 A, B shows current records of retinal CNGA1 channels in the presence of saturating (2 mM) and sub-saturating (30 μM) concentrations of intracellular cGMP. At 2 mM, currents develop instantaneously following a voltage step whereas at 30 μM they develop slowly. The macroscopic I-V relation is nearly linear at 2 mM but tends toward outward rectification with decreasing cGMP concentration (Fig. 3.1 C). To better illustrate the voltage dependence of the macroscopic conductance (G), we calculated the conductance from the current:electrochemical driving force ratio and plotted it against voltage (Fig. 3.1 D). The CNGA1 conductance exhibits insignificant voltage sensitivity at high concentrations of cGMP, and modest sensitivity at low concentrations of cGMP. In addition, the cGMP dose-response curves barely differ between -200 and 200 mV (Fig. 3.1 E). These results confirm previous reports (Karpen et al., 1988; Kaupp et al., 1989; Benndorf et al., 1999; Nache et al., 2006).

3.4.1 Mutations around the external end of the selectivity filter render the channels voltage gated even in saturating cGMP

The modest voltage sensitivity of CNGA1 at low cGMP concentrations signifies that the conformation of part of the ion conduction pore, e.g., the selectivity filter, is directly or indirectly influenced by membrane voltage. In Kv channels and bacterial KcsA channels, the external end of the selectivity filter is structurally attached to the pore helix (Perozo et al., 1993; Yang et al., 1997; Doyle et al., 1998; Zhou et al., 2001; Long et al., 2005; Blunck et al., 2006; Long et al., 2007; Cordero-Morales et al., 2007). Disruption of that interaction affects voltage gating in these channels (e.g., C-type inactivation; López-Barneo et al., 1993; Cordero-Morales et al., 2006b). We therefore wondered whether similar disruption of the analogous contact in CNG channels would also affect their voltage sensitivity. To test this idea, we mutated six residues (^{350}SLYWST^{355}) in the pore helix of CNGA1, one at a time, to alanine; five mutants express sufficient current for examination. The macroscopic conductance of the S350A, L351A, S354A and T355A mutants, like that of wild type, exhibits little voltage sensitivity (Fig. 3.2 B, C, E, F). In stark contrast, the Y352A pore-helix mutant becomes strongly voltage sensitive even in the presence of saturating cGMP concentrations (Fig. 3.2 D): depolarization elicits large outward currents with resolvable time courses but hyperpolarization induces little inward current. We note that some residual current persists at extreme negative voltages.

CNGA1's Y352 corresponds to Shaker's W434 whose mutation profoundly affects the ability of voltage to switch the selectivity filter between conducting and non-conducting conformations (Perozo et al., 1993; Yang et al., 1997). Intriguingly, the corresponding residue W362 in Kv1.2 of known structure is within hydrogen-bonding reach of D375 (Fig. 3.2 A), a residue that corresponds to E363 in CNGA1. The, by

analogy, likely spatial proximity of Y352 and E363 in CNGA1 suggests that mutation of E363 too, like that of Y352 shown above, might render the channels voltage sensitive. We thus mutated E363 to all 19 other natural variants; eleven mutants express detectable currents. Only the E363D channels exhibit wild-type-like behavior (Fig. 3.3 B), whereas the remaining ten E363 mutants display strong outward rectification (E363Q is shown in Fig. 3.4 A, C; all others in Fig. 3.3). At negative voltages the conductance of these E363 mutants is greatly reduced, in the case of E363Q and E363H dramatically so (E363H expresses much less well). These latter two mutants are essentially completely shut down by hyperpolarization (see below), i.e. they appear to be fully voltage gated, even in the presence of a saturating concentration of cGMP. The kinetics of E363Q current development following a voltage jump become faster with increasing cGMP concentration (compare Figs. 3.4 A, B). However, the shape of the steady-state G-V curves at saturating and subsaturating concentrations of cGMP are superimposable (Fig. 3.4 C). Depolarization lowers the EC_{50} for channel activation by cGMP only modestly (Fig. 3.4 D). Therefore, cGMP and voltage are unlikely to affect the same gating step(s).

We further investigated the mechanism underlying the voltage sensitivity of the fully gated E363Q mutant by comparing the single-channel and macroscopic current-voltage relations. The single-channel i-V curve rectifies only mildly over the -200 to 200 mV range (Fig. 3.5 A; filled symbols). For illustration, single-channel currents at 120 and at -120 mV are shown in Fig. 3.5 C, E. In sharp contrast, the macroscopic I-V curve rectifies steeply (Fig. 3.5 A; open symbols). The dramatic difference in the degree of rectification seen in these two current-voltage relations indicates that the rectification of the macroscopic I-V curve is due mainly to voltage gating. As expected, an E363Q

channel-containing membrane patch carries large macroscopic outward currents at positive voltages but only brief individual channel events at very negative voltages (Fig. 3.5 G, H). The following criteria confirm that the latter are indeed individual E363Q-mutant channel events. First, the events occur only when patches are exposed to intracellular cGMP (compare Fig. 3.5 G, H with I, J). Second, we observe inward current events only in patches containing a large number of channels, i.e., carrying outward macroscopic currents. Third, the frequency of individual channel events at negative voltages correlates with the amount of macroscopic current in the same patch at positive voltages (compare Fig. 3.5 G with H). Lastly, the single-channel events are less strongly inhibited by Mg^{2+} than the wild-type current. The wild-type channel is known to be blocked by Mg^{2+} in a voltage dependent manner such that mainly the inward current is blocked. Neutralizing E363 reduces the apparent Mg^{2+} affinity (Root and MacKinnon, 1993; Eismann et al., 1994; Park and MacKinnon, 1995). As expected for single-channel currents presumably carried by E363Q mutant channels, their amplitude at -120 mV is reduced 37% by 100 μM external Mg^{2+} (Fig. 3.5 B-F). This yields an estimated K_i of 170 μM, compared to 20 μM for the wild type (Root and MacKinnon, 1993; Eismann et al., 1994; Park and MacKinnon, 1995). We conclude, therefore, that the extreme macroscopic rectification of some E363 mutants over the wide voltage range mostly reflects voltage gating not single-channel rectification.

To recapitulate, we find that the Y352A pore helix mutant becomes strongly voltage sensitive; that mutation of its putative structural contact, residue E363, similarly reveals strong rectification; and that this latter behavior reflects voltage gating not single-channel rectification. To confirm that E363 does interact with Y352, we produced the

Y352A/E363Q double-mutant channel (Fig. 3.6 A, B). Were the two mutations to act independently and therefore additively, the residual voltage-independent conductance of the double mutant at extreme negative voltages would be even lower than that of either single mutant. Instead, it falls between those of the single mutants (Fig. 3.6 C; also compare Figs. 3.2 D, 3.4 C, and 3.6 B). The finding that the two mutations affect gating in an energetically non-additive manner confirms that Y352 and E363 indeed interact.

3.4.2 Mutations in S6 near the internal end of the selectivity filter also render the channels voltage gated in saturating cGMP

Whereas the selectivity filter's external end is attached to the pore helix, its internal end, which extends from the pore helix, is attached to S6 (Fig. 3.7 A). To test whether perturbing the relevant part of S6 also enhances voltage sensitivity, we mutated seven S6 residues near the internal end of the selectivity filter (^{380}FLIGVLI^{386}), one at a time, to alanine. Among the five mutants that express sufficient current for examination, those with F380A and G383A substitutions (colored red in Fig. 3.7 A) are also voltage gated (Fig. 3.7 B, D). The tail-current kinetics of the F380A mutant are sufficiently slow to be measured and, as expected, the G-V curve obtained directly from tail currents (open circles) matches that calculated from the I-V curve (filled circles in Fig. 3.7 B). In contrast, the remaining three mutants, with substitutions (I382A, V384A and I386A, colored grey in Fig. 3.7 A) internal to the filter and/or on the other side of the helix, exhibit little voltage sensitivity (Fig. 3.7 C, E, F). This spatial distribution pattern of S6 mutations that result in voltage gating further supports the notion that proper attachment

of the selectivity filter to the surrounding shell is essential to minimize voltage gating in CNG channels.

3.4.3 Alanine scan of the entire region from the pore helix to S6

The hypothesis that proper anchoring of the selectivity filter to the surrounding structural shell prevents undesirable voltage gating implies that mutations that result in voltage gating (in saturating cGMP) will be confined to the external part of the pore around the selectivity filter. In particular, no S6 mutations in the internal part of the pore should confer voltage sensitivity, even though architectural similarities with Kv channels suggest the possible existence of an intracellular gate. To test this prediction, we replaced each of the remaining 53 residues in the region from the N-terminal end of the pore helix to the C-terminal end of S6, one at a time, with alanine (native alanine residues were replaced with valine; Fig. 3.8 A). Of the 65 mutant channels (including those already discussed), 59 express sufficient current for examination (Figs. 3.9 – 3.13). Phenotypically, the 65 mutant channels fall into four categories, characterized by their degree of rectification which we express as the ratio of currents at 200 and -200 mV (I_{200}/I_{-200}) or for comparison (see below), that at 200 and 10 mV (I_{200}/I_{10}) (Fig. 3.8 C). The first category, colored grey in the sequence alignment (Fig. 3.8 A) and in the chimeric Kv channel structure (Fig. 3.8 B) exhibits, like the wild type, no significant voltage gating in saturating cGMP. The second group (colored red in Fig. 3.8) is strongly voltage gated, i.e., little or no macroscopic current remains at hyperpolarized potentials. The third group (colored yellow in Fig. 3.8) exhibits modest voltage gating, i.e., the channels conduct significant, if diminished, macroscopic current at very hyperpolarized

potentials. The fourth group (colored blue in Fig. 3.8) expresses no or insufficient current for examination.

Structural mapping of these phenotypes yields an informative pattern (Fig. 3.8 B). All mutations that cause the appearance of voltage gating in saturating concentrations of cGMP (labeled positions; Fig. 3.8 B) are located in the external part of the pore around the selectivity filter. Thus, if voltage gating arises from the ion conduction pore, it must arise from this external region not from a more internal one, such as the C-terminal part of S6 which in Kv channels constitutes the activation gate. This pattern reinforces the view that proper anchoring of the selectivity filter is critical in minimizing voltage gating.

It is noteworthy that the F387A mutation in the cavity, unlike mutations at neighboring residues, renders the I-V relation "super-linear" (compare Fig. 3.14 A, D; filled symbols). As a result, the current exhibits little rectification as judged from the I_{200}/I_{-200} value but partial rectification based on the I_{200}/I_{10} value (categorization of all other mutants is qualitatively the same in both cases). In principle, the phenyl ring of F387 may be involved in forming an ion-binding site in the cavity of the channel. As illustrated in Fig. 3.15, the super-linearity of this mutant's I-V curve may simply result from the disruption of an ion-binding site. If that were the case, block of the mutant's pore should exhibit reduced voltage dependence because it contains fewer Na^+ ions that can be displaced by a blocker across the electric field (Armstrong, 1971; Spassova and Lu, 1998; Shin et al., 2005). Indeed, the F387A mutation, but not those at neighboring residues, reduces voltage dependence of channel block by philanthotoxin (PhTx) (Fig. 3.14; Table 3.1; see Guo and Lu, 2000 for PhTx block of CNGA1). For this reason, we did not categorize the F387A mutant as modestly voltage gated.

3.4.4 Charge-neutralizing mutations at arginine residues in S4 do not affect the voltage sensitivity of E363Q mutant channels

Voltage sensitivity in K^+ channels originates from two regions: the S4 voltage sensor and the ion selectivity filter. The S4 in CNGA1 channels resembles that of Kv channels in that it contains the four arginines that in Kv channels sense voltage (Kaupp et al., 1989; Jan and Jan, 1990; Aggarwal and MacKinnon, 1996; Seoh et al., 1996; Tang and Papazian, 1997). This similarity naturally raises the question whether the voltage sensitivity which we find to be brought out by numerous mutations around the selectivity filter arises, not from the filter after all, but from the arginines in S4. To address this issue, we made neutral substitutions at R1 through R4 on the background of the E363Q mutation and observed the following. R1 is intolerant of mutation, as all 19 mutants fail to produce detectable currents (a result consistent with R1's involvement in a critical hydrogen bond). R2 is so poorly tolerant that among the 19 possible substitutions only lysine and threonine yield measurable currents. R3 and R4 are more tolerant. If the voltage sensitivity of E363Q channels originates, as our results thus far suggest, mainly from the selectivity filter region rather than from S4, then neutral substitutions (R2T, R3Q or R4Q; Fig. 3.16 A-C) should have little effect on voltage sensitivity. This is indeed the case, as the G-V curves of the E363Q mutant with or without neutral substitutions for any one of these three arginine residues are all superimposable (Fig. 3.16 D). That is, these positive charges on S4 play no role in conferring voltage sensitivity to the mutants described above.

3.5 Discussion

In the present study we report four main findings. First, mutations at a number of sites render macroscopic CNGA1 currents strongly outwardly rectifying in the presence of saturating concentrations of cGMP. Second, the rectification mainly reflects voltage gating not single-channel current rectification. Third, mutations that bring out voltage gating are exclusively confined to the region around the ion selectivity filter. Fourth, the acquired voltage sensitivity is not affected by neutralizing any of the (second through fourth) positively charged residues in S4. We will analyze the characteristic features of the voltage-gated mutant channels using mainly the E363Q mutant as an example. This mutant not only is practically fully voltage gated but also expresses sufficient current for a relatively more detailed characterization. Additionally, E363 mutations have been extensively studied in the context of ion conduction.

Over a decade ago, mutations at E363 were shown to render the macroscopic I-V curve outwardly rectifying (Root and MacKinnon, 1993; Eismann et al., 1994; Sesti et al., 1995). These studies were carried out with voltage ramp protocols between -100 and 100 mV. Within this relatively restricted voltage range, rectification is not as extreme as we report here over a much wider (-200 to 200 mV) range. On the assumption that the glutamate residue is located near the external mouth of the ion conduction pore, and given the fact that the single-channel i-V curve exhibits rectification (although less than the macroscopic I-V curve), a natural conclusion is that neutralizing a negatively charged residue near the external end of the pore would lower the local electrostatic potential. This reduced potential could in turn lower the permeant ion concentration at the external mouth of the pore, causing the pore to conduct ions in an outwardly rectifying manner.

As detailed below, our voltage-pulse protocols over a much wider voltage range reveal that the extreme rectification following neutralization of E363 mainly reflects voltage gating not single-channel current rectification. First, if macroscopic rectification caused by neutralizing E363 were mainly due, not to channel gating, but to asymmetric ion conduction, the current induced by a voltage step should develop instantaneously without relaxation. On the contrary, several neutral E363 mutant channels, like other voltage-gated ones with mutations in the pore helix or in S6, clearly exhibit current relaxation. Second and as already mentioned, among those E363 mutants, E363Q channels display extreme outward rectification, i.e., they carry no significant inward current. If macroscopic rectification were mainly due to asymmetric conduction rather than gating, the single-channel i-V curve should exhibit a similar degree of outward rectification. Fig. 3.5 A shows that this is not the case: the single-channel i-V curve (filled symbols) rectifies only mildly over the -200 to 200 mV range, compared to the much more steeply rectifying macroscopic I-V curve (open symbols). This result leads to the conclusion that the rectification of the macroscopic I-V curve must mainly reflect voltage gating, a conclusion that is further supported by the observation that an E363Q channel-containing membrane patch carries large macroscopic outward current at positive voltages but only brief individual channel events at very negative voltages (Fig. 3.5 G, H).

To estimate the magnitude of the voltage-induced change in open probability of the E363Q channel, one could attempt to determine, from single-channel current recordings, the open probability at various voltages. This conceptually straightforward undertaking is very difficult in practice because, given the extremely low open probability at negative voltages, there is no reliable way to ensure that a membrane patch

contains only a single channel. Alternatively, we can obtain the information by comparing outward macroscopic current (= iNP_o) at a positive voltage with inward current at the corresponding negative voltage. At negative voltages where the open probability is extremely low, the inward current was calculated from the product of unitary current and the fraction of total open time for all channels (iNP_o) present in the patch. With this simple approach we obtained a ratio of channel open probabilities at -200 and at 200 mV of $1.6 \pm 0.5 \times 10^4$ (mean ± SEM, n = 8), reflecting a valence of ~0.6. A comparable value of 0.5 was estimated from the limiting slope (Almers, 1978) of the semi-logarithmic plot of macroscopic conductance against voltage (Fig. 3.17 A). Finally, a Boltzmann function fit to the entire experimentally accessible portion of the G-V curve yielded Z = 0.5 and $V_{1/2}$ = 240 mV, and a projected maximum around 400 mV (Fig. 3.17 B). Indeed, the experimental G-V curve shows no sign of saturation at 200 mV, the limit of our recording system. In biophysical terms, the voltage sensitivity (valence ~ 0.5) of CNGA1 mutants is rather modest, much lower than that of Kv channels which originates from S4 (Schoppa et al., 1992), but is comparable to that of KcsA K^+ channels which originates from the region around the selectivity filter (Heginbotham et al., 1999; Cordero-Morales et al., 2006a). In biological terms, however, a G-V relation with a Z of ~0.5 and $V_{1/2}$ of ~240 mV would pose significant problems, as it would surely result in closure of the channels at physiological voltages.

E363 located at the external end of the selectivity filter appears to interact with Y352 in the pore helix (Fig. 3.6). Neutralizing E363 could therefore conceivably loosen the attachment of the filter to the pore helix, thereby decreasing the probability of the filter remaining in a stable, open conformation. In fact, loosening of structural contacts

between the selectivity filter and the pore helix of K^+ channels has been shown to affect voltage gating (Alagem et al., 2003; Cordero-Morales et al., 2006a; Cordero-Morales et al., 2006b). Mutations at E363 and at other sites around the selectivity filter of CNGA1 channels evidently keep the gating equilibrium biased toward closed states, whereas positive voltages appear to help stabilize an open conformation of the selectivity filter. Voltage sensitivity may arise from ion movement within the selectivity filter as its conformation changes to an open state. In addition, given that the pore helix bears no charges but has a dipole moment and is located in a low-dielectric environment (Roux and MacKinnon, 1999), its motion may be voltage sensitive.

Sequential binding of cGMP to four potential sites of a wild-type CNGA1 channel drives it through a series of closed states to open states (Karpen et al., 1988; Tanaka et al., 1989; Goulding et al., 1994; Gordon and Zagotta, 1995; Varnum and Zagotta, 1996; Benndorf et al., 1999; Nache et al., 2006). This gating sequence consists of (at least) two processes: a ligand-binding transition followed by a closed-open channel transition (Fig. 3.18 A). Kinetic analyses have suggested that the closed-open transition is voltage dependent (valence ~ 0.2), and that this could account for the voltage gating observed at low concentrations of cGMP. Although a voltage sensitive step anywhere along the ligand-initiated gating sequence could mediate the observed enhancement of activation of certain mutant channels by depolarization, it cannot explain the failure of a sufficiently strong hyperpolarization to reduce conductance to zero. For any residual current to remain at extreme negative potentials (as is the case for most rectifying mutants described here; e.g. Figs. 3.2 D, 3.3, 3.6 B and 3.7 D) the voltage-sensitive transition must be between open states. In fact, more than one open state has been observed in

wild-type channels under low cGMP conditions, or in channels with neutral substitutions at E363 (Sesti et al., 1995; Bucossi et al., 1996; Sesti et al., 1996; Fodor et al., 1997; Bucossi et al., 1997; Becchetti et al., 1999; Kusch et al., 2004).

A model to describe voltage gating of mutant CNGA1 channels requires at least four states (Fig. 3.18 B): two closed (C and C_L) and two open (O_1 and O_2). Sequential binding of cGMP brings the mutant channel, like the wild type, to the final closed state (C_L), from which it may proceed to the first open state (O_1). None of the gating transitions to this point is assumed to be voltage sensitive. However, state O_1 is in voltage-sensitive equilibrium with a second open state O_2. Whereas in wild-type channels the (voltage-insensitive) transition from the last closed to the first open state is energetically favorable (i.e. high-probability), in mutant channels the first open state is energetically unstable (i.e. low-probability) with respect to the last closed state. Strong depolarization (favoring O_2) will therefore be required to pull a sizeable fraction of channels into an open configuration. For the scheme in Fig. 3.18 B, relative conductance (G/G_{max}) is given by the ratio of the open states to the sum of all states:

$$\frac{G}{G_{\max}} = \frac{[O_1] + [O_2]}{[C] + [O_1] + [O_2]}.$$

The equilibrium constants in the absence of an electric field are defined as $K_L = [C][cGMP]^n/[C_L]$, $K_1=[O_1]/[C]$ and $K_2=[O_2]/[O_1]$. Assuming for simplicity that only the transition between open states is voltage sensitive, we define $K_2(V) = K_2\exp(Z_{K2}FV/RT)$ where Z_{K2} is the effective valence associated with the O_1 - O_2 transition, V is the membrane voltage, and F, R and T have their usual meaning. The relative conductance is then given by:

$$\frac{G}{G_{\max}} = \frac{1}{1 + \frac{1 + \left(\frac{K_L}{[cGMP]}\right)^n}{K_1\left(1 + K_2 e^{\frac{Z_{K2}FV}{RT}}\right)}}. \tag{3.1}$$

At saturating concentrations of cGMP, the ligand-binding transition is extremely biased toward the C_L state and scheme B (Fig. 3.18 B) is then reduced to scheme C (Fig. 3.18 C), and Eq. 3.1 to

$$\frac{G}{G_{\max}} = \frac{1}{1 + \frac{1}{K_1\left(1 + K_2 e^{\frac{ZFV}{RT}}\right)}}. \tag{3.2}$$

At sufficiently negative voltages $K_2\exp(Z_{K2}FV/RT)$ vanishes and Eq. 3.2 reduces to:

$$\frac{G}{G_{\max}} = \frac{1}{1 + \frac{1}{K_1}}, \tag{3.3}$$

that is, K_1 governs the height of the asymptotic, voltage-insensitive plateau at negative voltages, i.e., the fraction of conductance that will not be further reduced by any degree of hyperpolarization. The remaining, voltage-sensitive fraction is described by a Boltzmann function with valence $Z = Z_{K2}$ and $V_{1/2} = (RT/Z_{K2}F)\ln[(K_1+1)/K_1K_2]$. In the limit where K_1 becomes very small (i.e., state O_1 has very low probability), the conductance plateau at extreme negative voltages vanishes and the conductance becomes voltage gated over its entire range, such that Eq. 3.2 (red dashed curve in Fig. 3.17 B)

reduces to a Boltzmann function (black curve). The valence Z_{K2} governs the steepness of the G-V curve; K_2 influences only $V_{1/2}$ not the height of the plateau.

Fig. 3.18 D shows G-V plots (normalized to the conductance at 200 mV) at saturating cGMP concentrations for wild-type and eleven E363 mutant channels. We restricted our analysis to the voltage range between 10 and 200 mV where the single-channel i-V curve is linear (Fig. 3.5 A) and variations in macroscopic conductance therefore primarily reflect changes in channel open probability, not confounded by altered ion conduction. Given the saturating cGMP concentrations, the relevant scheme is model C in Fig. 3.18, governed by Eq. 3.2. A simultaneous fit of Eq. 3.2 to the entire data set yields $K_2 = 1.04 \pm 0.14$ common to all twelve channels, as well as K_1 and Z_{K2} values for each individual channel. These best-fit K_1 and Z_{K2} values are listed in Table 3.2, and their relationship is plotted in Fig. 3.18 E. Generally, a mutation that has a greater destabilizing effect on the O_1 state (i.e., smaller K_1) seems to exhibit a somewhat larger Z_{K2}. This trend suggests that a larger voltage-driven conformational change can occur around the selectivity filter of mutants with a more disrupted interaction between selectivity filter and pore helix – a not implausible scenario. Of all viable mutations, E363H has the largest effect on both parameters, lowering K_1 150 fold and raising Z_{K2} 2.5 fold from the wild-type values. These sole changes account for the appearance of nearly full-range voltage gating in E363H channels. Thus, mutations produce voltage gating not just by modestly increasing the valence associated with the open - open transition, but mainly by lowering the stability of an open state. The latter effect creates a condition in which strong depolarization is now needed to achieve high open probability.

To recapitulate, our analysis is consistent with a model where the whole range of observed voltage sensitivities, from barely detectable in wild-type channels to full-fledged in certain mutants, reflects a common property inherent in all channels including wild type. In the case of wild-type channels in the presence of saturating ligand concentrations, where the closed - open gating equilibrium is already biased to approach maximal open probability, inherent voltage gating is largely obscured because depolarization cannot further enhance open probability to any significant extent. Extension of this model for saturating cGMP concentrations (Fig. 3.18 C, governed by Eq. 3.2) to include a ligand-binding transition of negligible voltage sensitivity (Fig. 3.18 B, governed by Eq. 3.1) also adequately accounts for – without any adjustments of K_1, $K_2(V)$ or Z_{K2} – the voltage gating behavior of wild-type and E363Q mutant channels at subsaturating ligand concentrations. We fit the data of Fig. 3.18 F with Eq. 3.1, keeping K_1, $K_2(V)$ and Z_{K2} fixed at their values obtained from Fig. 3.18 D. The resulting best fit values for the two remaining adjustable parameters are $K_L = 78 \pm 4$ μM and Hill coefficient = 1.44 ± 0.06. This Hill coefficient value is comparable to those obtained from Hill fits of the cGMP dose-response curves in Figs. 3.1 E and 3.4 D.

To assess the voltage sensitivity, if any, of the ligand-binding step, we fitted Eq. 3.1 to the cGMP dose-response relations at -200 and 200 mV simultaneously. The fits of the wild-type data yield K_L (-200 mV) = 96 ± 2 μM and K_L (200 mV) = 182 ± 5 μM, a twofold variation over 400 mV (red dashed lines, Fig. 3.1 E), which corresponds to K_L (0 mV) = 132 μM with a valence factor of 0.04. Similar fits to the E363Q data yield K_L (40 mV) = 166 ± 6 μM and K_L (200 mV) = 67 ± 2 μM, a 2.5 fold variation over a 160 mV range (Fig. 3.4 D), which corresponds to K_L (0 mV) = 196 μM with a valence factor of

-0.1. The relatively small variation of K_L with voltage further supports the notion that the observed voltage sensitivity is mainly associated with the open - open transition whereas cGMP binding per se exhibits little voltage sensitivity.

In summary, we have found that certain mutations around the selectivity filter render CNGA1 channels practically fully voltage gated. These mutations loosen the attachment of the selectivity filter to the surrounding structures. As a result, saturated binding of cGMP by itself can only help the channel enter a low-probability, i.e. unstable open state. Membrane depolarization, which favors a second open state in equilibrium with the first, is required to move a sizeable fraction of the channels into an open configuration. In other words, the channels become voltage gated even in the presence of saturating concentrations of cGMP. Such voltage gating would have a profoundly adverse functional consequence, as the mutant channels could remain mostly closed at physiological voltages. Thus, proper attachment of the selectivity filter to the surrounding supporting structure is essential to ensure that the CNGA1 channel remains primarily gated by ligands not voltage.

Figure 3.1. cGMP activation of wild-type CNGA1 channels. (A, B) Macroscopic current traces recorded in symmetric 130 mM Na^+ from inside-out patches containing CNGA1 channels in the presence of 2 mM (A) or 30 μM (B) intracellular cGMP. Currents were elicited by stepping from the -80 mV holding potential to voltages between -200 and 200 mV in 10-mV increments. Only traces every 20 mV are shown for clarity. Dotted line indicates zero current level. (C) I-V curves (mean ± SEM; n = 3-6) in the presence of 0.01 mM (filled inverted triangles), 0.03 mM (open triangles), 0.1 mM (filled circles), and 2 mM (open squares) cGMP, each normalized to the current at 200 mV. (D) Corresponding normalized G-V curves (mean ± SEM; n = 3-6). (E) Fraction of maximal current (I/I_{max}; mean ± SEM; n = 7) plotted against cGMP concentration for -200 mV (open circles) and 200 mV (filled circles). Black dashed curves are Hill equation fits with a common Hill coefficient (n) yielding EC_{50} = 66 ± 2 μM at -200 mV, EC_{50} = 53 ± 1 μM at 200 mV and n = 1.48 ± 0.03. Red dashed curves are fits of Eq. 3.1 to both data sets simultaneously, with a single adjustable K_L and all other parameters fixed (n = 1.48, K_1 = 0.62, K_2 = 1.04 and Z_{K2} = 0.25), which yield K_L = 96 ± 2 μM at -200 mV and K_L = 182 ± 5 μM at 200 mV.

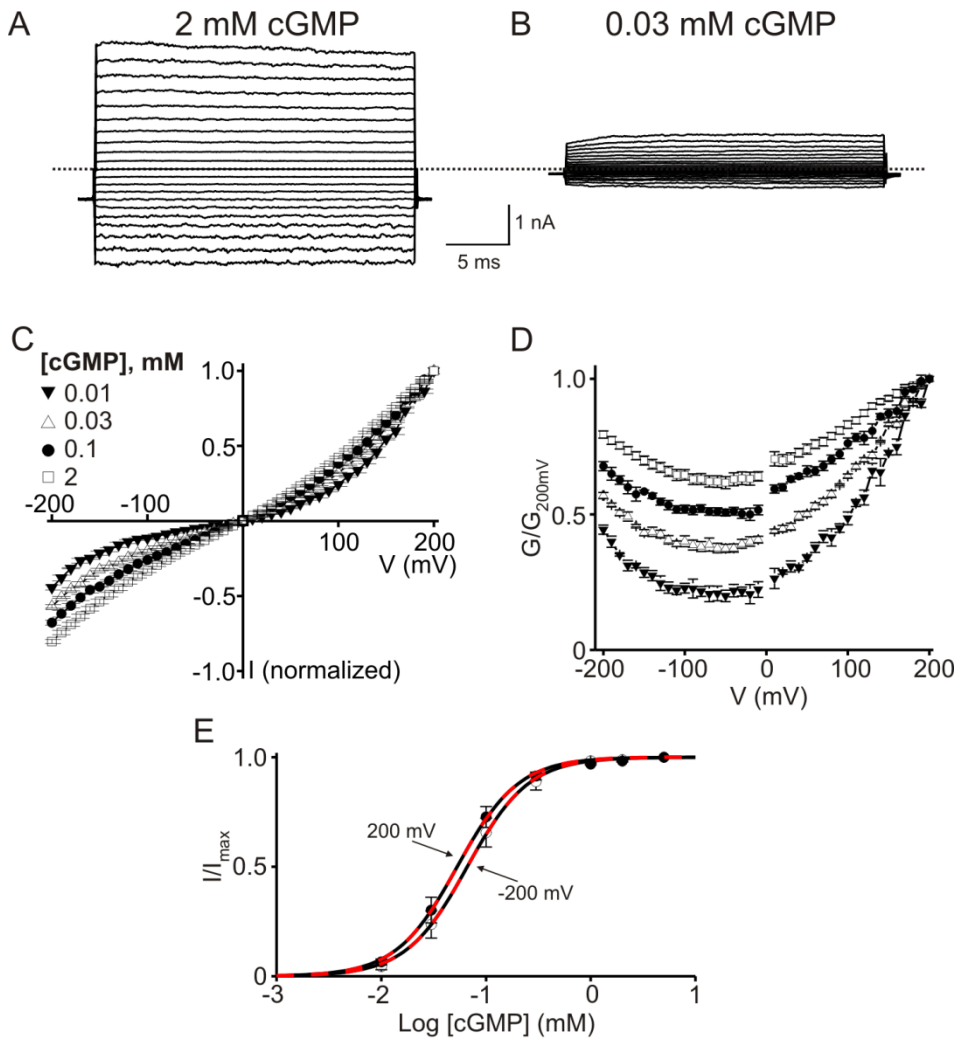
A
2 mM cGMP
B
0.03 mM cGMP
1 nA
5 ms
C
[cGMP], mM
0.01
0.03
0.1
2
1.0
0.5
-0.5
-1.0
-200
-100
100
200
V (mV)
I (normalized)
D
1.0
0.5
0
G/G200mV
-200
-100
0
100
200
V (mV)
E
1.0
0.5
0
I/Imax
200 mV
-200 mV
-3
-2
-1
0
1
Log [cGMP] (mM)

Figure 3.1

Figure 3.2. A point mutation in CNGA1's pore helix renders the channel voltage sensitive. (A) Partial crystal structure model of the Kv1.2-Kv2.1 chimeric channel (PDB 2R9R) featuring the pore helix and the selectivity filter in two diagonally opposite subunits. An oxygen in the side-chain of the chimera's D375 is hydrogen-bonded to the nitrogen of W362. (B-F) Left: macroscopic currents in 2 mM cGMP for the S350A, L351A, Y352A, S354A, and T355A mutants. Each current trace for Y352A or T355A is the average of 5 or 3 individual traces. Right: corresponding G-V curves (mean ± SEM, n = 4-6).

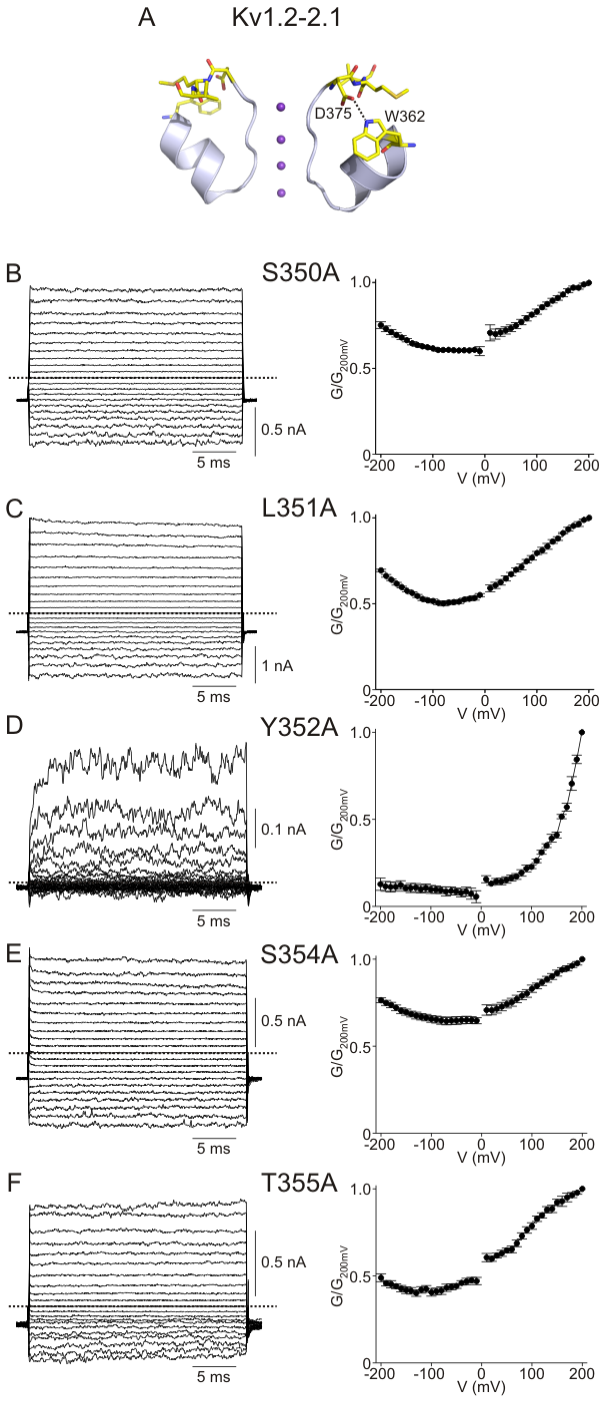
A
Kv1.2-2.1
D375
W362
B
S350A
0.5 nA
5 ms
C
L351A
1 nA
5 ms
D
Y352A
0.1 nA
5 ms
E
S354A
0.5 nA
5 ms
F
T355A
0.5 nA
5 ms
G/G200mV
V (mV)

Figure 3.2

Figure 3.3. Neutral E363 mutations undergo voltage gating. Macroscopic currents in 2 mM cGMP (left) and corresponding G-V curves (right; mean ± SEM, n = 4-6) for the CNGA1 mutants indicated. Currents were elicited by stepping from the -80 mV holding potential to voltages between -200 and 200 mV in 10-mV increments. For clarity, only traces every 20 mV are shown. Current traces for E363F, E363G, E363H, and E363P are averages of 3 - 5 individual traces. Dotted lines indicate zero current level.

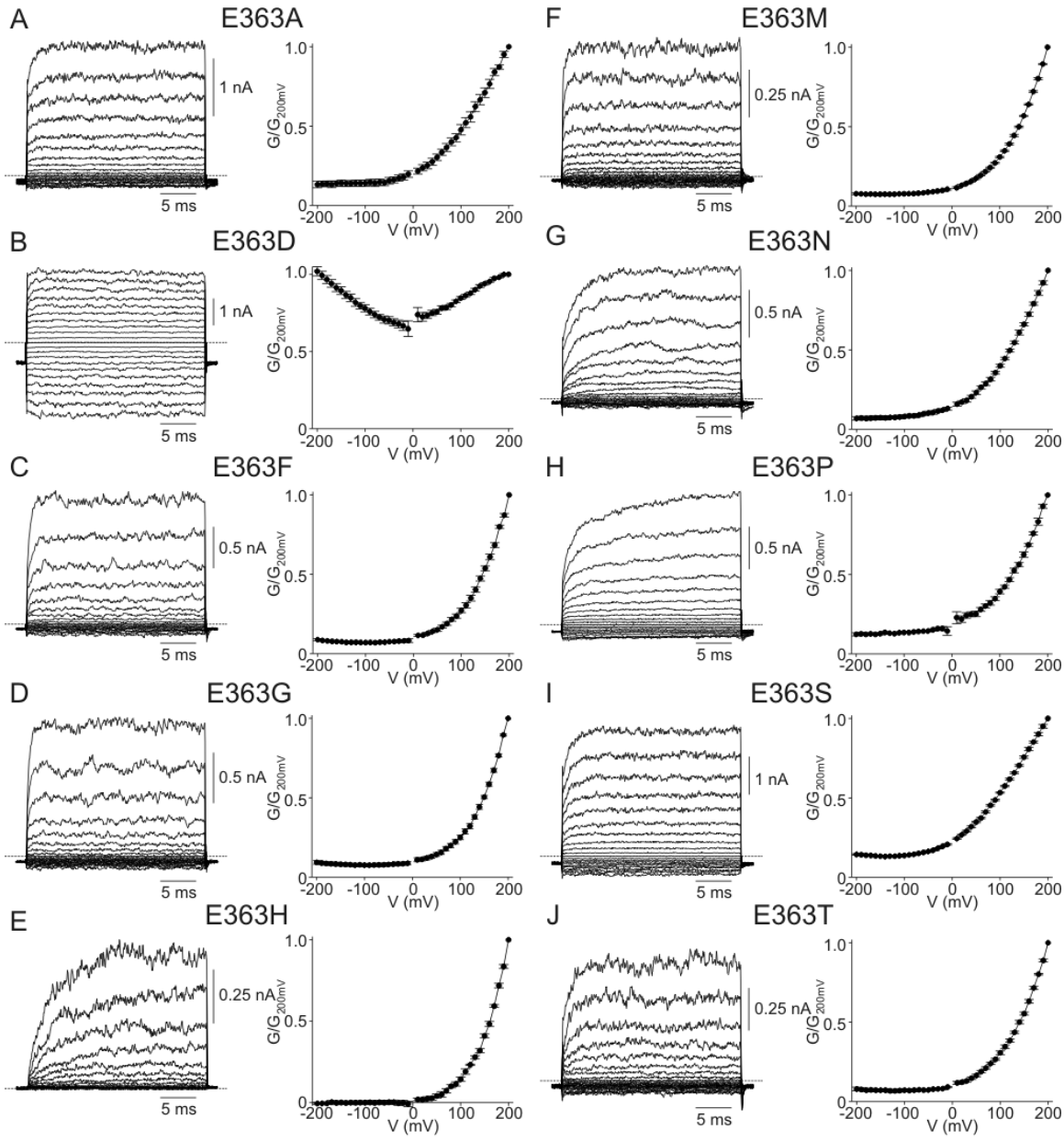
A
E363A
1 nA
5 ms
G/G200mV
V (mV)
F
E363M
0.25 nA
B
E363D
1 nA
G
E363N
0.5 nA
C
E363F
0.5 nA
H
E363P
0.5 nA
D
E363G
0.5 nA
I
E363S
1 nA
E
E363H
0.25 nA
J
E363T
0.25 nA

Figure 3.3

Figure 3.4. The E363Q mutant channel shows extreme outward rectification at saturating cGMP concentrations. (A, B) Macroscopic currents of the E363Q mutant in 2 mM (A) and 0.1 mM (B) cGMP. (C) G-V curves (mean ± SEM; n = 5) for 2 mM (open circles) and 0.1 mM (filled circles) cGMP. (D) I/I_{max} (mean ± SEM; n = 3-7) plotted against cGMP concentration for 40 mV (open circles) and 200 mV (filled circles). Black dashed curves are Hill equation fits with a common Hill coefficient (n), yielding EC_{50} = 163 ± 10 μM at 40 mV, EC_{50} = 65 ± 3 μM at 200 mV and n = 1.44 ± 0.01. Red dashed curves are fits of Eq. 3.1 to both data sets simultaneously, with a single adjustable K_L and all other parameters fixed (n = 1.44, $K_1 = 5 \times 10^{-3}$, K_2 = 1.04 and Z_{K2} = 0.58), which yield K_L = 166 ± 6 μM at 40 mV and K_L = 67 ± 2 μM at 200 mV.

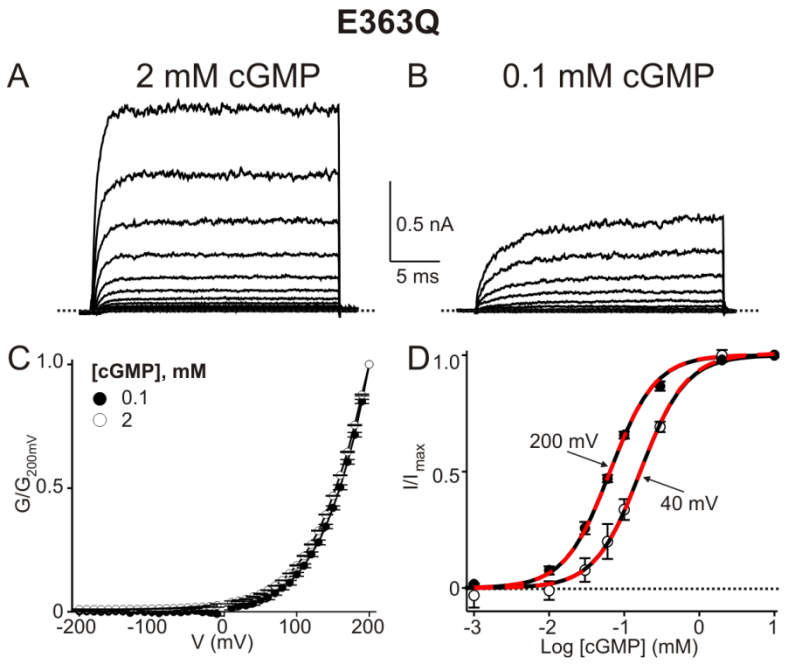
E363Q
A
2 mM cGMP
B
0.1 mM cGMP
0.5 nA
5 ms
C
[cGMP], mM
0.1
2
G/G200mV
V (mV)
D
200 mV
40 mV
I/Imax
Log [cGMP] (mM)

Figure 3.4

Figure 3.5. Macroscopic rectification of the E363Q mutant reflects voltage gating not asymmetric ion conduction. (A) Single-channel i-V curve (mean ± SEM; n = 4-7) of the E363Q mutant (filled circles) and the (arbitrarily scaled) macroscopic I-V curve (mean ± SEM; n = 5) in the presence of 2 mM cGMP (open circles). The dotted line through the single-channel data points is hand drawn. (B) Single-channel current amplitude of the E363Q mutant (mean ± s.e.m.; n = 5-20) at 120 mV or -120 mV and in the presence or absence of 0.1 mM extracellular Mg^{2+}. * indicates $P < 0.001$ (one-way ANOVA). (C-F) Representative single-channel currents of the E363Q mutant recorded at 120 mV (C, D) or -120 mV (E, F) and in the absence (C, E) or presence (D, F) of 0.1 mM extracellular Mg^{2+}; each trace was recorded from a separate inside-out patch. (G-J) Longer-duration macroscopic current traces recorded in 2 mM cGMP (G, H) from membrane patches of two oocytes expressing different densities of E363Q channels. Traces at -200 mV were magnified to show individual channel activity; the control traces recorded from the same patches at -200 mV and in the absence of cGMP are shown below (I, J).

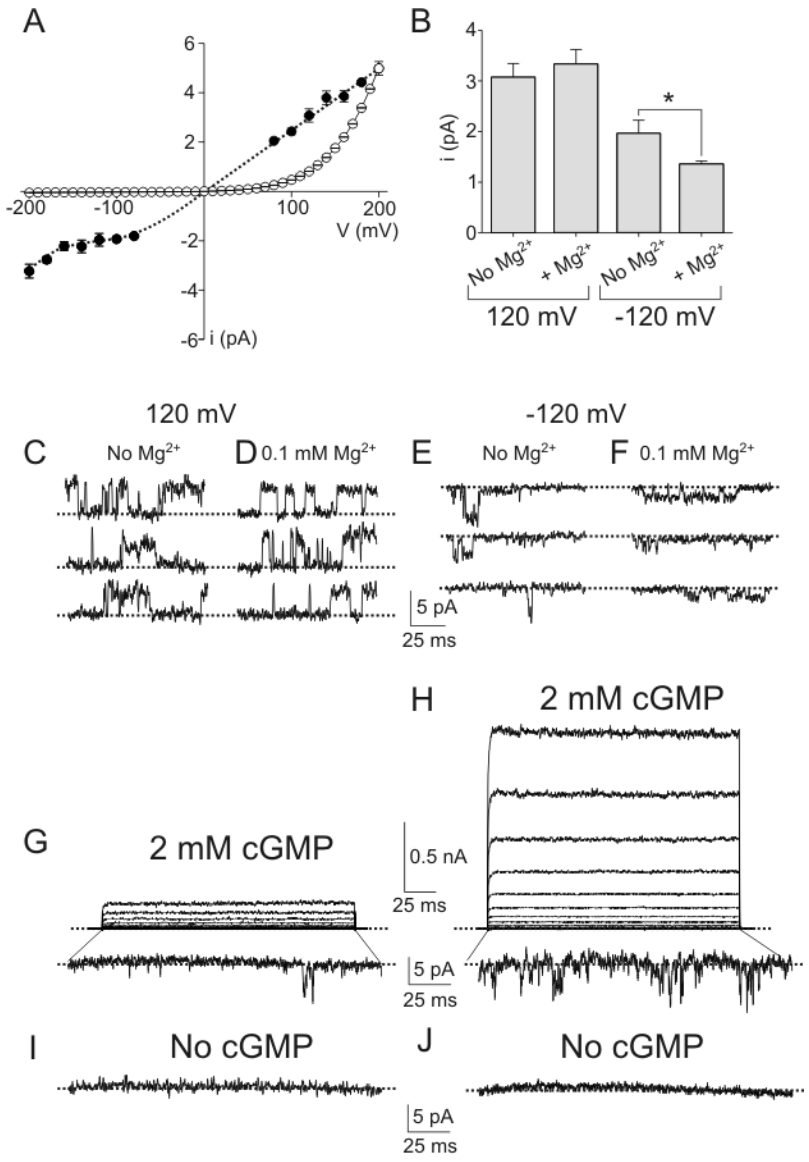
A
B
i (pA)
V (mV)
No Mg2+
+ Mg2+
120 mV
-120 mV
C
D 0.1 mM Mg2+
E
F 0.1 mM Mg2+
5 pA
25 ms
H
2 mM cGMP
G
0.5 nA
I
No cGMP
J

Figure 3.5

Figure 3.6. Gating effects of mutations at Y352 and E363 are not additive. (A) Macroscopic currents of the Y352A/E363Q double mutant in 2 mM cGMP; each trace is the average of 9 individual traces. (B) Corresponding G-V curve (mean ± SEM; n = 5). (C) Residual conductance (mean ± SEM; n = 4-5) at very negative voltages of the channels containing a single E363Q (squares) or Y352A (circles) mutation, or a Y352A/ E363Q double mutation (triangles).

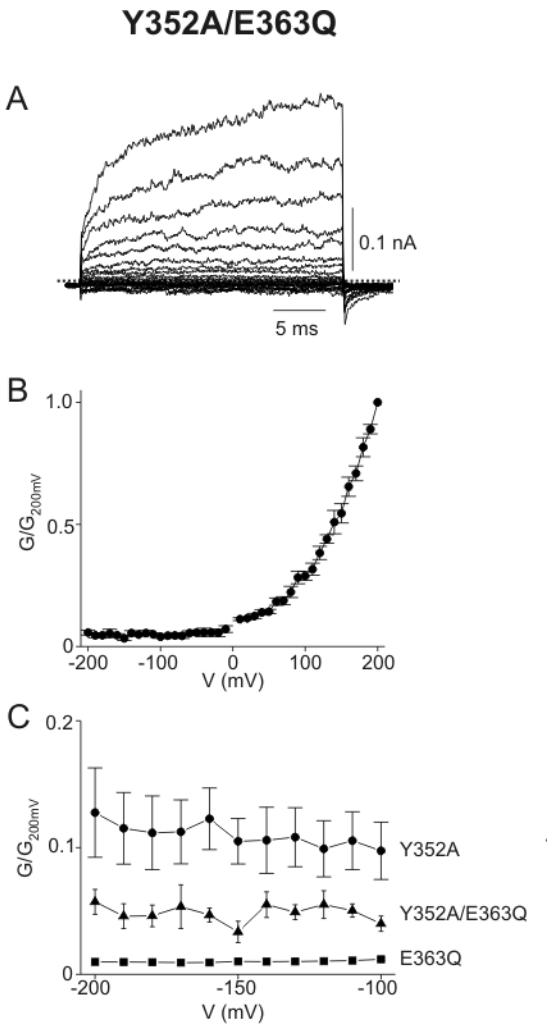
Y352A/E363Q
A
0.1 nA
5 ms
B
1.0
0.5
0
G/G200mV
-200
-100
0
100
200
V (mV)
C
0.2
0.1
0
G/G200mV
Y352A
Y352A/E363Q
E363Q
-200
-150
-100
V (mV)

Figure 3.6

Figure 3.7. S6 mutations and voltage gating. (A) Partial crystal structure model of the Kv1.2-Kv2.1 chimeric channel (PDB 2R9R) featuring the selectivity filter, the pore helix, and the external part of S6 in two diagonally opposite subunits. Residue numbers are those of the corresponding residues in CNGA1. Mutations at red- and grey-colored S6 residues produce voltage-gated and non-voltage-gated channels, respectively, whereas those at blue-colored ones produce non-conductive channels. (B-F) Macroscopic currents in 2 mM cGMP (left) and corresponding G-V curves (right; mean ± SEM, n = 3-7) for various CNGA1 mutants. The normalized conductance values were calculated from the current : electrochemical driving force ratio, except for those indicated by open circles in panel B, which were determined from isochronal tail-current measurements.

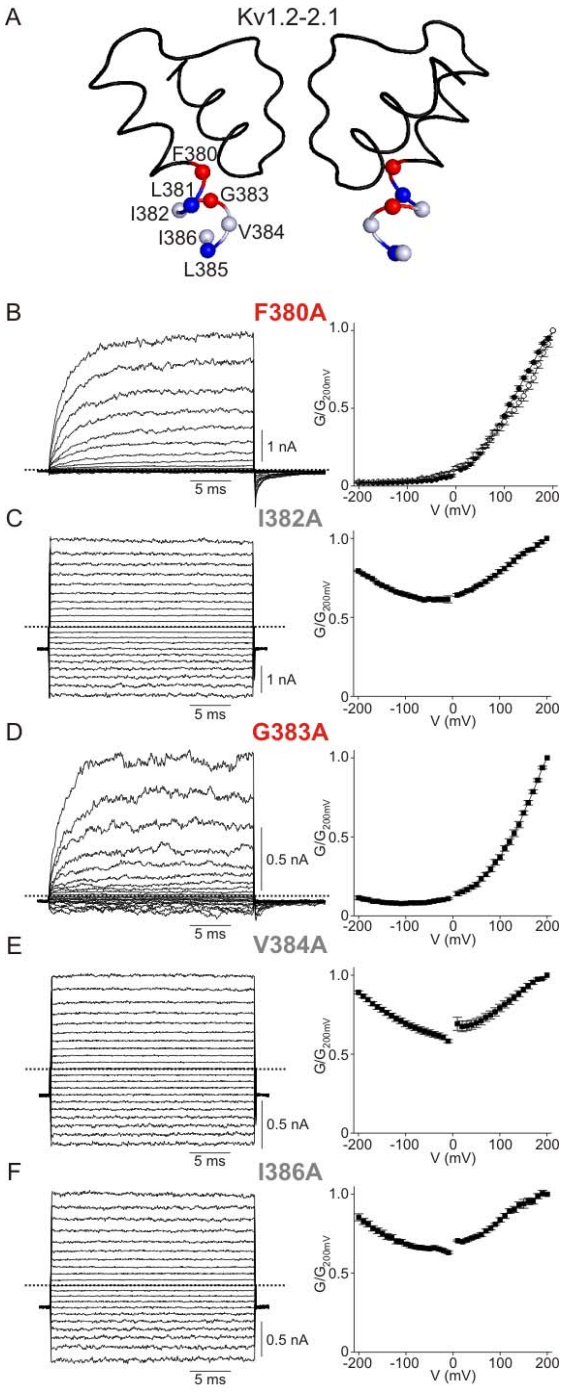
A
Kv1.2-2.1
F380
L381
G383
I382
I386
V384
L385
B
F380A
1 nA
5 ms
G/G200mV
V (mV)
C
I382A
1 nA
5 ms
D
G383A
0.5 nA
5 ms
E
V384A
0.5 nA
5 ms
F
I386A
0.5 nA
5 ms

Figure 3.7

Figure 3.8. Distribution pattern of point mutations that produce voltage gating in the CNGA1 channel. (A) Partial sequence alignment of the CNGA1 (GI 31342442) and Kv1.2 (GI 1235594) channels for the region in which the alanine scan was performed. Mutations at red- and yellow-colored positions produce strongly and modestly voltage-gated currents, respectively, whereas those at blue-colored ones produce no or unmeasurable currents. The remaining mutations (grey-colored positions) produce non-voltage-gated currents. Residues in the dashed box are absent from the crystal structure model of the Kv1.2-Kv2.1 chimeric channel. (B) Partial crystal structure model of the Kv1.2-Kv2.1 chimeric channel (PDB 2R9R) corresponding to the entire alignment shown in panel A, featuring the selectivity filter, the pore helix, and S6 in one subunit. Labeled positions (numbering is that of corresponding residues in CNGA1) indicate the mutations that produce voltage gated or partially voltage gated channels. Structure within the dashed box, absent from the crystal structure, is arbitrary. (C) I_{200}/I_{-200} (top) and I_{200}/I_{10} (bottom) values (mean ± SEM, n = 3-7) of mutant channels. Red bars signify $I_{200}/I_{-200} > 5$, yellow bars $4 > I_{200}/I_{-200} > 2.5$ and grey bars I_{200}/I_{-200} near unity in top panel, whereas in the bottom panel they signify $I_{200}/I_{10} > 95$, $85 > I_{200}/I_{10} > 45$ and $I_{200}/I_{10} < 35$, respectively, except for mutant F387A mutant (arrow) which is discussed in Results.

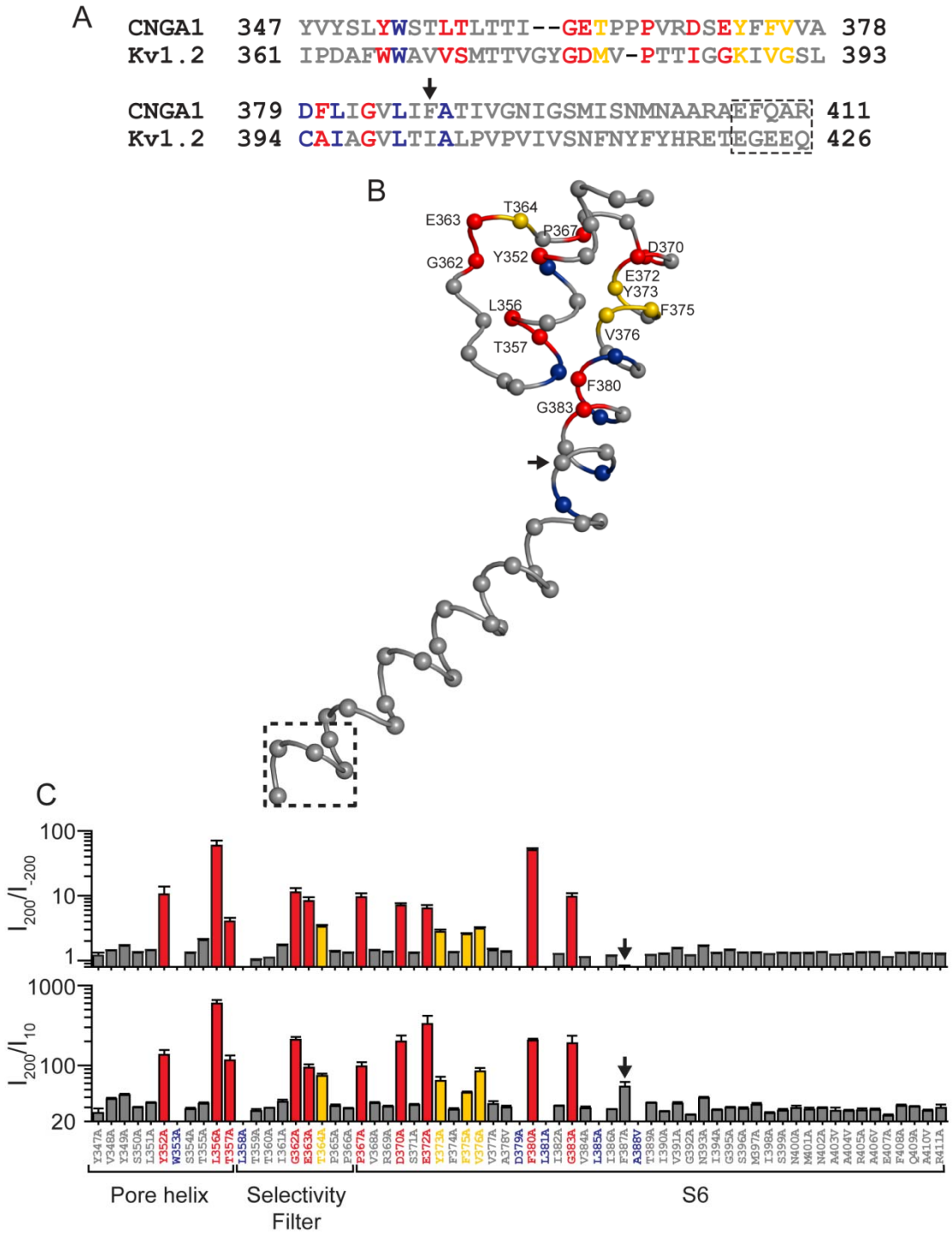
A
CNGA1 347 YVYSLYWSTLTLTTI--GETPPPVRDSEYFFVVA 378
Kv1.2 361 IPDAFWWAVVSMTTVGYGDMV-PTTIGGKIVGSL 393
CNGA1 379 DFLIGVLIFATIVGNIGSMISNMNAARAEFQAR 411
Kv1.2 394 CAIAGVLTIALPVPVIVSNFNYFYHRETEGEEQ 426
B
T364
E363
P367
D370
G362
Y352
E372
Y373
L356
F375
V376
T357
F380
G383
C
100
10
1
I200/I-200
1000
100
20
I200/I10
Pore helix
Selectivity Filter
S6

Figure 3.8

Figure 3.9. Alanine scan from the pore-helix to the N-terminus of the selectivity filter (Y347-T360). Macroscopic currents in 2 mM cGMP (left) and corresponding G-V curves (right; mean ± SEM., n = 4-7) for the CNGA1 mutants indicated. Current traces for Y352A, T355A, and T357A are averages of 3 - 10 individual traces.

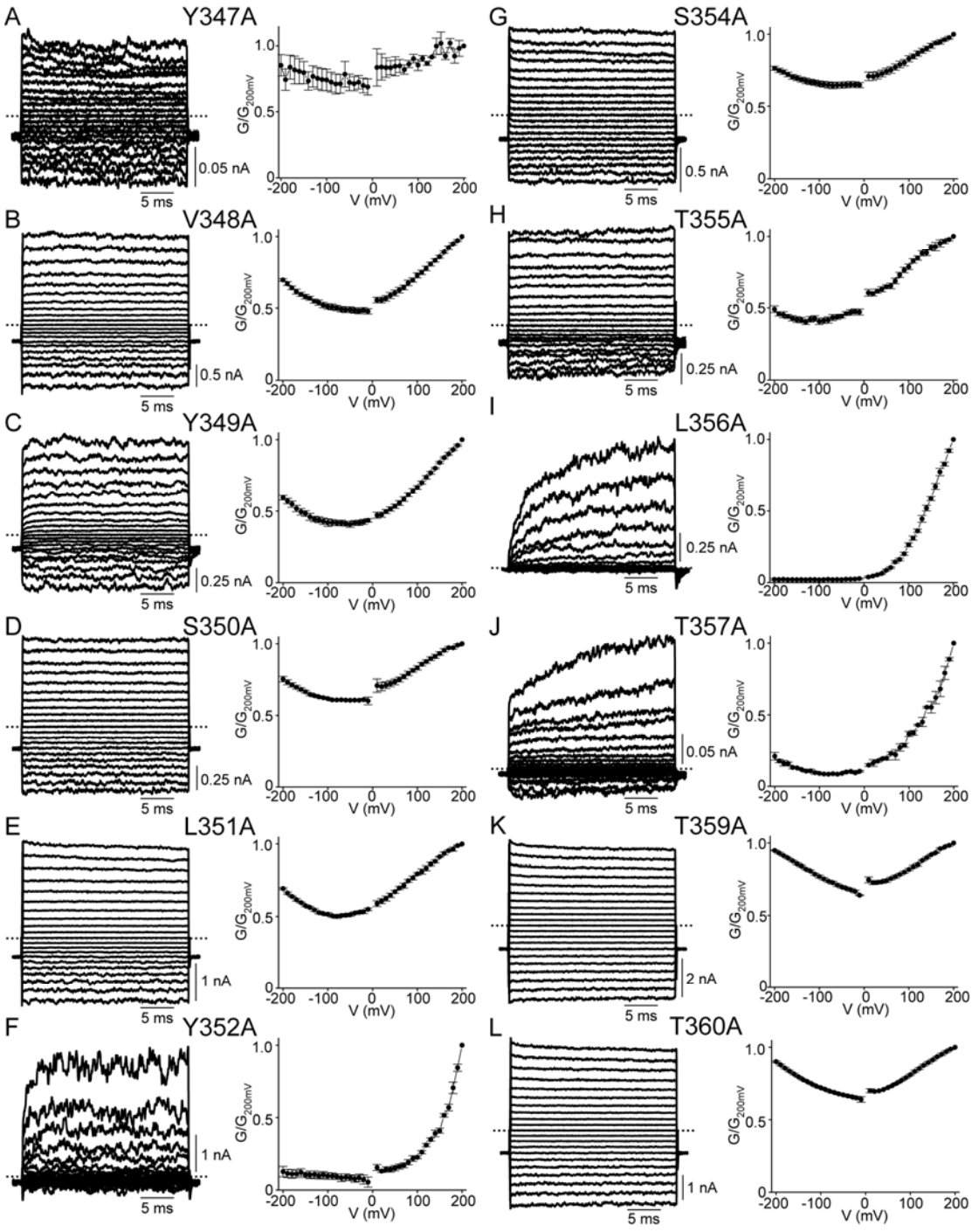
A
Y347A
0.05 nA
5 ms
B
V348A
0.5 nA
5 ms
C
Y349A
0.25 nA
5 ms
D
S350A
0.25 nA
5 ms
E
L351A
1 nA
5 ms
F
Y352A
1 nA
5 ms
G
S354A
0.5 nA
5 ms
H
T355A
0.25 nA
5 ms
I
L356A
0.25 nA
5 ms
J
T357A
0.05 nA
5 ms
K
T359A
2 nA
5 ms
L
T360A
1 nA
5 ms
G/G200mV
V (mV)
1.0
0.5
0
-200
-100
0
100
200

Figure 3.9

Figure 3.10. Alanine scan from the N-terminus of the selectivity filter to the N-terminus of S6 (I361-E372). Macroscopic currents in 2 mM cGMP (left) and corresponding G-V curves (right; mean ± SEM., n = 4-7) for the CNGA1 mutants indicated. Current traces for G362A, T364A, P367A, D370 and E372A are averages of 3 - 10 individual traces.

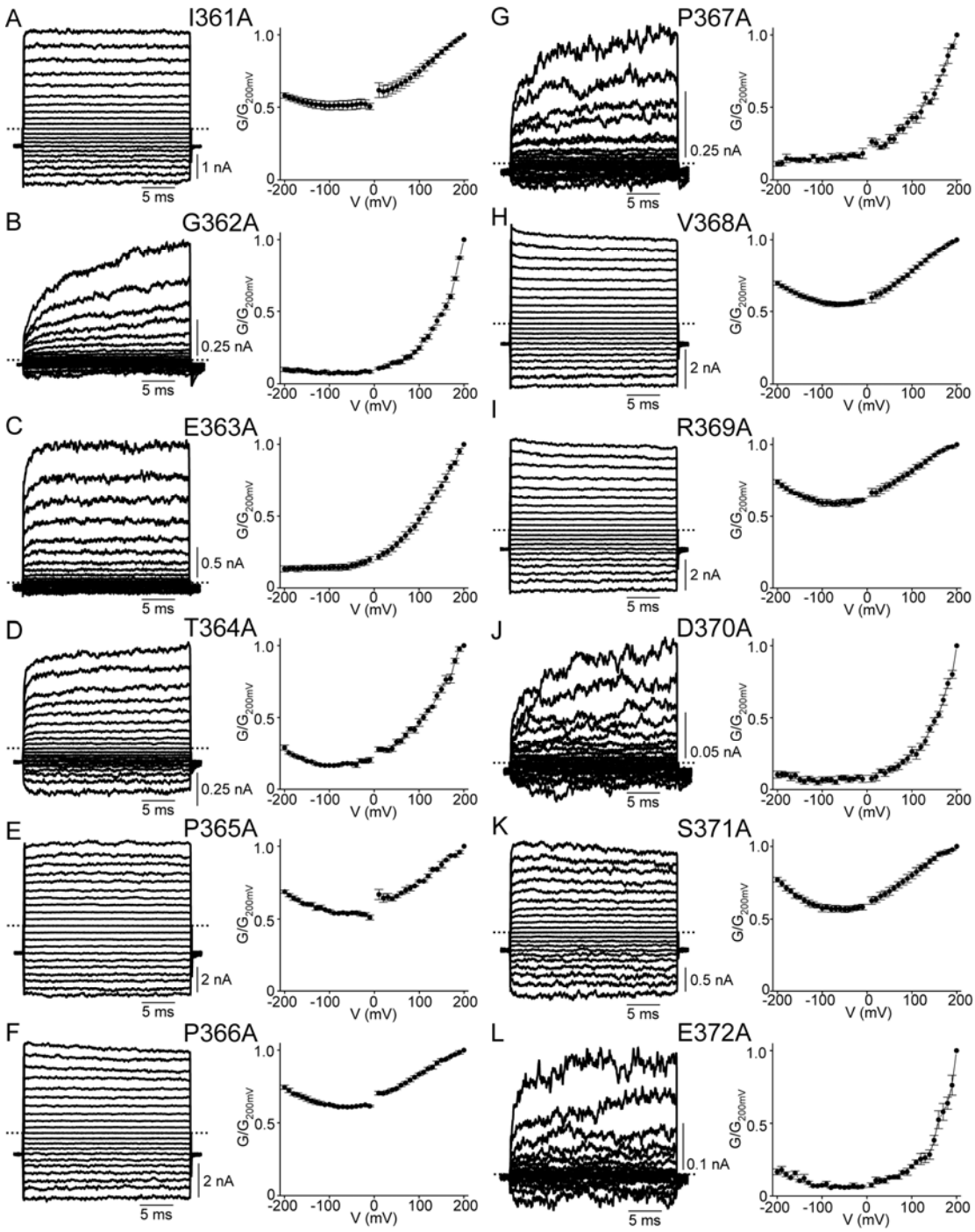
A
I361A
1 nA
5 ms
G/G200mV
V (mV)
B
G362A
0.25 nA
C
E363A
0.5 nA
D
T364A
0.25 nA
E
P365A
2 nA
F
P366A
2 nA
G
P367A
0.25 nA
H
V368A
2 nA
I
R369A
2 nA
J
D370A
0.05 nA
K
S371A
0.5 nA
L
E372A
0.1 nA

Figure 3.10

Figure 3.11. Alanine scan of S6 (Y373-F387). Macroscopic currents in 2 mM cGMP (left) and corresponding G-V curves (right; mean ± SEM, n = 4-7) for the CNGA1 mutants indicated. Current traces for Y373A and V376A are averages of 6 individual traces.

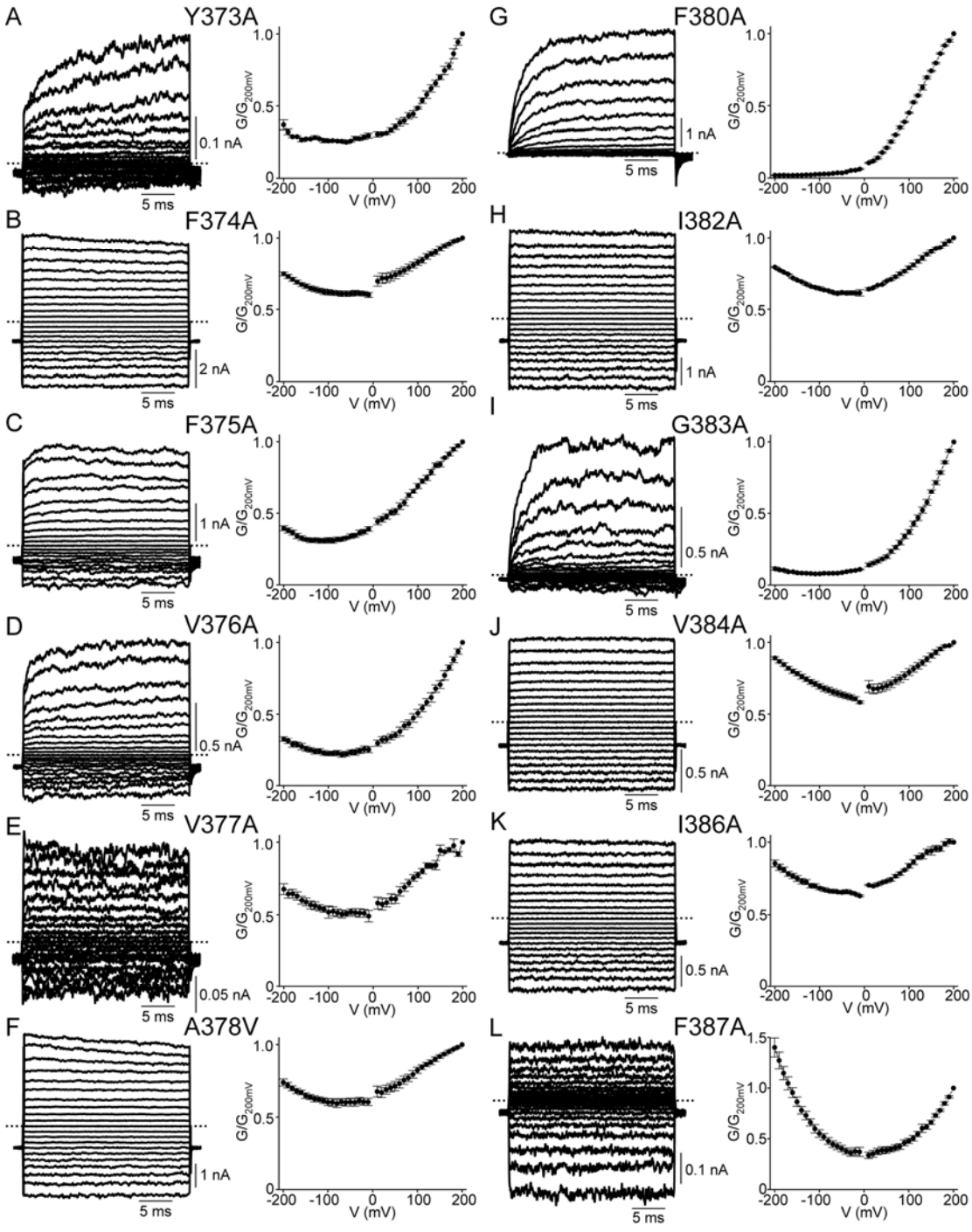
A
Y373A
0.1 nA
5 ms
G/G200mV
V (mV)
B
F374A
2 nA
C
F375A
1 nA
D
V376A
0.5 nA
E
V377A
0.05 nA
F
A378V
1 nA
G
F380A
H
I382A
I
G383A
0.5 nA
J
V384A
K
I386A
L
F387A
0.1 nA

Figure 3.11

Figure 3.12. Alanine scan of S6 (T389-N400). Macroscopic currents in 2 mM cGMP (left) and corresponding G-V curves (right; mean ± SEM, n = 3-7) for the CNGA1 mutants indicated.

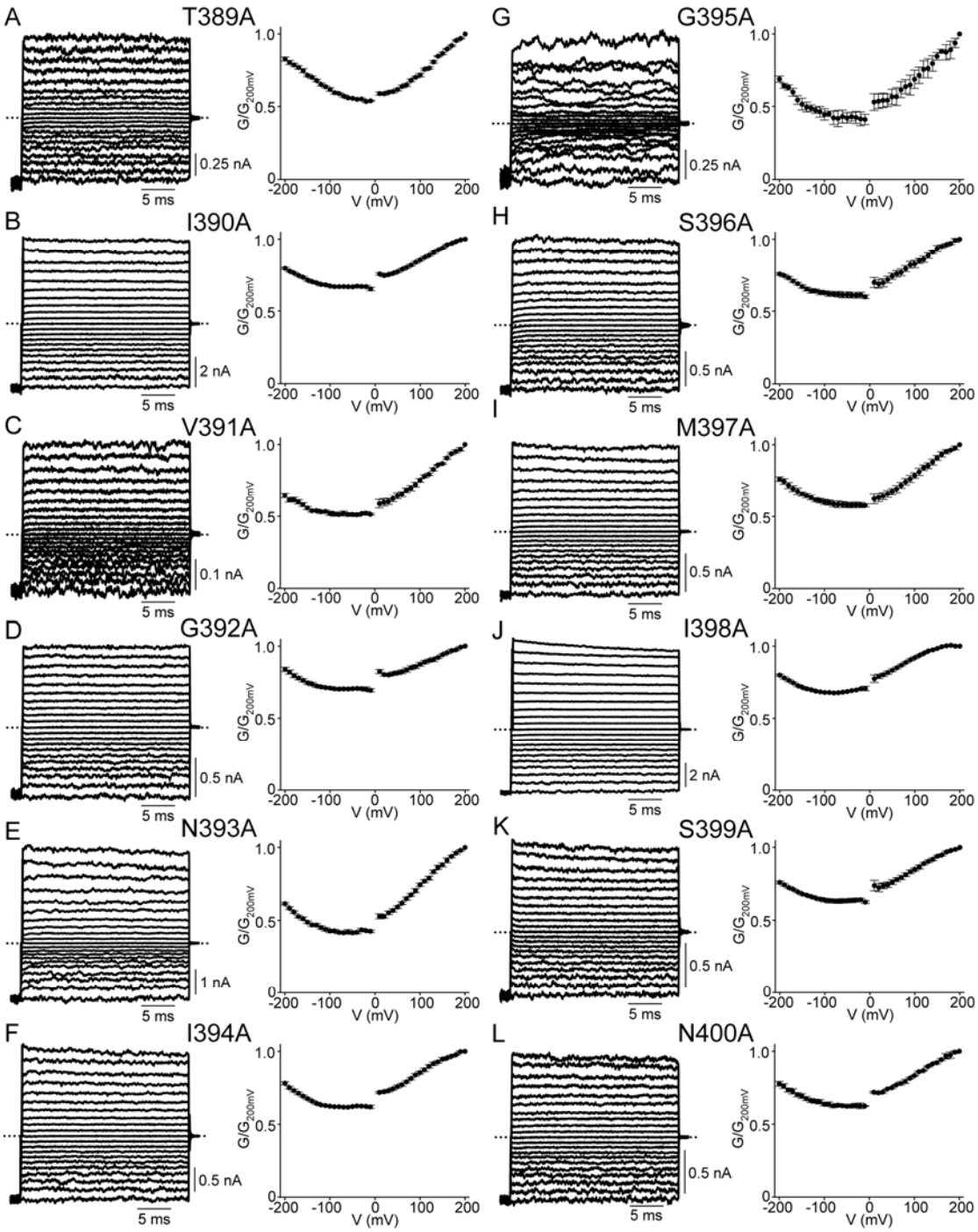
A
T389A
0.25 nA
5 ms
G/G200mV
V (mV)
B
I390A
2 nA
C
V391A
0.1 nA
D
G392A
0.5 nA
E
N393A
1 nA
F
I394A
0.5 nA
G
G395A
0.25 nA
H
S396A
0.5 nA
I
M397A
0.5 nA
J
I398A
2 nA
K
S399A
0.5 nA
L
N400A
0.5 nA

Figure 3.12

Figure 3.13. Alanine scan of S6 (M401-R411). Macroscopic currents in 2 mM cGMP (left) and corresponding G-V curves (right; mean ± SEM, n = 4) for the CNGA1 mutants indicated.

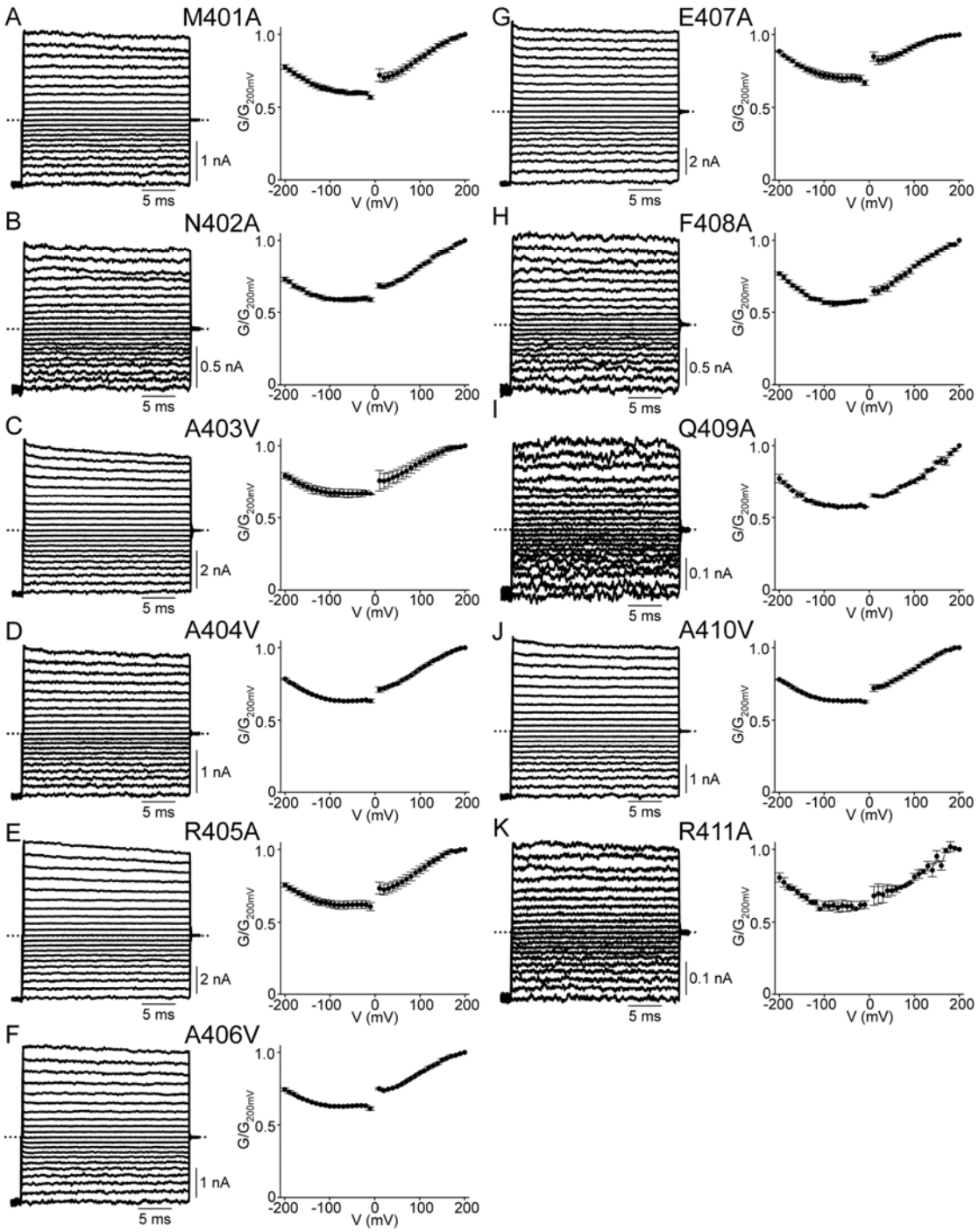
A
M401A
1 nA
5 ms
G/G200mV
V (mV)
B
N402A
0.5 nA
C
A403V
2 nA
D
A404V
1 nA
E
R405A
2 nA
F
A406V
1 nA
G
E407A
2 nA
H
F408A
0.5 nA
I
Q409A
0.1 nA
J
A410V
1 nA
K
R411A
0.1 nA

Figure 3.13

Figure 3.14. Voltage-dependent block of wild-type and mutant CNGA1 channels by intracellular PhTx. (A-F) I-V curves (mean ± SEM; n = 4-6) of wild-type (WT) and mutant channels in the presence (open circles) and absence (filled circles) of 10 μM intracellular PhTx. (G) Fraction of current not blocked (I/I_o; mean ± SEM; n = 4-6) by 10 μM PhTx for wild-type and mutant channels, plotted against membrane voltage. Curves are fits of a Boltzmann function, $I/I_o = 1/(1 + [PhTx]/^{app}K_d exp^{-ZFV/RT})$; the fitted parameter values are listed in Table 3.1.

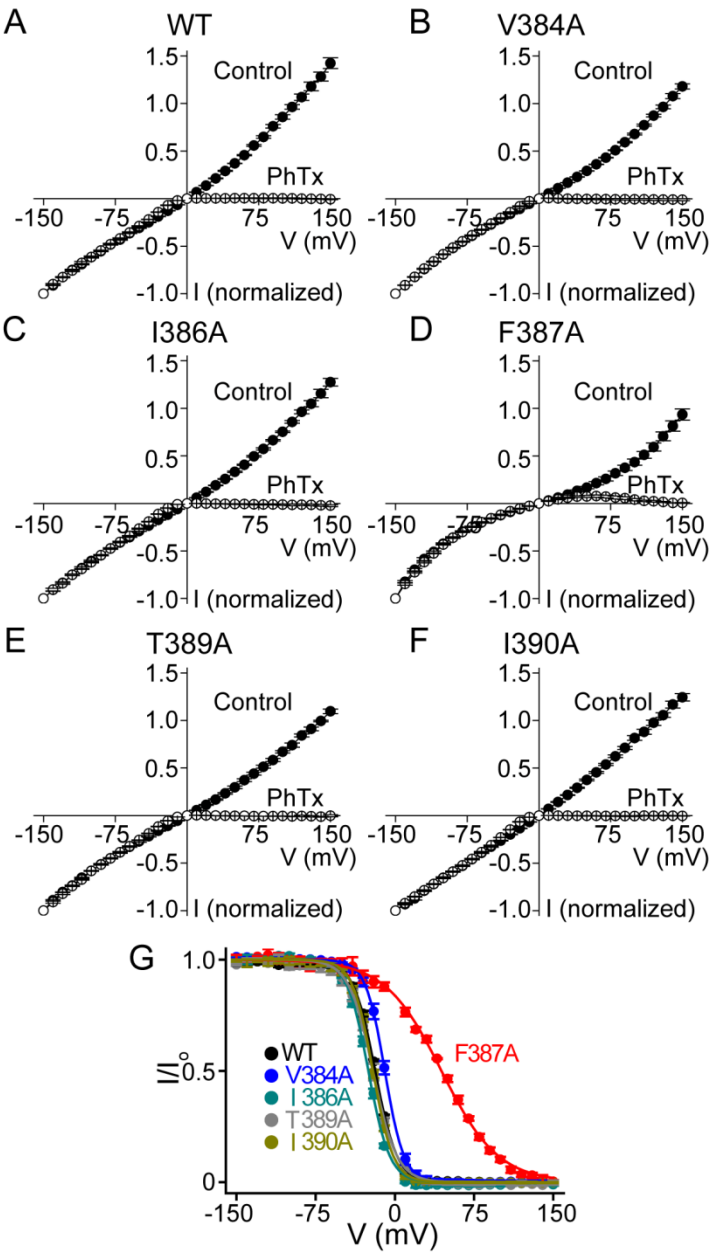
A
WT
B
V384A
C
I386A
D
F387A
E
T389A
F
I390A
Control
PhTx
1.5
1.0
0.5
-0.5
-1.0
-150
-75
75
150
V (mV)
I (normalized)
G
I/I°
WT
V384A
I 386A
T389A
I 390A
F387A
0
V (mV)

Figure 3.14

Figure 3.15. Simulations of wild-type and F387A mutant I-V curves. (A, B) Energy profiles of a permeation model with three ion sites (Begenisich and Cahalan, 1980; Begenisich and Smith, 1984), where the free energy (in RT units) is plotted against the assumed linearly related physical and electric transmembrane distance for wild type (A) and F387A mutant channels (B). (C) I-V relations for wild-type (black) and mutant (red) channels (taken from Fig. 3.14), where curves correspond to the models in A and B.

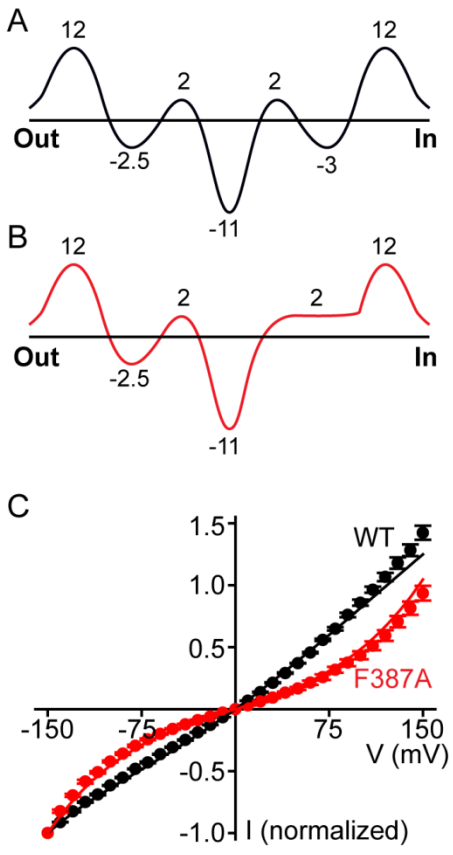
A
12
12
2
2
Out
In
-2.5
-3
-11
B
12
12
2
2
Out
In
-2.5
-11
C
1.5
1.0
0.5
WT
F387A
-150
-75
75
150
V (mV)
-0.5
-1.0
I (normalized)

Figure 3.15

Figure 3.16. Effect of S4 mutations on voltage gating induced by the E363Q mutation. (A-C) Macroscopic currents recorded in 2 mM cGMP from E363Q mutant channels containing an additional substitution in S4: R272T (R2T; A), R275Q (R3Q; B), or R278Q (R4Q; C). (D) G-V curves (mean ± SEM; n = 3-8) for the E363Q mutants without (open squares) or with an additional S4 substitution: R272T (filled circles), R275Q (open triangles), or R278Q (filled inverted triangles). The four curves are superimposed.

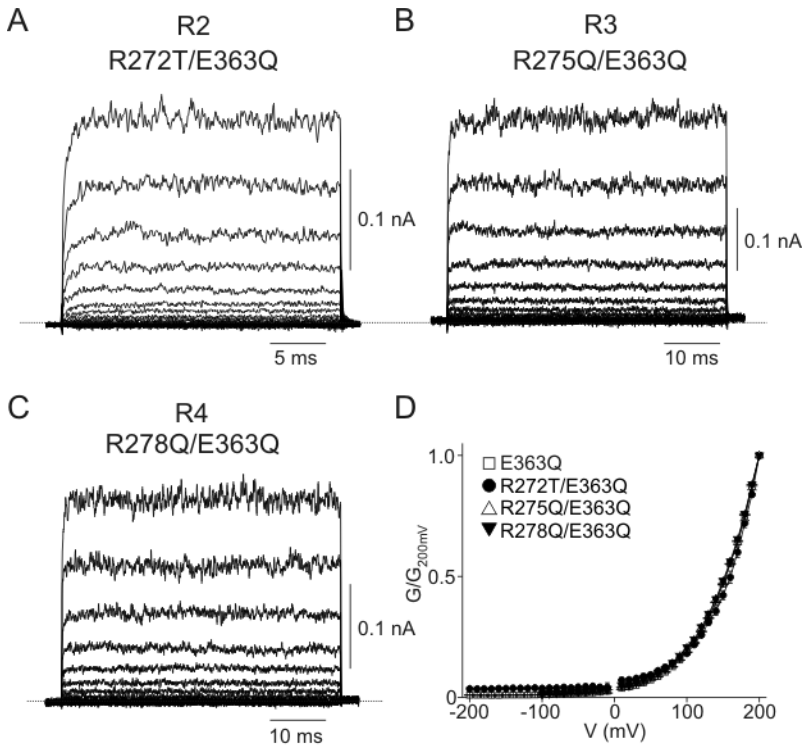
A
R2
R272T/E363Q
0.1 nA
5 ms
B
R3
R275Q/E363Q
0.1 nA
10 ms
C
R4
R278Q/E363Q
0.1 nA
10 ms
D
E363Q
R272T/E363Q
R275Q/E363Q
R278Q/E363Q
G/G200mV
1.0
0.5
0
-200
-100
0
100
200
V (mV)

Figure 3.16

Figure 3.17. Voltage dependence of the activation of E363Q mutant channels exposed to a saturating cGMP concentration. (A) Semi-logarithmic plot of relative conductance against voltage between 10 mV and 200 mV (taken from Fig. 3.4 C). The data points from 10 to 150 mV were fitted with a straight line, yielding a valence of 0.47 ± 0.01 (mean ± SEM, n = 5); the rest of the line was extrapolated. (B) Entire G-V curve (mean ± SEM; n = 5) of the E363Q mutant in the presence of 2 mM cGMP taken from Fig. 3.4 C. Black curve superimposed on the plot of relative conductance against voltage is a Boltzmann function fit yielding $Z = 0.51 \pm 0.01$ and $V_{1/2} = 240 \pm 7$ mV. Red dashed curve is a simulation of Eq. 3.2 with $K_1 = 5 \times 10^{-3}$, $K_2 = 1.04$, and $Z_{K2} = 0.58$ (taken from Table 3.2). The asymptotic maximum was rescaled to one to produce the plot.

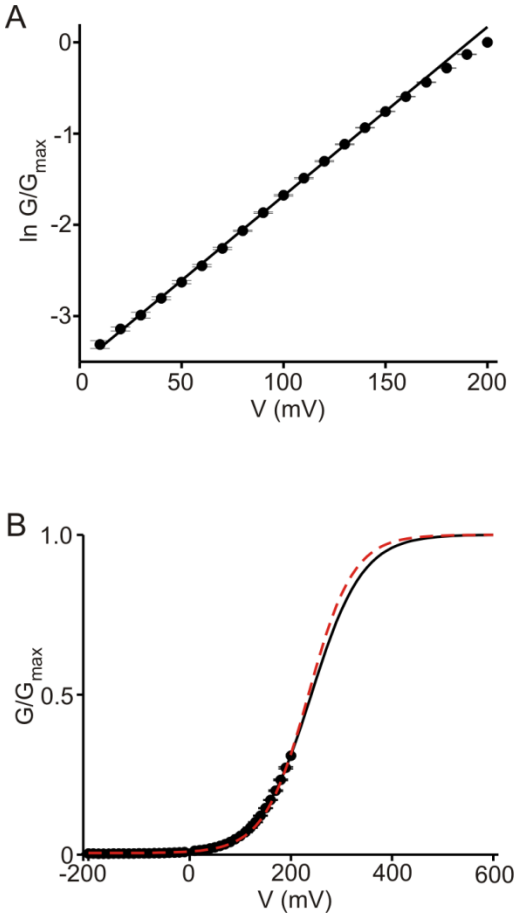
A
0
-1
-2
-3
ln G/G_max
0
50
100
150
200
V (mV)
B
1.0
0.5
0
G/G_max
-200
0
200
400
600
V (mV)

Figure 3.17

Figure 3.18. Analysis of voltage gating of wild-type and E363 mutants. (A-C) Schemes representing gating of the CNGA1 channel, in which C and C_L represent closed channel states without and with cGMP bound, respectively, whereas O_1 and O_2 (lumped into a single open state in A) are two sequential open states in voltage-sensitive equilibrium. (D) G-V relations (mean ± SEM, n = 4-7) between 10 mV and 200 mV for wild-type and E363 mutant channels. Curves correspond to a simultaneous fit of Eq. 3.2 to the data sets with common K_2. Best-fit parameters were (common) $K_2 = 1.04 \pm 0.14$, and individual K_1 and Z_{K2} values for each mutant (listed in Table 3.2). (E) Z_{K2} for each wild-type and mutant channel plotted against the channel's K_1, both obtained from the simultaneous fit described above and listed in Table 3.2. (F) G-V relations (mean ± SEM, n = 4-7) between 10 mV and 200 mV for WT and E363Q channels at saturating and subsaturating cGMP concentrations (taken from Figs. 3.1 D and 3.4 C). Curves are fits of Eq. 3.1 with adjustable parameters $K_L = 78 \pm 4$ μM and $n = 1.44 \pm 0.06$. Fixed parameters are $K_2 = 1.04$ (taken from panel D, common to all curves), $K_1 = 0.62$ and $Z_{K2} = 0.25$ for WT, and $K_1 = 5 \times 10^{-3}$ and $Z_{K2} = 0.58$ for E363Q channels (taken from Table 3.2).

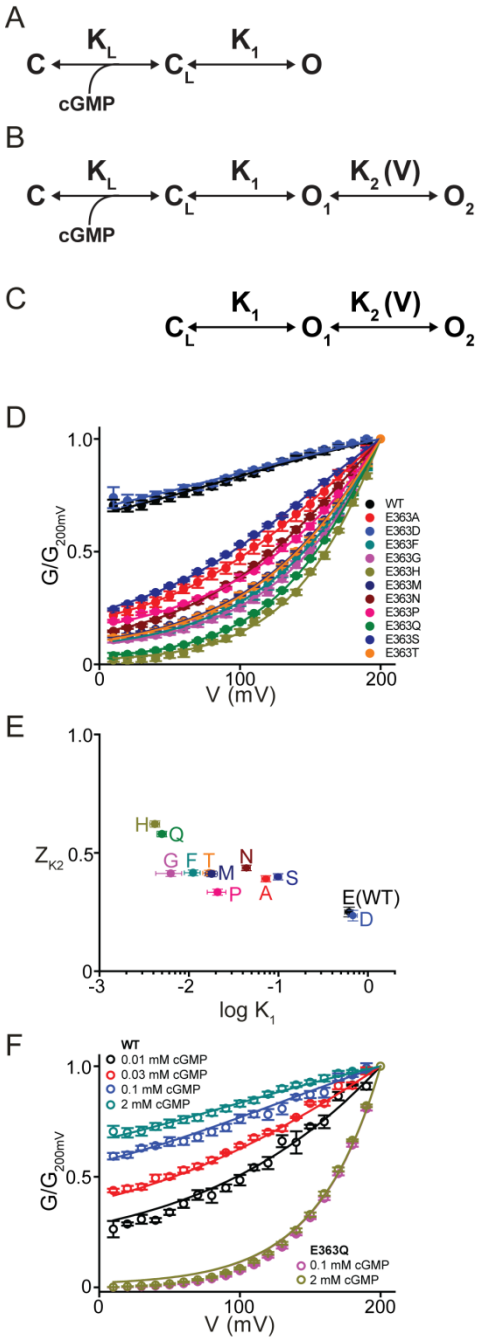
A
C
K_L
C_L
K_1
O
cGMP
B
C
K_L
C_L
K_1
O_1
K_2 (V)
O_2
cGMP
C
C_L
K_1
O_1
K_2 (V)
O_2
D
G/G_200mV
1.0
0.5
0
0
100
200
V (mV)
WT
E363A
E363D
E363F
E363G
E363H
E363M
E363N
E363P
E363Q
E363S
E363T
E
Z_K2
1.0
0.5
0
H
Q
G
F
T
M
N
S
P
A
E(WT)
D
-3
-2
-1
0
log K_1
F
G/G_200mV
1.0
0.5
0
WT
0.01 mM cGMP
0.03 mM cGMP
0.1 mM cGMP
2 mM cGMP
E363Q
0.1 mM cGMP
2 mM cGMP
0
100
200
V (mV)

Figure 3.18

Table 3.1

Best-fit values obtained from Fig. 3.14 G

Channels	$^{app}K_d$ (M)	**Z**
WT	$1.6 \pm 0.1 \times 10^{-6}$	2.48 ± 0.07
V384A	$3.5 \pm 0.2 \times 10^{-6}$	2.81 ± 0.09
I386A	$8.3 \pm 0.6 \times 10^{-7}$	2.55 ± 0.07
F387A	$5.2 \pm 0.2 \times 10^{-5}$	0.96 ± 0.02
T389A	$1.6 \pm 0.1 \times 10^{-6}$	2.25 ± 0.06
I390A	$1.2 \pm 0.1 \times 10^{-6}$	2.67 ± 0.08

Table 3.2

Best-fit values of Eq. 3.2

Channels	$\mathbf{K}_1$	$\mathbf{Z}_{K2}$
WT	$6.2 \pm 0.6 \times 10^{-1}$	0.25 ± 0.02
E363A	$7.2 \pm 0.7 \times 10^{-2}$	0.39 ± 0.01
E363D	$6.8 \pm 0.8 \times 10^{-1}$	0.23 ± 0.02
E363F	$1.1 \pm 0.2 \times 10^{-2}$	0.42 ± 0.01
E363G	$6.3 \pm 2.0 \times 10^{-3}$	0.41 ± 0.01
E363H	$4.2 \pm 0.5 \times 10^{-3}$	0.62 ± 0.01
E363M	$1.8 \pm 0.3 \times 10^{-2}$	0.41 ± 0.01
E363N	$4.4 \pm 0.5 \times 10^{-2}$	0.44 ± 0.01
E363P	$2.1 \pm 0.5 \times 10^{-2}$	0.33 ± 0.01
E363Q	$5.0 \pm 0.9 \times 10^{-3}$	0.58 ± 0.01
E363S	$9.9 \pm 0.9 \times 10^{-2}$	0.40 ± 0.01
E363T	$1.7 \pm 0.3 \times 10^{-2}$	0.41 ± 0.01

Chapter 4

Conclusions and future directions

This thesis addresses two mechanisms of CNG channel function: voltage-dependent block and suppression of the inherent voltage gating in these channels. In this chapter, I will recapitulate the conclusions of the previously presented studies and will discuss possible future directions to gain further understanding of these features of the channel.

4.1 Mechanism of voltage-dependence of pore block in a retinal CNG channel.

Two models have been proposed to explain the voltage dependence of ion channel block. One model, which has been predominantly used for three decades, postulates that the voltage-dependence of block is directly conferred to a charged blocker as it binds in the transmembrane electric field and is therefore an intrinsic property of the blocking process (Woodhull, 1973). This model predicts that the extent of block increases with membrane depolarization in the entire voltage range, as described by a Boltzmann function (Eq. 2.1; see also Fig. 2.13). An alternate model assumes that the blocker does not bind in the electric field, and the voltage dependence reflects the displacement of the permeant ions across the field by the blocker and is therefore an extrinsic property of the blocking process (Armstrong, 1971). This model predicts that strong depolarization lowers the permeant ion occupancy in the pore, and the blocker can then bind in the pore

without the need to displace permeant ions across the electric field. In this case, the apparent voltage dependence of channel block will decrease, approaching zero, with depolarization (Fig. 2.13). By blocking CNGA1 channels with PhTx which binds in the electric field, we showed that its block is indeed described by a Boltzmann function, however, when we blocked the channels with QAs that do not interact with the electric field their block deviated markedly from a Boltzmann function at depolarized voltages. This is the key experimental observation that allows the biophysical distinction of these two types of blocker interactions in the pore of ion channels.

Block by intracellular PhTx requires a model of at least two blocked states, similar to polyamine block of inward-rectifier channels (Shin and Lu, 2005; Shin et al., 2005). If we consider a minimal model in which these two states are arranged in sequence (Fig. 2.14 A), formation of the first (shallow) blocked state is practically voltage independent, and most voltage dependence occurs during the transition between the two blocked states. We also showed that QA block in these channels produces at least two sequential blocked states. One important consequence of the sequential blocked mechanism is that the apparent blocking kinetics do not directly relate to the channel open probability unless the gate is located at or before the first blocked state. Thus, the channel-blocking rate cannot be automatically used to probe the gating transition, an approach that is currently widely used. This observation thus serves as a warning in future studies that seek to relate kinetic measurements of block with molecular movements in the channel protein.

If the two sequential blocker sites are physically separate, they should be able to be differentially perturbed by point mutations in the pore of the channel. In other words,

mutations in specific residues lining the pore of the channel should only affect the affinity of a blocker for the shallow or the deep sites. By doing systematic mutagenesis, these particular residues could be located to delineate the blocker binding sites. The relevant mutations underlying the binding sites could be identified as they would cause an alteration in the equilibrium constant describing blocker binding to the shallow (K_{B1}) or the deep site (K_{B2}; Fig. 2.14 D) of the mutant channel compared to wild-type. In this way, by making point mutations along S6 one could obtain physical evidence for the two separate blocker binding sites.

4.2 Mutations bring about voltage sensitivity in the CNGA1 channel

During our studies of voltage-dependent block, we found that certain point mutations around the extracellular part of the CNGA1 channel pore produced mutant channels that displayed voltage gating. This observation interested us because it is unknown why CNGA1 channels exhibit only very modest voltage sensitivity, even though they have the analogous structure as Kv channels. The suppression of the inherent voltage sensitivity of the CNGA1 channel is physiologically important because the channels could be unable to open at the physiological voltages where they normally operate (-65 to -35 mV).

By analyzing the effect of point mutations in the conductance of the CNGA1 channel we observed the following. First, a number of mutations render the channels voltage gated in the presence of a saturating concentrations of cGMP. Second, those mutations are exclusively confined within the region around the ion selectivity filter. Third, the voltage sensitivity is not affected by neutralizing the positively charged

residues in the S4. These observations led us to conclude that mutations that bring out voltage gating loosen the attachment the selectivity filter to the surrounding structure. Several lines of evidence support the notion that proper attachment of the selectivity filter is important for proper gating in different types of channels (Seebohm et al., 2003; Kurata and Fedida, 2006). A point mutation in Kv2.1 or KcsA channels, at a residue corresponding to E363 in CNGA1, affects gating of those K^+ channels at the single-channel level by destabilizing the open state (Chapman et al., 2006; Cordero-Morales et al., 2006b). Furthermore, mutations in the selectivity filter and pore helix of other types of K^+ channels also have dramatic effects on the gating behavior (Ficker et al., 1998; Lu et al., 2001; Yifrach and MacKinnon, 2002; Alagem et al., 2003). Interestingly, a point mutation in the selectivity filter of the CNGA3 channel expressed in cone photoreceptors is associated with achromatopsia (Tränkner et al., 2004), an autosomal recessively inherited retinal disorder (Sharpe et al., 1999). This mutation produces a homomeric channel that has altered single channel gating properties. Similarly, mutations in or near the selectivity filter in CNGA1 channels produce altered single-channel gating behavior (Sesti et al., 1995; 1996; Bucossi et al., 1996; 1997; Fodor et al., 1997; Becchetti et al., 1999; Contreras et al., 2008). These observations, taken together with our studies, reinforce the notion that proper attachment of the selectivity filter is crucial for the correct physiological function of ion channels.

By loosening the attachment of the selectivity filter to the surrounding structure, mutations could decrease the probability of the filter to remain in a stable, conducting conformation. These mutations would thus bias the gating equilibrium toward closed states, and voltage would help stabilize an open state of the selectivity filter. This would

give rise to apparent voltage gating of the channel. Voltage sensitivity may arise from two sources. First, ion movement associated with the conformational change of the filter where the electric field drops steeply. Second, through the movement of the dipole moment of the pore helix which is located in a low-dielectric environment (Roux and MacKinnon, 1999). We show that the voltage sensitivity of the mutant channels can be well described by a minimal three-state model (Fig. 3.18 C) where the voltage sensitivity is associated with the transition between two open states. In this model, the binding of cGMP only allows the mutant channel (with an unstable selectivity filter) to enter an unstable open state, whereas strong depolarization switches this unstable state to a more stable open state.

In future studies, it would be interesting to determine the contribution to the voltage gating process coming from movement of ions in the pore and that coming from rearrangements of the pore helix structure. For example, one could analyze single-channel currents using K^+ or Rb^+ as permeant ions. These ions permeate more slowly than Na^+ and stabilize the channel in the open conformation (Holmgren, 2003; Kusch et al., 2004). If permeating ions indeed help stabilize the pore of the voltage sensitive mutant channels and such stabilization is related to voltage gating, then an apparent decrease in the voltage sensitivity (an increase in K_1) would be expected in the presence of ions that permeate more slowly. Alternatively, if movements of the side chains of the pore helix or movements of the helix itself contribute to the observed voltage sensitivity, mutating residues in the pore helix to charged ones could result in an altered Z_{K2} value of the G-V relation.

By engineering salt bridges between residues it would be possible to show

specific interactions between residues whose mutation produces voltage gating. For example, by determining if a E363K/Y352D double mutant channel displays voltage gating. If such double mutant channel is not voltage gated, it would suggest that both mutated residues interact. This could be further proven by mutating pairs of residues to cysteine in order to observe if they form disulfide bonds. For example, if the non-functional E363C mutant channel can be rescued by adding the Y352C mutation. Disulfide bonds formed in the double mutant channels could then be broken by addition of the reducing agent dithiothreitol (DTT) which would probably abolish channel activity.

It would also be interesting to investigate the number of subunits in the channel that have to be mutated for the channel to start exhibiting voltage sensitivity. This question could be approached by making tandem constructs in which a known number of the subunits forming the channel and their arrangement have a certain mutation. If a single mutant subunit is sufficient to produce closure of the channels at negative potentials, that could indicate that any of these mutations could potentially be a clinically important dominant negative phenotype in disorders like achromatopsia, where point mutations around the selectivity filter of a CNG channel have been linked to the disease.

Bibliography

Aggarwal, S.K., and R. MacKinnon. 1996. Contribution of the S4 segment to gating charge in the Shaker K^+ channel. *Neuron* 16:1169-1177.

Ahmad, I., C. Korbmacher, A.S. Segal, P. Cheung, E.L. Boulpaep, and C.J. Barnstable. 1992. Mouse cortical collecting duct cells show nonselective cation channel activity and express a gene related to the cGMP-gated rod photoreceptor channel. *Proc. Natl. Acad. Sci. U. S. A.* 89:10262-10266.

Alagem, N., S. Yesylevskyy, and E. Reuveny. 2003. The pore helix is involved in stabilizing the open state of inwardly rectifying K^+ channels. *Biophys. J.* 85:300-312.

Almers, W. 1978. Gating currents and charge movements in excitable membranes. *Rev. Physiol. Biochem. Pharmacol.* 82:96-190.

Anselmi, C., P. Carloni, and V. Torre. 2007. Origin of functional diversity among tetrameric voltage-gated channels. *Proteins.* 66:136-146.

Armstrong, C.M. 1971. Interaction of tetraethylammonium ion derivatives with the potassium channels of giant axons. *J. Gen. Physiol.* 58:413-437.

Bacigalupo, J., E.C. Johnson, C. Vergara, and J.E. Lisman. 1991. Light-dependent channels from excised patches of *Limulus* ventral photoreceptors are opened by cGMP. *Proc. Natl. Acad. Sci. U. S. A.* 88:7938-7942.

Bähring, R., D. Bowie, M. Benveniste, and M.L. Mayer. 1997. Permeation and block of rat GluR6 glutamate receptor channels by internal and external polyamines. *J. Physiol.* 502 (Pt 3):575-589.

Baumann, A., S. Frings, M. Godde, R. Seifert, and U.B. Kaupp. 1994. Primary structure and functional expression of a Drosophila cyclic nucleotide-gated channel present in eyes and antennae. *EMBO J.* 13:5040-5050.

Baylor, D.A., T.D. Lamb, and K.W. Yau. 1979. Responses of retinal rods to single photons. *J. Physiol.* 288:613-634.

Baylor, D.A., B.J. Nunn, and J.L. Schnapf. 1984. The photocurrent, noise and spectral sensitivity of rods of the monkey *Macaca fascicularis*. *J. Physiol.* 357:575-607.

Becchetti, A., K. Gamel, and V. Torre. 1999. Cyclic nucleotide-gated channels: pore topology studied through the accessibility of reporter cysteines. *J. Gen. Physiol.* 114:377-392.

Becchetti, A., and P. Roncaglia. 2000. Cyclic nucleotide-gated channels: intra- and extracellular accessibility to Cd^{2+} of substituted cysteine residues within the P-loop. *Pflügers Arch.* 440:556-565.

Begenisich, T.B., and M.D. Cahalan. 1980. Sodium channel permeation in squid axons. I: Reversal potential experiments. *J. Physiol.* 307:217-242

Begenisich, T., and C. Smith. 1984. Multi-ion nature of potassium channels in squid axons. *Current topics in membranes and transport.* 22:353-369

Benndorf, K., R. Koopmann, E. Eismann, and U.B. Kaupp. 1999. Gating by cyclic GMP and voltage in the alpha subunit of the cyclic GMP-gated channel from rod photoreceptors. *J. Gen. Physiol.* 114:477-490.

Bernèche, S., and B. Roux. 2003. A microscopic view of ion conduction through the K^+ channel. *Proc. Natl. Acad. Sci. U. S. A.* 100:8644-8648.

Bezanilla, F. 2008. Ion channels: from conductance to structure. *Neuron* 60:456-468.

Biel, M., W. Altenhofen, R. Hullin, J. Ludwig, M. Freichel, V. Flockerzi, N. Dascal, U.B. Kaupp, and F. Hofmann. 1993. Primary structure and functional expression of a cyclic nucleotide-gated channel from rabbit aorta. *FEBS Lett.* 329:134-138.

Biel, M., X. Zong, M. Distler, E. Bosse, N. Klugbauer, M. Murakami, V. Flockerzi, and F. Hofmann. 1994. Another member of the cyclic nucleotide-gated channel family, expressed in testis, kidney, and heart. *Proc. Natl. Acad. Sci. U. S. A.* 91:3505-3509.

Blatz, A.L., and K.L. Magleby. 1984. Ion conductance and selectivity of single calcium-activated potassium channels in cultured rat muscle. *J. Gen. Physiol.* 84:1-23.

Blaustein, R.O., and A. Finkelstein. 1990. Voltage-dependent block of anthrax toxin channels in planar phospholipid bilayer membranes by symmetric tetraalkylammonium ions. Effects on macroscopic conductance. *J. Gen. Physiol.* 96:905-919.

Blunck, R., J.F. Cordero-Morales, L.G. Cuello, E. Perozo, and F. Bezanilla. 2006. Detection of the opening of the bundle crossing in KcsA with fluorescence lifetime

spectroscopy reveals the existence of two gates for ion conduction. *J. Gen. Physiol.* 128:569-581.

Bradley, J., S. Frings, K.W. Yau, and R. Randall. 2001. Nomenclature for ion channel subunits. *Science* 294:2095-2096.

Bradley, J., Y. Zhang, R. Bakin, H.A. Lester, G.V. Ronnett, and K. Zinn. 1997. Functional expression of the heteromeric "olfactory" cyclic nucleotide-gated channel in the hippocampus: a potential effector of synaptic plasticity in brain neurons. *J. Neurosci.* 17:1993-2005.

Bräu, M.E., M. Dreimann, A. Olschewski, W. Vogel, and G. Hempelmann. 2001. Effect of drugs used for neuropathic pain management on tetrodotoxin-resistant Na^+ currents in rat sensory neurons-depolarized resting membrane potential and repetitive. *Anesthesiology* 94:137-144.

Bucossi, G., E. Eismann, F. Sesti, M. Nizzari, M. Seri, U.B. Kaupp, and V. Torre. 1996. Time-dependent current decline in cyclic GMP-gated bovine channels caused by point mutations in the pore region expressed in *Xenopus* oocytes. *J. Physiol.* 493:409-418.

Bucossi, G., M. Nizzari, and V. Torre. 1997. Single-channel properties of ionic channels gated by cyclic nucleotides. *Biophys. J.* 72:1165-1181.

Burns, M.E., and D.A. Baylor. 2001. Activation, deactivation, and adaptation in vertebrate photoreceptor cells. *Annu. Rev. Neurosci.* 24:779-805.

Carmeliet, E., and K. Mubagwa. 1998. Antiarrhythmic drugs and cardiac ion channels: mechanisms of action. *Progr. Biophys. Mol. Biol.* 70:1-72.

Chapman,M.L., M.L.Blanke, H.S.Krovetz, and A.M.VanDongen. 2006. Allosteric effects of external K^+ ions mediated by the aspartate of the GYGD signature sequence in the Kv2.1 K^+ channel. *Pflügers Arch.* 451:776-792.

Chen, T.Y., Y.W. Peng, R.S. Dhallan, B. Ahamed, R.R. Reed, and K.W. Yau. 1993. A new subunit of the cyclic nucleotide-gated cation channel in retinal rods. *Nature* 362:764-767.

Choi, K.L., C. Mossman, J.Aubé, and G. Yellen. 1993. The internal quaternary ammonium receptor site of Shaker potassium channels. *Neuron* 10:533-541.

Clayton, G.M., S. Altieri, L. Heginbotham, V.M. Unger, and J.H. Morais-Cabral. 2008. Structure of the transmembrane regions of a bacterial cyclic nucleotide-regulated channel. *Proc. Natl. Acad. Sci. U.S.A.* 105:1511-1515.

Coburn, C.M., and C.I. Bargmann. 1996. A putative cyclic nucleotide-gated channel is required for sensory development and function in *C. elegans*. *Neuron* 17:695-706.

Colamartino, G., A. Menini, and V. Torre. 1991. Blockage and permeation of divalent cations through the cyclic GMP-activated channel from tiger salamander retinal rods. *J. Physiol.* 440:189-206.

Contreras, J.E., and M. Holmgren. 2006. Access of quaternary ammonium blockers to the internal pore of cyclic nucleotide-gated channels: implications for the location of the gate. *J. Gen. Physiol.* 127:481-494.

Contreras, J.E., D. Srikumar, and M. Holmgren. 2008. Gating at the selectivity filter in cyclic nucleotide-gated channels. *Proc. Natl. Acad. Sci. U. S. A.* 105:3310-3314.

Cook, N.J., C. Zeilinger, K.W. Koch, and U.B. Kaupp. 1986. Solubilization and functional reconstitution of the cGMP-dependent cation channel from bovine rod outer segments. *J. Biol. Chem.* 261:17033-17039.

Cordero-Morales, J.F., L.G. Cuello, and E. Perozo. 2006a. Voltage-dependent gating at the KcsA selectivity filter. *Nat. Struct. Mol. Biol.* 13:319-322.

Cordero-Morales, J.F., L.G. Cuello, Y. Zhao, V. Jogini, D.M. Cortes, B. Roux, and E. Perozo. 2006b. Molecular determinants of gating at the potassium-channel selectivity filter. *Nat. Struct. Mol. Biol.* 13:311-318.

Cordero-Morales, J.F., V. Jogini, A. Lewis, V. Vasquez, D. M.Cortes, B. Roux, and E. Perozo. 2007. Molecular driving forces determining potassium channel slow inactivation. *Nat. Struct. Mol. Biol.* 14:1062-1069.

Coronado, R., and C.Miller. 1979. Voltage-dependent caesium blockade of a cation channel from fragmented sarcoplasmic reticulum. *Nature* 280:807-810.

Craven, K.B., and W.N. Zagotta. 2006. CNG and HCN channels: two peas, one pod. *Annu. Rev. Physiol.* 68:375–401

del Camino, D., and G. Yellen. 2001. Tight steric closure at the intracellular activation gate of a voltage-gated K^+ channel. *Neuron* 32:649-656.

Delgado, R., P. Hidalgo, F. Diaz, R. Latorre, and P. Labarca. 1991. A cyclic AMP-activated K^+ channel in Drosophila larval muscle is persistently activated in dunce. *Proc. Natl. Acad. Sci. U. S. A.* 88:557-560.

Dingledine, R., K. Borges, D. Bowie, and S.F. Traynelis. 1999. The glutamate receptor ion channels. *Pharmacol. Rev.* 51:7-62.

Distler, M., M. Biel, V. Flockerzi, and F. Hofmann. 1994. Expression of cyclic nucleotide-gated cation channels in non-sensory tissues and cells. *Neuropharmacology* 33:1275-1282.

Doyle, D.A., J. Morais-Cabral, R.A. Pfuetzner, A. Kuo, J.M. Gulbis, S.L. Cohen, B.T. Chait, and R. MacKinnon. 1998. The structure of the potassium channel: molecular basis of K^+ conduction and selectivity. *Science* 280:69-77.

Dryer, S.E., and D. Henderson. 1991. A cyclic GMP-activated channel in dissociated cells of the chick pineal gland. *Nature* 353:756-758.

Eismann, E., F.Müller, S.H. Heinemann, and U.B. Kaupp. 1994. A single negative charge within the pore region of a cGMP-gated channel controls rectification, Ca^{2+} blockage, and ionic selectivity. *Proc. Natl. Acad. Sci. U. S. A.* 91:1109-1113.

Fesenko, E.E., S.S. Kolesnikov, and A.L. Lyubarsky. 1985. Induction by cyclic GMP of cationic conductance in plasma membrane of retinal rod outer segment. *Nature* 313:310-313.

Ficker,E., W.Jarolimek, J.Kiehn, A.Baumann, and A.M.Brown. 1998. Molecular determinants of dofetilide block of HERG K^+ channels. *Circ. Res.* 82:386-395.

Flynn, G.E., and W.N.Zagotta. 2001. Conformational changes in S6 coupled to the opening of cyclic nucleotide-gated channels. *Neuron* 30:689-698.

Flynn, G.E., and W.N. Zagotta. 2003. A cysteine scan of the inner vestibule of cyclic nucleotide-gated channels reveals architecture and rearrangement of the pore. *J. Gen. Physiol.* 121:563-582.

Fodor, A.A., K.D. Black, and W.N. Zagotta. 1997a. Tetracaine reports a conformational change in the pore of cyclic nucleotide-gated channels. *J. Gen. Physiol.* 110:591-600.

Fodor, A.A., S.E. Gordon, and W.N. Zagotta. 1997b. Mechanism of tetracaine block of cyclic nucleotide-gated channels. *J. Gen. Physiol.* 109:3-14.

Furman, R.E., and J.C. Tanaka. 1990. Monovalent selectivity of the cyclic guanosine monophosphate-activated ion channel. *J. Gen. Physiol.* 96:57-82.

Gavazzo, P., C. Picco, E. Eismann, U.B. Kaupp, and A. Menini. 2000. A point mutation in the pore region alters gating, Ca^{2+} blockage, and permeation of olfactory cyclic nucleotide-gated channels. J. *Gen. Physiol.* 116:311-326.

Ghatpande, A.S., R. Uma, and J.W. Karpen. 2002. A multiply charged tetracaine derivative blocks cyclic nucleotide-gated channels at subnanomolar concentrations. *Biochemistry* 42:265-270.

Gordon, S.E., and W.N. Zagotta. 1995. Localization of regions affecting an allosteric transition in cyclic nucleotide-activated channels. *Neuron* 14:857-864.

Goulding, E.H., G.R. Tibbs, D. Liu, and S.A. Siegelbaum. 1993. Role of H5 domain in determining pore diameter and ion permeation through cyclic nucleotide-gated channels. *Nature* 364:61-64.

Goulding, E.H., G.R. Tibbs, and S.A. Siegelbaum. 1994. Molecular mechanism of cyclic-nucleotide-gated channel activation. *Nature* 372:369-374.

Guo, D. and Z. Lu. 2000. Mechanism of cGMP-gated channel block by intracellular polyamines. *J. Gen. Physiol.* 115:783-798.

Guo, D., Y. Ramu, A.M. Klem, and Z. Lu. 2003. Mechanism of rectification in inward-rectifier K^+ channels. *J. Gen. Physiol.* 121:261-275.

Hackos, D.H., and J.I. Korenbrot. 1999. Divalent cation selectivity is a function of gating in native and recombinant cyclic nucleotide-gated ion channels from retinal photoreceptors. *J. Gen. Physiol.* 113:799-818.

Hagiwara, S., S. Miyazaki, W. Moody, and J. Patlak. 1978. Blocking effects of barium and hydrogen ions on the potassium current during anomalous rectification in the starfish egg. *J. Physiol.* 279:167-185.

Hamill, O.P., A. Marty, E. Neher, B. Sakmann, and F.J. Sigworth. 1981. Improved patch-clamp techniques for high-resolution current recording from cells and cell-free membrane patches. *Pflügers Arch.* 391:85-100.

Hanke, W., N.J. Cook, and U.B. Kaupp. 1988. cGMP-dependent channel protein from photoreceptor membranes: single-channel activity of the purified and reconstituted protein. *Proc. Natl. Acad. Sci. U. S. A.* 85:94-98.

Haynes, L., and K.W. Yau. 1985. Cyclic GMP-sensitive conductance in outer segment membrane of catfish cones. *Nature* 317:61-64.

Haynes, L.W., A.R. Kay, and K.W. Yau. 1986. Single cyclic GMP-activated channel activity in excised patches of rod outer segment membrane. *Nature* 321:66-70.

Heginbotham, L., T. Abramson, and R. MacKinnon. 1992. A functional connection between the pores of distantly related ion channels as revealed by mutant K^+ channels. *Science* 258:1152-1155.

Henn, D.K., A. Baumann, and U.B. Kaupp. 1995. Probing the transmembrane topology of cyclic nucleotide-gated ion channels with a gene fusion approach. *Proc. Natl. Acad. Sci. U. S. A.* 92:7425-7429.

Hille, B. 2001. Ion channels of excitable membranes. 3rd ed. Sinauer Associates, Inc. Sunderland, MA. 814 pp.

Hille, B., and W. Schwarz. 1978. Potassium channels as multi-ion single-file pores. *J. Gen. Physiol.* 72:409-442.

Holmgren, M., P.L. Smith, and G. Yellen. 1997. Trapping of organic blockers by closing of voltage-dependent K^+ channels . Evidence for a trap door mechanism of activation gating. *J. Gen. Physiol.* 109:527-535.

Holmgren, M. 2003. Influence of permeant ions on gating in cyclic nucleotide-gated channels. *J. Gen. Physiol.* 121:61-72.

Jan, L.Y., and Jan, Y.N. 1990. A superfamily of ion channels. *Nature* 345:672.

Jiang, Y., A. Lee, J. Chen, M. Cadene, B.T. Chait, and R. MacKinnon. 2002. The open pore conformation of potassium channels. *Nature* 417:523-526.

Karpen, J.W., A.L. Zimmerman, L. Stryer, and D.A. Baylor. 1988. Gating kinetics of the cyclic-GMP-activated channel of retinal rods: flash photolysis and voltage-jump studies. *Proc. Natl. Acad. Sci. U. S. A.* 85:1287-1291.

Karpen, J.W., R.L. Brown, L. Stryer, and D.A. Baylor. 1993. Interactions between divalent cations and the gating machinery of cyclic GMP-activated channels in salamander retinal rods. *J. Gen. Physiol.* 101:1-25.

Kaupp, U.B., W. Hanke, R. Simmoteit, and H. Lühring. 1988. Electrical and biochemical properties of the cGMP-gated cation channel from rod photoreceptors. *Cold Spring Harb. Symp. Quant. Biol.* 53:407-415.

Kaupp, U.B., T. Niidome, T. Tanabe, S. Terada, W. Bönigk, W. Stühmer, N.J. Cook, K. Kangawa, H. Matsuo, T. Hirose, T. Miyata, and S. Numa. 1989. Primary structure and functional expression from complementary DNA of the rod photoreceptor cyclic GMP-gated channel. *Nature* 342:762-766.

Kaupp, U.B., and R. Seifert. 2002. Cyclic nucleotide-gated ion channels. *Physiol. Rev.* 82:769-824.

Keating, M.T., and M.C. Sanguinetti. 2001. Molecular and cellular mechanisms of cardiac arrhythmias. *Cell* 104:569-580.

Komatsu, H., I. Mori, J.S. Rhee, N. Akaike, and Y. Ohshima. 1996. Mutations in a cyclic nucleotide-gated channel lead to abnormal thermosensation and chemosensation in *C. elegans. Neuron* 17:707-718.

Körschen, H.G., M. Illing, R. Seifert, F. Sesti, A. Williams, S. Gotzes, C. Colville, F. Müller, A. Dose, M. Godde, L. Molday, U.B. Kaupp, and R.S. Molday. 1995. A 240 kDa protein represents the complete beta subunit of the cyclic nucleotide-gated channel from rod photoreceptor. *Neuron* 15:627-636.

Kurata, H.T., and D. Fedida. 2006. A structural interpretation of voltage-gated potassium channel inactivation. *Progr. Biophys. Mol. Biol.* 92:185-208.

Kusch, J., V. Nache, and K. Benndorf. 2004. Effects of permeating ions and cGMP on gating and conductance of rod-type cyclic nucleotide-gated (CNGA1) channels. *J. Physiol.* 560:605-616.

Leng, Q., R.W. Mercier, W. Yao, and G.A. Berkowitz. 1999. Cloning and first functional characterization of a plant cyclic nucleotide-gated cation channel. *Plant Physiol.* 121:753-761.

Liman, E.R., J. Tytgat, and P. Hess. 1992. Subunit stoichiometry of a mammalian K^+ channel determined by construction of multimeric cDNAs. *Neuron* 9:861-871.

Liu, D.T., G.R. Tibbs, and S.A. Siegelbaum. 1996. Subunit stoichiometry of cyclic nucleotide-gated channels and effects of subunit order on channel function. *Neuron* 16:983-990.

Liu, J., and S.A. Siegelbaum. 2000. Change of pore helix conformational state upon opening of cyclic nucleotide-gated channels. *Neuron* 28:899-909.

Liu, Y., M. Holmgren, M.E. Jurman, and G. Yellen. 1997. Gated access to the pore of a voltage-dependent K^+ channel. *Neuron* 19:175-184.

Long, S.B., E.B. Campbell, and R. MacKinnon. 2005. Crystal structure of a mammalian voltage-dependent Shaker family K^+ channel. *Science* 309:897-903.

Long, S.B., X. Tao, E.B. Campbell, and R. MacKinnon. 2007. Atomic structure of a voltage-dependent K^+ channel in a lipid membrane-like environment. *Nature* 450:376-382.

López-Barneo, J., T. Hoshi, S.H. Heinemann, and R.W. Aldrich. 1993. Effects of external cations and mutations in the pore region on C-type inactivation of Shaker potassium channels. *Receptors. Channels* 1:61-71.

Lu, T., A.Y. Ting, J. Mainland, L.Y. Jan, P.G. Schultz, and J. Yang. 2001. Probing ion permeation and gating in a K^+ channel with backbone mutations in the selectivity filter. *Nat. Neurosci.* 4:239-246.

Lu, Z. 2004. Mechanism of rectification in inward-rectifier K^+ channels. *Annu. Rev. Physiol.* 66:103-129.

Lu, Z., and L. Ding. 1999. Blockade of a retinal cGMP-gated channel by polyamines. *J. Gen. Physiol.* 113:35-43.

Macdonald, R.L., and K.M. Kelly. 1995. Antiepileptic drug mechanisms of action. *Epilepsia* 36:S2-S12.

MacKinnon, R., and C. Miller. 1988. Mechanism of charybdotoxin block of the high-conductance, Ca^{2+}-activated K^+ channel. *J. Gen. Physiol.* 91:335-349.

Mayer, M.L., and G.L. Westbrook. 1987. Permeation and block of N-methyl-D-aspartic acid receptor channels by divalent cations in mouse cultured central neurones. *J. Physiol.* 394:501-527.

Menini, A. 1990. Currents carried by monovalent cations through cyclic GMP-activated channels in excised patches from salamander rods. *J. Physiol.* 424:167-185.

Moczydlowski, E., and R. Latorre. 1983. Gating kinetics of Ca^{2+}-activated K^+ channels from rat muscle incorporated into planar lipid bilayers. Evidence for two voltage-dependent Ca^{2+} binding reactions. *J. Gen. Physiol.* 82:511-542.

Molday, R.S., L.L. Molday, A. Dose, I. Clark-Lewis, M. Illing, N.J. Cook, E. Eismann, and U.B. Kaupp. 1991. The cGMP-gated channel of the rod photoreceptor cell

characterization and orientation of the amino terminus. *J. Biol. Chem.* 266:21917-21922.

Nache, V., J. Kusch, V. Hagen, and K. Benndorf. 2006. Gating of cyclic nucleotide-gated (CNGA1) channels by cGMP jumps and depolarizing voltage steps. *Biophys. J.* 90:3146-3154.

Nakamura, T., and G.H. Gold. 1987. A cyclic nucleotide-gated conductance in olfactory receptor cilia. *Nature* 325:442-444.

Nasi, E. and M.del Pilar Gomez. 1999. Divalent cation interactions with light-dependent K channels. Kinetics of voltage-dependent block and requirement for an open pore. *J. Gen. Physiol.* 114:653-672.

Neher, E., and J.H. Steinbach. 1978. Local anaesthetics transiently block currents through single acetylcholine-receptor channels. *J. Physiol.* 277:153-176.

Newman, E.A. 1993. Inward-rectifying potassium channels in retinal glial (Müller) cells. *J. Neurosci.* 13:3333-3345.

Neyton, J., and C. Miller. 1988. Potassium blocks barium permeation through a calcium-activated potassium channel. *J. Gen. Physiol.* 92:549-567.

Nichols, C.G., and A.N. Lopatin. 1997. Inward rectifier potassium channels. *Annu. Rev. Physiol.* 59:171-191.

Nicol, G.D., P.P. Schnetkamp, Y. Saimi, E.J. Cragoe, and M.D. Bownds. 1987. A derivative of amiloride blocks both the light-regulated and cyclic GMP-regulated conductances in rod photoreceptors. *J. Gen. Physiol.* 90:651-669.

Nimigean, C.M., and C. Miller. 2002. Na^+ block and permeation in a K^+ channel of known structure. *J. Gen. Physiol.* 120:323-335.

Nimigean, C.M., T. Shane, and C. Miller. 2004. A cyclic nucleotide modulated prokaryotic K^+ channel. *J. Gen. Physiol.* 124:203-210.

Nizzari, M., F. Sesti, M.T. Giraudo, C. Virginio, A. Cattaneo, and V. Torre. 1993. Single-channel properties of cloned cGMP-activated channels from retinal rods. *Proc. R. Soc., B* 254:69-74.

Noda, M., H. Takahashi, T. Tanabe, M. Toyosato, S. Kikyotani, T. Hirose, M. Asai, H. Takashima, S. Inayama, T. Miyata, and S. Numa. 1983. Primary structures of β- and

δ-subunit precursors of Torpedo californica acetylcholine receptor deduced from cDNA sequences. *Nature* 301:251-255.

Park, C.S., and C. Miller. 1992. Interaction of charybdotoxin with permeant ions inside the pore of a K^+ channel. *Neuron* 9:307-313.

Park, C.S., and R. MacKinnon. 1995. Divalent cation selectivity in a cyclic nucleotide-gated ion channel. *Biochemistry* 34:13328-13333.

Penn, R.D., and W.A. Hagins. 1972. Kinetics of the photocurrent of retinal rods. *Biophys. J.* 12:1073-1094.

Perozo, E., R. MacKinnon, F. Bezanilla, and E. Stefani. 1993. Gating currents from a nonconducting mutant reveal open-closed conformations in Shaker K^+ channels. *Neuron* 11:353-358.

Rieke, F., and D.A .Baylor. 1998. Single-photon detection by rod cells of the retina. *Rev. Mod. Phys.* 70:1027-1036.

Root, M.J., and R. MacKinnon. 1993. Identification of an external divalent cation-binding site in the pore of a cGMP-activated channel. *Neuron* 11:459-466.

Rosenbaum, T., A. Gordon-Shaag, L.D. Islas, J. Cooper, M. Munari, and S.E. Gordon. 2004. State-dependent block of CNG channels by dequalinium. *J. Gen. Physiol.* 123:295-304.

Rosenbaum, T., L.D. Islas, A.E. Carlson, and S.E. Gordon. 2002. Dequalinium: a novel, high-affinity blocker of CNGA1 channels. *J. Gen. Physiol.* 121:37-47.

Roux, B., and R. MacKinnon. 1999. The cavity and pore helices in the KcsA K^+ channel: electrostatic stabilization of monovalent cations. *Science* 285:100-102.

Ruiz, M., and J.W. Karpen. 1997. Single cyclic nucleotide-gated channels locked in different ligand-bound states. *Nature* 389:389-392.

Ruppersberg, J.P., E.V. Kitzing, and R. Schoepfer. 1994. The mechanism of magnesium block of NMDA receptors. *Seminars in the Neurosciences* 6:87-96.

Sakmann, B., and E. Neher. 1995. Single-Channel Recording. 2nd ed. Springer. New York, NY. 728 pp.

Schoppa, N.E., K. McCormack, M.A. Tanouye, and F.J. Sigworth. 1992. The size of gating charge in wild-type and mutant Shaker potassium channels. *Science* 255:1712-1715.

Seebohm, G., M.C. Sanguinetti, and M. Pusch. 2003. Tight coupling of rubidium conductance and inactivation in human KCNQ1 potassium channels. *J. Physiol.* 552:369-378.

Seifert, R., E. Eismann, J. Ludwig, A. Baumann, and U.B. Kaupp. 1999. Molecular determinants of a Ca^{2+}-binding site in the pore of cyclic nucleotide-gated channels: S5/S6 segments control affinity of intrapore glutamates. *EMBO J.* 18:119-130.

Seoh, S.A., D. Sigg, D.M. Papazian, and F. Bezanilla. 1996. Voltage-sensing residues in the S2 and S4 segments of the Shaker K^+ channel. *Neuron* 16:1159-1167.

Sesti, F., E. Eismann, U.B. Kaupp, M. Nizzari, and V. Torre. 1995. The multi-ion nature of the cGMP-gated channel from vertebrate rods. *J. Physiol.* 487:17-36.

Sesti, F., M. Nizzari, and V. Torre. 1996. Effect of changing temperature on the ionic permeation through the cyclic GMP-gated channel from vertebrate photoreceptors. *Biophys. J.* 70:2616-2639.

Sharpe, L.T., A. Stockman, H. Jägle, and J. Nathans. 1999. Opsin genes, cone photopigments, color vision and color blindness. *In* Color Vision: From Genes to Perception. K.R. Gegenfurtner and L.T. Sharpe, editors. Cambridge University Press, New York. 48-51.

Shin, H.G., and Z. Lu. 2005. Mechanism of the voltage sensitivity of IRK1 inward-rectifier K^+ channel block by the polyamine spermine. *J. Gen. Physiol.* 125:413-426.

Shin, H.G., Y. Xu, and Z. Lu. 2005. Evidence for sequential ion-binding loci along the inner pore of the IRK1 inward-rectifier K^+ channel. *J. Gen. Physiol.* 126:123-135.

Spassova, M., and Z. Lu. 1998. Coupled ion movement underlies rectification in an inward-rectifier K^+ channel. *J. Gen. Physiol.* 112:211-221.

Spassova, M., and Z. Lu. 1999. Tuning the voltage dependence of tetraethylammonium block with permeant ions in an inward-rectifier K^+ channel. *J. Gen. Physiol.* 114:415-426.

Stern, J.H., H. Knutsson, and P.R. MacLeish. 1987. Divalent cations directly affect the conductance of excised patches of rod photoreceptor membrane. *Science* 236:1674-1678.

Stotz, S.C., and L.W. Haynes. 1996. Block of the cGMP-gated cation channel of catfish rod and cone photoreceptors by organic cations. *Biophys. J.* 71:3136-3147.

Strassmaier, T., R. Uma, A.S. Ghatpande, T. Bandyopadhyay, M. Schaffer, J. Witte, P.G. McDougal, R.L. Brown, and J.W. Karpen. 2005. Modifications to the tetracaine scaffold produce cyclic nucleotide-gated channel blockers with widely varying efficacies. *J. Med. Chem.* 48:5805-5812.

Stryer, L. 1986. Cyclic GMP cascade of vision. *Annu. Rev. Neurosci.* 9:87-119.

Sun, Z.P., M.H. Akabas, E.H. Goulding, A. Karlin, and S.A. Siegelbaum. 1996. Exposure of residues in the cyclic nucleotide-gated channel pore: P region structure and function in gating. *Neuron* 16:141-149.

Swartz, K.J. 2004. Towards a structural view of gating in potassium channels. *Nat. Rev. Neurosci.* 5:905-916.

Tanaka, J.C., J.F. Eccleston, and R.E. Furman. 1989. Photoreceptor channel activation by nucleotide derivatives. *Biochemistry* 28:2776-2784.

Tang, C.Y., and D.M. Papazian. 1997. Transfer of voltage independence from a rat olfactory channel to the *Drosophila* ether-a-go-go K^+ channel. *J. Gen. Physiol.* 109:301-311.

Thompson, J., and T. Begenisich. 2001. Affinity and location of an internal K^+ ion binding site in shaker K channels. *J. Gen. Physiol.* 117:373-384.

Thompson, J., and T. Begenisich. 2003. External TEA block of shaker K^+ channels is coupled to the movement of K^+ ions within the selectivity filter. *J. Gen. Physiol.* 122:239-246.

Tränkner, D., H. Jägle, S. Kohl, E. Apfelstedt-Sylla, L.T. Sharpe, U.B. Kaupp, E. Zrenner, R. Seifert, and B. Wissinger. 2004. Molecular basis of an inherited form of incomplete achromatopsia. *J. Neurosci.* 24:138-147.

Varnum, M.D., and W.N. Zagotta. 1996. Subunit interactions in the activation of cyclic nucleotide-gated ion channels. *Biophys. J.* 70:2667-2679.

Weitz, D., N. Ficek, E. Kremmer, P.J. Bauer, and U.B. Kaupp. 2002. Subunit stoichiometry of the CNG channel of rod photoreceptors. *Neuron* 36:881-889.

Weyand, I., M. Godde, S. Frings, J. Weiner, F. Müller, W. Altenhofen, H. Hatt, and U.B. Kaupp. 1994. Cloning and functional expression of a cyclic-nucleotide-gated channel from mammalian sperm. *Nature* 368:859-863.

Wohlfart, P., W. Haase, R.S. Molday, and N.J. Cook. 1992. Antibodies against synthetic peptides used to determine the topology and site of glycosylation of the cGMP-gated channel from bovine rod photoreceptors. *J. Biol. Chem.* 267:644-648.

Woodhull, A.M. 1973. Ionic blockage of sodium channels in nerve. *J. Gen. Physiol.* 61:687-708.

Yang, Y., Y. Yan, and F.J. Sigworth. 1997. How does the W434F mutation block current in Shaker potassium channels? *J. Gen. Physiol.* 109:779-789.

Yau, K.W., and D.A. Baylor. 1989. Cyclic GMP-activated conductance of retinal photoreceptor cells. *Annu. Rev. Neurosci.* 12:289-327.

Yellen, G. 1984a. Ionic permeation and blockade in Ca^{2+}-activated K^+ channels of bovine chromaffin cells. *J. Gen. Physiol.* 84:157-186.

Yellen, G. 1984b. Relief of Na^+ block of $Ca2^+$-activated K^+ channels by external cations. *J. Gen. Physiol.* 84:187-199.

Yellen, G. 1998. The moving parts of voltage-gated ion channels. *Q. Rev. Biophys.* 31:239-295.

Yellen, G. 2002. The voltage-gated potassium channels and their relatives. *Nature* 419:35-42.

Yifrach, O. and R. MacKinnon. 2002. Energetics of pore opening in a voltage-gated K^+ channel. *Cell* 111:231-239.

Zagotta, W.N., and S.A. Siegelbaum. 1996. Structure and function of cyclic nucleotide-gated channels. *Annu. Rev. Neurosci.* 19:235-263.

Zheng, J., M.C. Trudeau, and W.N. Zagotta. 2002. Rod cyclic nucleotide-gated channels have a stoichiometry of three CNGA1 subunits and one CNGB1 subunit. *Neuron* 36:891-896.

Zhong, H., L.L. Molday, R.S. Molday, and K.W. Yau. 2002. The heteromeric cyclic nucleotide-gated channel adopts a 3A:1B stoichiometry. *Nature* 420:193-198.

Zhou, Y., J.H. Morais-Cabral, A. Kaufman, and R. MacKinnon. 2001. Chemistry of ion coordination and hydration revealed by a K^+ channel-Fab complex at 2.0 Å resolution. *Nature* 414:43-48.

Zimmerman, A.L., and D.A. Baylor. 1992. Cation interactions within the cyclic GMP-activated channel of retinal rods from the tiger salamander. *J. Physiol.* 449:759-783.

Zufall, F., and H. Hatt. 1991. Dual activation of a sex pheromone-dependent ion channel from insect olfactory dendrites by protein kinase C activators and cyclic GMP. *Proc. Natl. Acad. Sci. U. S. A.* 88:8520-8524.